# Synthesis and characterization of alkali metal borides and *closo*-hydroborates

Dissertation

zur Erlangung des Grades

"Doktor der Naturwissenschaften"

(Doctor of rer. nat.)

am Fachbereichs Chemie

der Universität Hamburg

vorgelegt von

Monalisa Panda

geboren in Cuttack (INDIA)

Hamburg, December 2006

Dekan : Prof. Dr. Chris Meier

1. Gutachterin: Prof. Dr. Barbara Albert

2. Gutachter: Prof. Dr. Dieter Rehder

Tag der Disputation: December 21, 2006

*I declare that I myself wrote this work and carried out the experimental study described in it, without using any other sources and aids than those that are stated.*

Hamburg, November 2006

# Abstract
## Synthesis and characterization of alkali metal borides and
## *closo*-hydroborates

Alkali metal borides and *closo*-hydroborates were synthesized and characterized. For alkali metal borides two different synthetic approaches were applied. Starting materials were either the elements or suitable precursor compounds. Alkali metal *closo*-hydroborates were synthesized as ammoniates in liquid ammonia.

In the Li-B system, $Li_2B_9$ has been successfully synthesized from the elements as well as from $Li_2[B_{10}H_{10}]$ as precursor. The products were thoroughly investigated via powder diffractometry (synchrotron radiation) and electron energy loss spectroscopy. They were found to be free from oxygen. The crystal structure was determined by refinement of the powder diffraction data. It exhibits an open channel framework of the boron atoms. The presence of lithium atoms inside the channels suggests a lithium ion mobility. This was confirmed by impedance spectroscopy. $LiB_{13}$ was synthesized from the elements and characterized by Rietveld refinement. In the Na-B system, $Na_2B_{29}$ and $Na_3B_{20}$ were synthesized from precursor compounds such as sodium azide and sodium decahydro-*closo*-decaborate and characterized via powder diffractometry.

Ammoniated compounds like $[Li(NH_3)_4]_2[B_6H_6] \cdot 2\,NH_3$, $[Na(NH_3)_4]_2\,[B_6H_6] \cdot 2\,NH_3$, $[Li(NH_3)_4]_2[B_{12}H_{12}] \cdot 2\,NH_3$ and $M_2[B_{10}H_{10}] \cdot 5\,NH_3$ (M = Rb and Cs) as well as $[N(C_4H_9)_4]_2[B_6H_6]$ were obtained in form of single crystals from liquid ammonia and investigated via single crystal diffractometry at 123 K. Their crystal structures were determined. All of these compounds are highly sensitive to moisture and air and decompose far below room temperature, for example by loosing ammonia. The symmetry of the anions and the coordination sphere of the cations as well as the role of the ammonia molecules and their structure-directing influence through hydrogen bonding was carefully analyzed.

# Kurzzusammenfassung

## Synthese und Charakterisierung von Alkalimetalboriden und *closo*-Hydroboraten

Alkalimetallboride und *closo*-Hydroborate wurden synthetisiert und charakterisiert. Die Darstellung der Alkalimetallboride erfolgte auf zwei unterschiedlichen Synthesewegen. Ausgangsstoffe waren entweder die Elemente oder geeignete Precursor-Verbindungen. Die Darstellung der *closo*-Hydroborate gelang in flüssigem Ammoniak.

Im Li-B System wurde $Li_2B_9$ synthetisiert, sowohl durch Umsetzung der Elemente als auch aus $Li_2[B_{10}H_{10}]$ als Precursor-Verbindung. Die Charakterisierung erfolgte mittels Pulverdiffraktometrie (Synchrotron) und Elektronenenergieverlustspektroskopie. Die Produckte waren Sauerstoff-frei. Die Kristallstruktur wurde auf Basis der Pulverbeugungsdaten bestimmt. Sie zeigt ein Boratomgerüst mit offenen Kanälen. Die Gegenwart von Lithiumatomen in diesen Kanälen legt deren Beweglichkeit nahe. Diese wurde mittels Impedanzspektroskopie bestätigt. Zudem konnte $LiB_{13}$ als eine weitere Verbindung im System Li-B synthetisiert und mittels Röntgendiffraktometrie charakterisiert werden. Im System Na-B gelang es, $Na_2B_{29}$ und $Na_3B_{20}$ aus den Precursor-Verbindungen Natriumazid und Natrium-*closo*-decahydrodecaborat darzustellen und durch Pulverdiffraktometrie zu charakterisieren.

Ammoniakhaltige Verbindungen wie $[Li(NH_3)_4]_2[B_6H_6] \cdot 2\,NH_3$, $[Na(NH_3)_4]_2[B_6H_6]$ $\cdot 2\,NH_3$, $[Li(NH_3)_4]_2[B_{12}H_{12}] \cdot 2\,NH_3$ und $M_2[B_{10}H_{10}] \cdot 5\,NH_3$ (M = Rb and Cs) sowie $[N(C_4H_9)_4]_2[B_6H_6]$ wurden in Form von Einkristallen aus flüssigem Ammoniak erhalten und bei 123 K mittels Röntgenstrukturanalyse untersucht. Ihre Kristallstrukturen wurden bestimmt. Alle beschrieben Verbindungen sind feuchtigkeits- und luftempfindlich. Die ammoniakhaltigen Verbindungen zersetzen sich weit unterhalb der Raumtemperatur durch den Verlust von Ammoniakmolekülen. Die Symmetrie der Anionen, Kationen und deren Koordinationssphären wurden analysiert. Der Einfluss der Ammoniakmoleküle auf die Struktur der Verbindungen durch die Bildung von Wasserstoffbrückenbindungen wurde analysiert.

# Acknowledgements

# Contents

# 1 Introduction

## 1.1 Background

Solid state chemistry is the study of solid materials, which may have either molecular, supramolecular or extended structures. It includes their syntheses, structure analyses and the determination of the physical properties. There are various methods available for the preparation of solids, like the high temperature reaction, precipitation reaction or electrochemical methods. Among these methods the high temperature solid state reaction route is the most widely used.

Numerous phases of borides are synthesized by using this high temperature solid state route combining boron with almost all elements of the periodic table. Borides are the subject of much interest due to their crystal structures, bonding situations, physical properties and applications. In the crystal structure of borides, the arrangement of boron atoms varies with boron concentration. In metal-rich borides isolated boron atoms are found with widely differing interatomic B-B distances. As the boron atom concentration increases isolated pairs, chains and planar like arrangements are observed. In the boron-rich borides, the structures comprise of three dimensional networks of boron atoms and clusters dominated by inter-boron bonding [1]. Therefore, the bonding situations of the boron atoms in the frameworks of boron-rich solids are not easy to understand properly. Alkali metal borides can be used to study the complex electronic situation of the boron atom framework because of the usually well defined oxidation state of alkali metals in compounds.

The aim of this study is to synthesize alkali metal borides, mainly lithium and sodium borides by solid state reactions from the elements or precursors. Few compounds in Li-B series are known and the thermodynamic equilibrium phase diagram is also not available [2]. It has been a constant challenge for the synthetic chemists to prepare pure alkali metal borides because of the stringent experimental procedure. The synthesis procedures are often difficult due to high differences in melting points and reactivities between the reactants. The structurally characterized compounds

in the Li-B system are $LiB_{13}$ [3], $Li_3B_{14}$ [4], $Li_2B_6$ [5] and $LiB_x$ (0.82$\leq$ x $\leq$ 1) [6] in the order of increasing Li/B ratio. Except for these four compounds, all other reported compounds are ambiguous and controversial. Further compounds which have been mentioned in the literature so far but remain to be unconfirmed concerning the composition and structure are given in the table 1.1.

| Comp. name | Structure information | Characterization techniques |
|---|---|---|
| $LiB_{10.85}$ [7] | Tetragonal (indexed) | XRD |
| $LiB_{10}$ [8] | - | XPS, XRD and chemical analysis |
| $LiB_4$ [9] | - | Chemical analysis and XRD |
| $LiB_2$ [8] | - | XPS, XRD and chemical analysis |
| LiB [10] | - | XRD, Thermogravimetry |
| $Li_7B_6$ [11] | - | DSC and XRD |
| $Li_5B_4$ [12] | $R\bar{3}m$, $I4\bar{3}m$ | XRD, TGA, DTA |
| $Li_2B$ [13] | - | LiCl-KCl eutectic melt |
| $Li_3B$ [14] | - | DSC, chemical analysis |

Table 1.1: List of controversial compounds reported in the Li-B system

A compound which was described by different formula like " $Li_6B_{18}X$ " (X = $BH_3$ or $Li_2O$) [15] or " $Li_2B_9$ " [16] exhibits a very interesting framework structure but was never synthesized and characterized in a pure and monophasic form. This compound is reinvestigated in the present work and described in chapter 3.1.

In the sodium-boron system, crystal structures of only two binary sodium borides have been published. These are $Na_2B_{29}$ and $Na_3B_{20}$. A boron-rich sodium boride with a chemical formula $NaB_{15}$ was first reported by Naslain $et$ $al.$ [17–19]. Albert $et$ $al.$ [20] studied this compound with a comprehensive structural investigation using X-ray single-crystal and powder diffraction, low-temperature neutron and electron diffraction, high resolution transmission electron microscopy and $^{23}$Na solid-state NMR spectroscopy. They concluded that the composition "$NaB_{15}$" and the orthorhombic space group were incorrect. Consistent with all the experimental results they proposed a modified chemical formula as $Na_2B_{29}$, indexed in the monoclinic crystal system and structurally described in the space group $I1m1$. $Na_3B_{20}$ is also a modified structure of a binary compound called $NaB_6$ which was earlier reported by Hagenmüller and Naslain [17–19]. Albert $et$ $al.$ [21, 22] found that the chemical formula of this compound was $Na_3B_{20}$ instead of $NaB_6$ and that it crystallizes in the orthorhombic system with a space group $Cmmm$. Now a new synthetic procedure

was developed and $Na_3B_{20}$ and $Na_2B_{29}$ were prepared from precursor compounds as described in section 3.4.

In the present work, another class of compounds known as *closo*-hydroborates was given much importance because of their possible use as precursor materials. These compounds contain anions in the form of closed polyhedral clusters of $n$ boron atoms. The general formula is $[B_nH_n]^{2-}$ (n = 5 to 12). Only a few *closo*-hydroborates of the alkali metals have been investigated concerning their crystal structures, electron density distributions and the exact symmetry of the polyhedra, as it was difficult to obtain single crystals of these compounds. In the present study liquid ammonia was used as a solvent to crystallize alkali metal hydroborates. The idea behind this was to prepare an ammoniated alkali metal hydroborate, which can be used as a precursor material for synthesizing ultra pure alkali metal borides by evaporating the ammonia and hydrogen. Another long-term motivation is to use these crystals (mainly crystals containg light elements like lithium and boron) to evaluate the experimental charge densities in multi-center bonds in *closo*-hydroborates and compare with electron localisation function (ELF) calculations. *Closo*-hydroborates discussed in this work are those with the anions $[B_6H_6]^{2-}$, $[B_{10}H_{10}]^{2-}$ and $[B_{12}H_{12}]^{2-}$ and are described in chapter 4.

The various characterization techniques used in this study are X-ray diffraction, electron energy loss spectroscopy (EELS), infrared spectroscopy (IR), nuclear magnetic spectroscopy (NMR) and impedance spectroscopy (IS). Single crystal X-ray diffraction is used for solving the crystal structures whereas the powder X-ray diffraction method is used as the fingerprint characterization of crystalline materials and for solving the crystal structure. EELS was found to be an important tool for verifying the presence of light elements such as B, C, N and O. Impedance spectroscopy, was used for electrical characterization of solids. IR and NMR were used for verifying the content and purity of the sample. All these techniques are described in detail in the chapter 2.

## 1.2 Aim of the present work

This research work is mainly focussed on the synthesis and characterization of extremely pure, monophasic, homogeneous alkali metal borides and the study of their ionic conductivity. To obtain these ultra pure compounds different synthesis routes were attempted either from elements or precursors. Most often, it is difficult to

obtain a pure and homogeneous product by synthesis from the elements due to difficulties like impurities in starting materials, unavoidable reactions of starting materials with crucible materials etc. Therefore, one of the alternative routes is synthesis using various precursors. Especially, alkali metal *closo*-hydroborates $M_2[B_nH_n]$ (n = 6, 10 and 12) (M = Li, Na, K, Rb, Cs) can be used as precursors for alkali metal boride synthesis as they contain the same kind of building block that are found in boron-rich borides. Even though the chemistry of hydroborates is an established field in inorganic chemistry, very few crystal structures had been reported for alkali metal *closo*-hydroborates. This is due to difficulties in obtaining single crystals.

The present work deals with implementation of precursor route along with the classical route for synthesizing alkali metal borides.

# 2 General Part

## 2.1 Equipment and experimental techniques

### 2.1.1 Working under inert gas techniques

Many of the starting materials like alkali metals, alkali metal *closo*-hydroborates and products like lithium borides and sodium borides used in this work are described in the literature as air and moisture sensitive materials. Therefore, the synthesis and handling of these substances is possible only with modified Schlenk techniques [23] under inert argon atmosphere. The filling of capillaries (Lindemann-glass capillaries 0.3 mm, 0.5 mm and 0.7 mm) for X-ray powder measurements, drying of the substances and distillation of excess sodium from the products was performed by the use of this technique.

### 2.1.2 Inert gas line with vacuum techniques

The Schlenk line providing vacuum and inert gas facilities is shown in figure 2.1. This setup consists of a vacuum strand, connected to a rotary valve oil vacuum pump (RV3, BOC Edwards) and a gas line. The glass parts are made of Duran glass. The ground glass joints are sealed with Ramsay high vacuum grease (Leybold), while the metal and glass joints are connected with pitch. The working glass ware is connected to the vacuum line by means of glass spirals. All these glass ware is evacuated to $3\times10^{-3}$ mbar approximately. The quality of the vacuum is examined by a manometer (Edwards). As inert gas, argon (Westphalengas, quality 4.6) is used. Argon flow is controlled by a pressure reducing valve. The flow is checked by bubbling of argon in a bubbling tube filled with paraffin oil.

Argon is dried before use, by passing through four drying towers. The drying towers are filled with silica gel, potassium hydroxide, molecular sieve (mesh size 3) and phosphorus pentaoxide (Merck) successively. This arrangement removes humidity traces from the inert gas argon. Subsequently, the argon flows through a quartz

glass tube, on which a safety relief valve (company Riegler, 0.3 bar) is attached. This quartz tube is filled with titanium sponge (Deutsche Titan). It is constantly heated by a furnace at 973 K. By this process the remaining oxygen and nitrogen are removed from the inert gas. Pure, free from moisture, nitrogen and oxygen, argon is available for further work. In order to prevent the penetration of air in the whole set up, the glass ware is always connected in flow of argon stream. All the required glass ware is heated with the Bunsen burner under vacuum. After cooling down it is flooded with argon, a procedure that is repeated for three times to get rid of air and moisture.
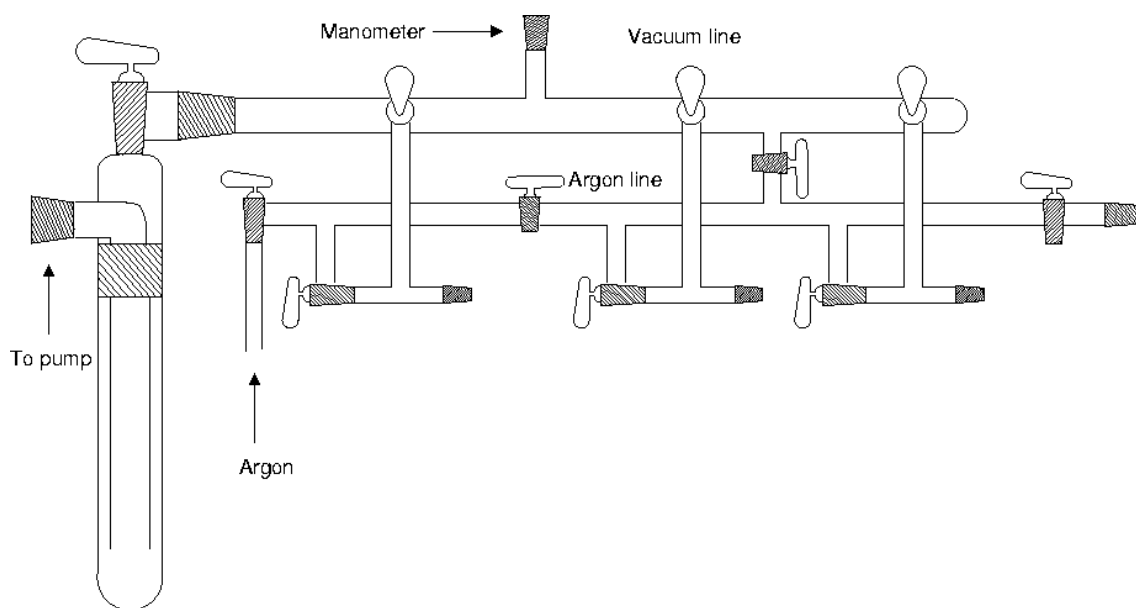


Figure 2.1: Inert gas line

## 2.1.3 Liquid ammonia line

The ammonia line is shown in figure 2.2. A part of this line is similar to the inert gas line. Condensation and storage of ammonia is possible in an additional part of this line. Both these parts are joined by glass. Mercury valves are used to check the pressure. The set up has two cooling traps. In one of the cooling traps, sodium pieces are used for drying ammonia. Both the cooling traps are joined by ground glass joints or through the bypass. When the cooling trap is filled with ammonia, evacuation of the set up is possible through a bypass. Before condensation of ammonia (Air Liquide Deutschland, GmbH (quality 3.8)), the whole set up has to be evacuated.

7

For condensation the cooling trap is cooled by a mixture of dry ice and isopropanol. Liquid ammonia is stored over sodium before use. The empty cooling trap is mainly used for removal of ammonia from the Schlenk tubes under vacuum through the mercury bubbler without contaminating the stored ammonia. The whole setup is always kept under vacuum.
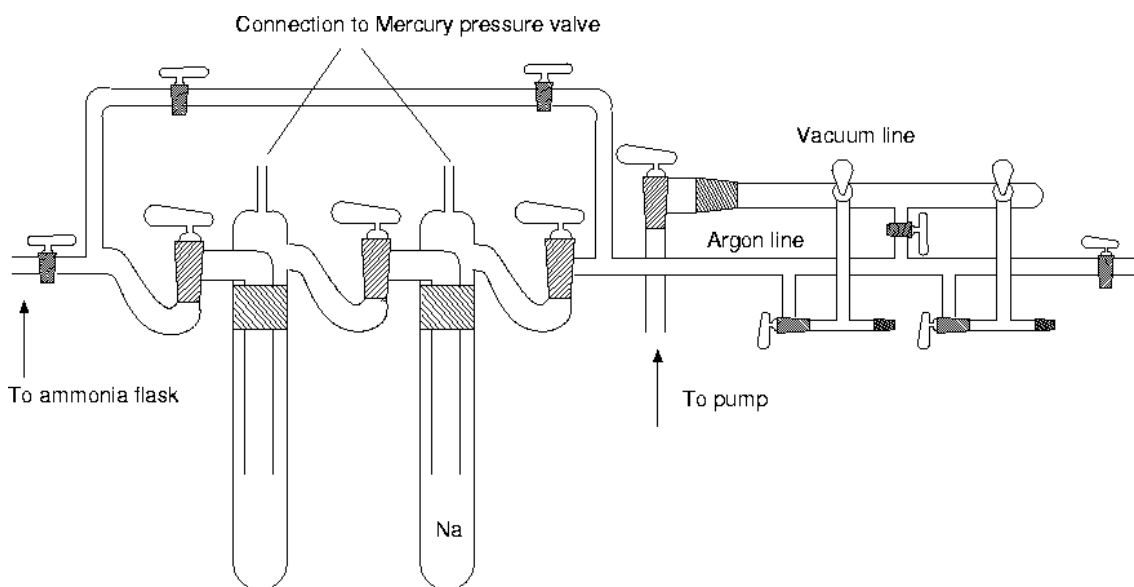


Figure 2.2: Liquid ammonia line

## 2.1.4 Arc-melting apparatus

The arc melting apparatuses is used for welding metal crucibles or as a reaction chamber for synthesizing materials above 2000° C [24]. The melting chamber is made up of either a brass base, attached with which a metal crucible for welding or a water cooled copper block with a small concavity in the center, for melting the sample. The metal piece is connected to the glass cylinder through a metal glass flange connection. The glass cylinder is connected to the inert gas line through glass joints. This results in an air tight system. The melting chamber is shown in figure 2.3. The glass cylinder is made up of Duran glass. So, during the melting process a quartz tube is used to protect the glass. A tungsten electrode is used for melting. The melting chamber is evacuated to a pressure of $8 \times 10^{-3}$ mbar, and then purged with pure argon. The process of evacuation and purging is repeated for three times. Melting of the sample is carried out at low pressure in argon atmosphere. The equipment is attached to a welding electric rectifier (Fronius, Transtig 1600)

with foot pedal operation. The arc is formed between the tungsten electrode and the metal crucible. The maximum attainable ampere is 160 A. The amount of ampere needed for melting depends upon the tube material and tube thickness.
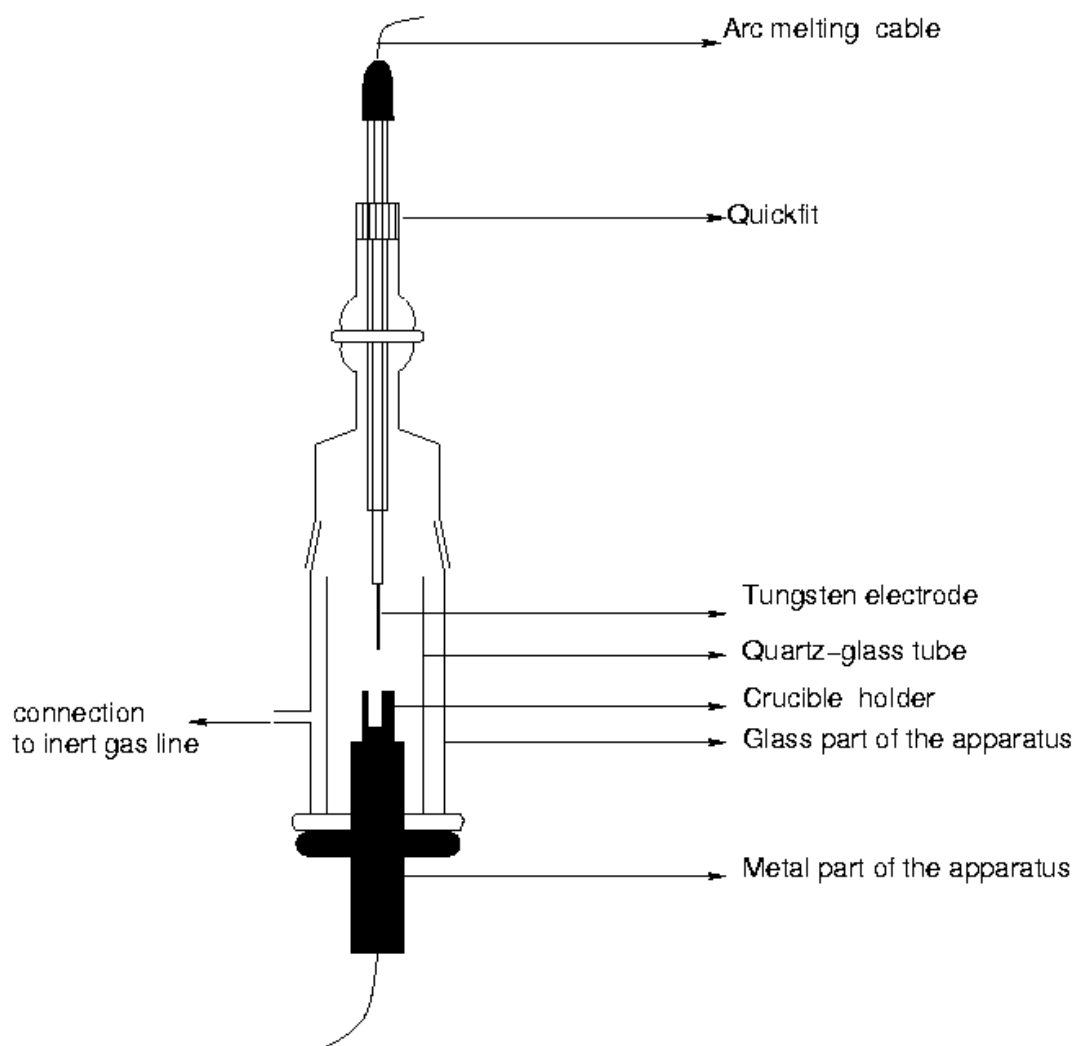
Figure 2.3: Arc-melting apparatus

## 2.1.5 Working equipments

All the glass ware is made from Duranglass. These apparatus is manufactured in the glass-technical workshops of the Institute of inorganic and applied chemistry, Hamburg. If necessary, the glass ware is cleaned with *aqua-regia* and washed carefully with distilled water.

9

### 2.1.5.1 Schlenk tubes

Schlenk tubes contain a special type of glass joints that allow to handle air sensitive substances. The joints consist of a ground glass joint male and a ground glass joint female as shown in the figure 2.4 (upper cross section: NS 29 mm, side cross section: NS 14.5 mm). A Schlenk tube is attached to the inert gas line through 14.5 mm connector. It is possible to keep moisture and air-sensitive substances in these tubes under argon. It can be used for drying the substances below 773 K under vacuum with approximately $3 \times 10^{-3}$ mbar and as a reaction vessel for liquid ammonia synthesis.
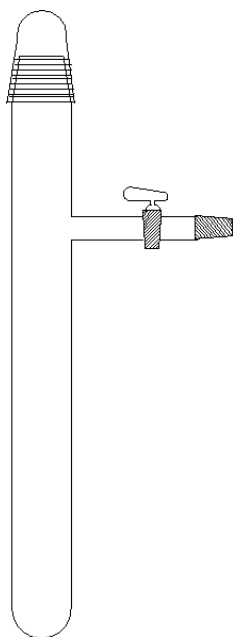


Figure 2.4: Schlenk tube

### 2.1.5.2 Filling apparatus

The filling equipment is shown in the figure 2.5 (upper cross sections: NS 29 mm, remaining cross sections NS 14.5 mm). This equipment is used to homogenize the substances with help of a dry and heated glass rod. Glass capillaries for X-ray powder measurements are filled. The remaining substance is portionated and kept in glass ampules (10-12 mm in diameter) under argon for further use.
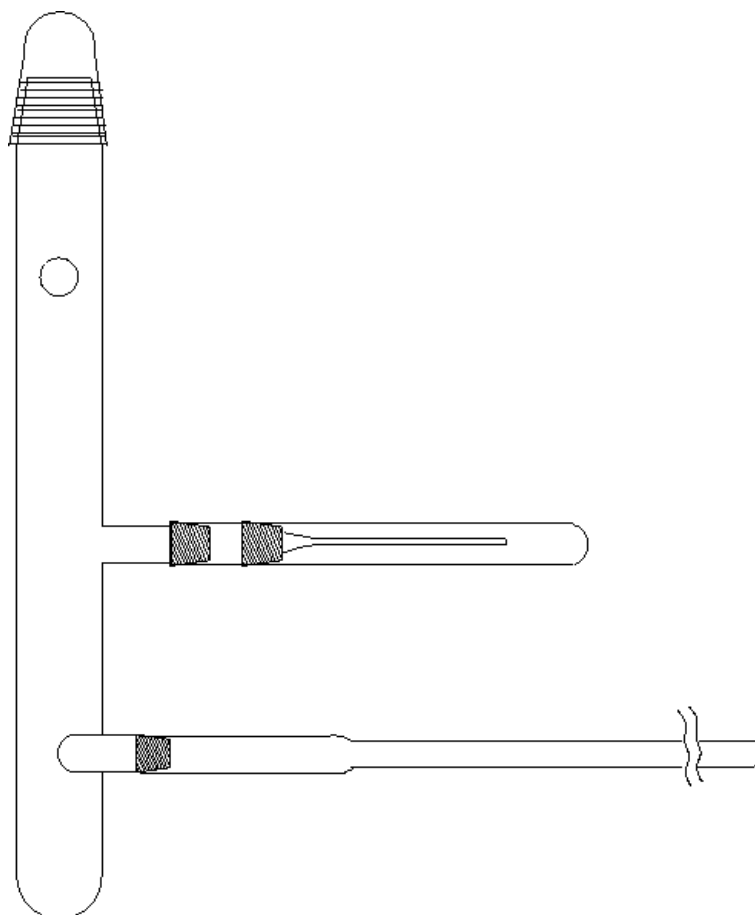
Figure 2.5: Apparatus for filling capillary and portionating air-sensitive samples

### 2.1.5.3 H-Schlenk tube

A line diagram of H-Schlenk tube is shown in figure 2.6. This apparatus consists of two closed tubes (200 mm long, inner diameter 30 mm) with male and female ground glass joints of NS 29 mm. Both these tubes are joined with a glass tube (50 mm long) which is separated by a glass frit (porosity G3). Both the parts of the H-tube have a 90° bent side arm, those are finally connected forming a U-shape. These side arms are also closed by glass stopcock. Finally, it has a NS 14.5 female joint through which it is connected to the vacuum line.

This tube is used for washing of excess alkali metals from the samples after the synthesis using liquid ammonia. First, the sample is filled in one part of the H-tube and then ammonia is condensed. Alkali metals are thus dissolved in liquid ammonia and the solution turns blue. This blue solution is transferred to the other part of the H-tube through the glass frit (G3). Again the ammonia is condensed from here to

the part where the sample is stored. This process is repeated till a colorless solution is obtained.
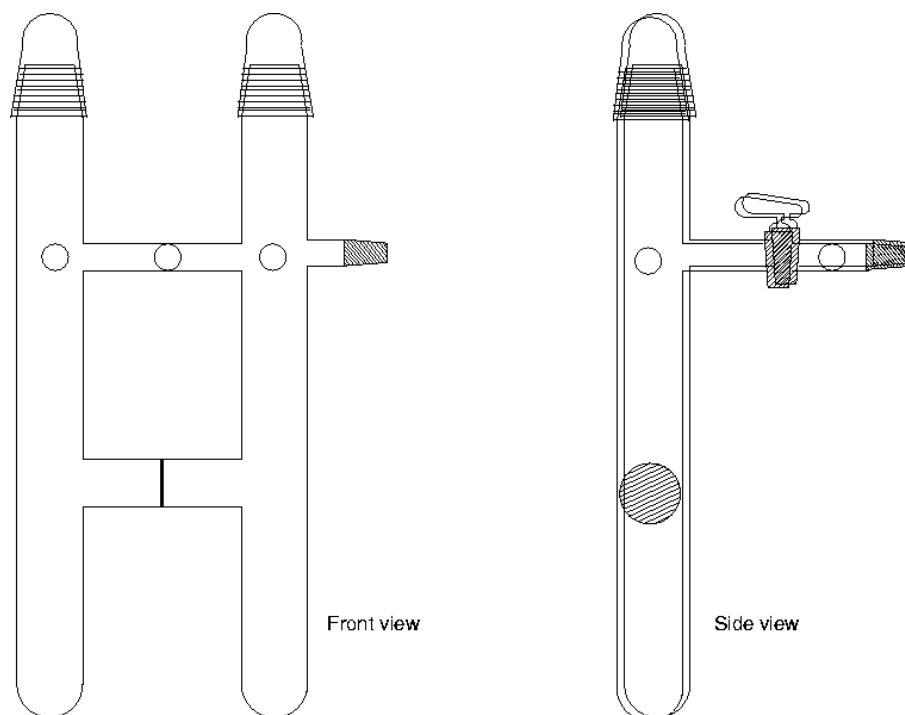
Figure 2.6: H-Schlenk tube

### 2.1.5.4 Crucibles

Most of the solid state reactions are carried out in iron or tantalum tubes. Diameter and length of these tubes vary for different reactions. Sometimes to obtain a pure sample, combination of two crucible materials are used. Boron nitride is used as an inner crucible material and sealed in an outer crucible material like tantalum. Some of the lithium borides are synthesized in a combination of molybdenum and niobium respectively. The iron tubes are sandblasted and washed with acetone, before use. Tantalum tubes are cleaned with a mixture of 2:1:1 conc. nitric acid, conc. sulphuric acid and conc. hydrofluoric acid respectively. The crucibles are kept in this mixture for about one minute and then carefully washed with distilled water and dried in a furnace. The metal tubes are heated under vacuum and stored in the Schlenk tubes under argon atmosphere. Some of the reactions are carried out in preboronated tantalum or niobium tubes. At higher temperatures tantalum reacts with boron to produce tantalum borides. To get rid of this problem, the tube is filled with an

excess of boron and placed in a quartz tube. This quartz tube is connected to the inert gas line by the help of quick fit and heated at 1273 K under vacuum for 12 h. After cooling down the excess of boron is removed. Hence, a thin film of tantalum boride will produce on the tube wall which will protect the reaction of the starting material with the crucible. These tubes are filled in the glove box and sealed with help of arc-melting apparatus.

For sodium azide reactions a tightly closed steel reactor is used. Both sides of this reactor are closed by a screw. Heating of azide in a close system will cause some explosion as the nitrogen pressure shoots up inside the crucible. So for safety reason only crucibles were used which allowed the gas to come out.

## 2.1.6 Glove-box

Some of the processing steps, e.g. filling up of the starting material in metal ampules or opening up of the metal ampules, preparing pellets etc, are not feasible in Schlenk techniques. Therefore, to get a high purity substance, these steps are handled in a "glove box" (M. Braun, Garching) under argon atmosphere. The quality of the inert gas can be judged over gas analyzers. The water and oxygen contents are below 1 ppm. Apparatus or sample can be taken inside or outside the glove box compartment through airtight evacuation chambers. The big chamber is evacuated for 15 minutes and then filled with argon. The process of evacuation and refilling with argon is repeated for three more times to make sure that the atmosphere inside the chamber is completely inert. Same process is repeated with the small evacuation chamber with the evacuation time of about 3 minutes.

## 2.1.7 Alkali metal distillation apparatus

Generally, alkali metals are available with some impurities like oxides, hydroxides, hydrides, nitrides, etc. To remove these impurities, distillation techniques are used. For alkali metals from Na to Cs (having relatively low melting points compared to lithium), the glass apparatus shown in figure 2.7 is used. Before use, it is cleaned with hot *aqua-regia* followed by washing with distilled water. Above mentioned alkali metal ampules are opened in argon stream with the help of a copper spiral hanging from a hook. The ampule is heated with the help of a bunsen burner inside this closed apparatus under argon. Then the liquified alkali metal is sucked to the flask with the help of vacuum. The ampule is then destroyed and liquified alkali

metal is distilled to a second round bottom flask in vacuum. It can be further distilled to the glass tubes and portionated to small ampules under argon. Sodium can also be handled by seggregation technique. This can be performed by using the left side apparatus in figure 2.7. Sodium is filled in the seggregation tube with the help of inert gas line in flow of argon. It is liquified by heating with a bunsen burner under vacuum. The liquid sodium is then poured to the connected glass tubes and closed under argon.
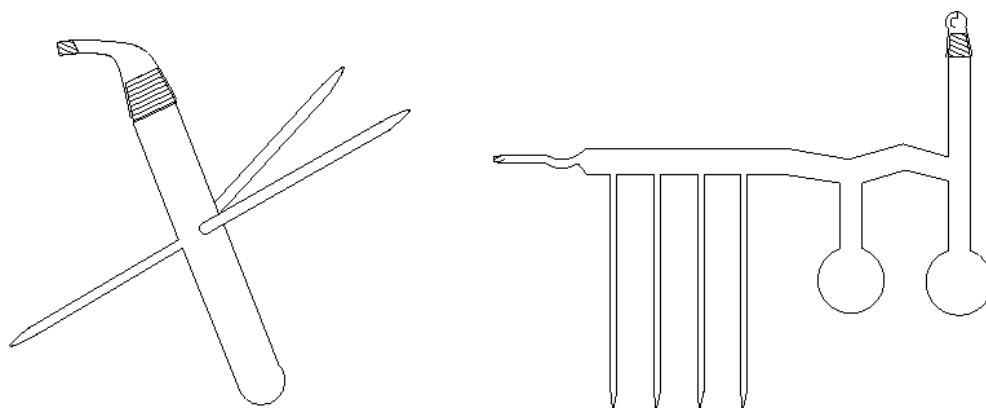


Figure 2.7: Apparatus for seggregating (left) and distillating (right) alkali metals like Na, K, Rb, Cs

Lithium can not be treated like this due to the higher melting point. A metal apparatus displayed in figure 2.8 is used for the distillation of lithium. It consists of a cylindrical steel apparatus which can be attached to the inert gas line. It has a connector for cold water flow. This setup is evacuated by using a diffusion pump (BOC Edwards) to obtain high vacuum varying from $3 \times 10^{-4}$ mbar to $3 \times 10^{-6}$ mbar. Before filling the sample, the steel apparatus is heated at 673 K by an oven and the other parts are heated by the hot plates under vacuum. A tantalum crucible (acts as sample holder) is placed inside this steel set up as displayed in left side of the figure 2.8. The required amount of lithium is filled inside the tantalum crucible. The entire set up is again evacuated till $2 \times 10^{-6}$ mbar vacuum is obtained. The temperature is raised at a rate of 5 K/minute till 823 K and then with 2 K/minute till 923 K. After rising the temperature, the cooling trap is cooled with liquid nitrogen. At this temperature, it is kept for 2 h and then cooled with 5 K/minute till room temperature. Distilled lithium is then collected in a Schlenk tube. In order to prevent the penetration of air in the whole setup, the steel apparatus is always connected while argon is streaming.

<div style="text-align:center">
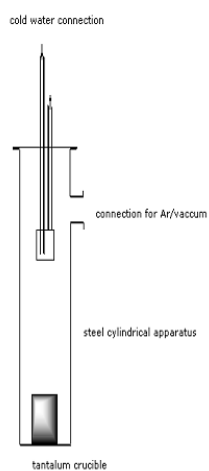
(a)          (b)

Figure 2.8: Apparatus for distillating lithium and alkaline earth metals

</div>

## 2.1.8 Oven

Reactions up to 1050 °C are carried out in an electrical resistance heating oven (Kanthal). In this kind of ovens, the crucibles are placed in an evacuated quartz ampule. For higher temperatures up to 1400 °C, a SiC high temperature oven is used. In the high temperature oven, a gas-tight aluminum oxide tube is used and is connected to an inert gas line. With the help of the inert gas line, it is possible to evacuate and flood the reaction chamber with argon stream. It is also possible to maintain the argon stream during the reaction. The crucibles are placed in an alumina boat. The temperature of the oven is measured by a platinum and platinum-rhodium thermocouple. Two thermocouple wires pass through separate

channels within a ceramic sheathe. At one end, these wires are joined together using an acetylene burner and the other sides are connected with appropriate (+ve and -ve) poles of the temperature controller.

## 2.1.9 Crystal picking apparatus

A mobile apparatus is used for the selection of temperature-moisture and air-sensitive crystals. A part of crystal picking apparatus contains vacuum and argon connections (principle same as inert gas line) which permit to open the Schlenk tubes under argon. As shown in figure 2.9, it also contains a sample holder made up of glass with a pit. Perfluoroether oil(Galden LS 230, Asscon Systemtechnik-Elektronik GmbH (Solvay Solexis)) is taken in this pit, which is cooled from the bottom by liquid nitrogen. The top of the sample holder is exposed to a stream of cooled nitrogen coming through a copper tube dipped in a liquid nitrogen bath. As the temperature decreases the perfluoroether becomes more viscous. Then the Schlenk tube is opened under argon and crystals are transferred to the oil. A crystal of particular size is selected under the microscope and picked up with the tip of a glass capillary mounted on a goniometer head. The crystal is then immediately submerged in liquid nitrogen and transferred to the X-ray diffractometer as soon as possible.
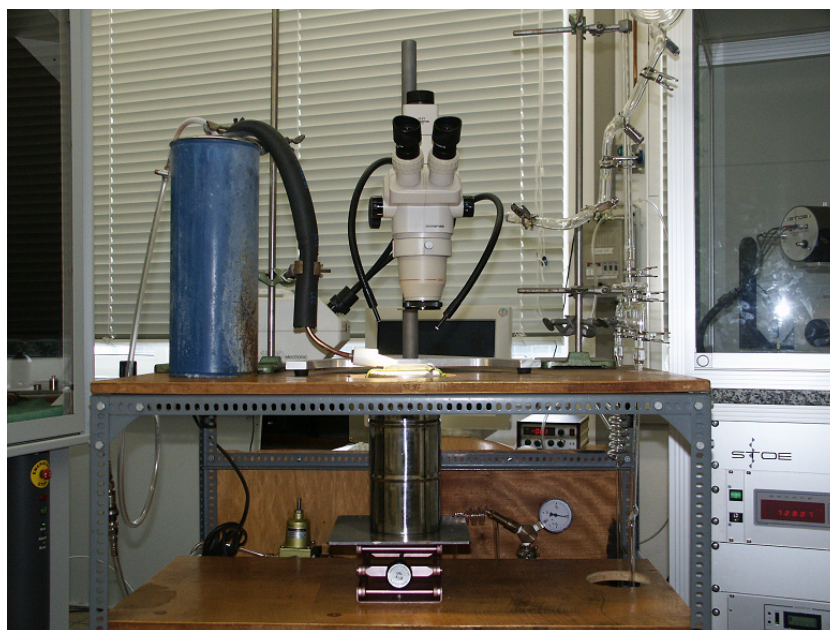


Figure 2.9: Apparatus for crystal picking at low temperature

## 2.2 Analysis techniques

### 2.2.1 X-ray diffraction

#### 2.2.1.1 Principle

X-ray diffraction is one of the most important characterization tools used in solid state chemistry as most of the substances dealt with are crystalline, meaning that their arrangement is periodic at the atomic scale. X-rays are useful as their wavelength is similar to the inter-atomic separation ($\approx 1$ Å ) in a crystal. A crystal is obtained by repetition of many billions of the unit cell (smallest repeating unit) in all three dimensions. A unit cell consists of sets of planes (lattice planes) designated by Miller indices (*hkl*) in various orientations and it is these planes which are considered in the derivation of Bragg,s law, which refers to the equation 2.1.

$$n \cdot \lambda = 2 \cdot d \cdot \sin \theta \qquad (2.1)$$

where:
n = diffraction order
$\lambda$ = wavelength of X-rays
d = distance between pairs of adjacent lattice planes
$\theta$ = angle of diffraction or Bragg angle


So Bragg's law indicates that diffraction is only observed when a set of plane makes a very specific angle with the incoming monochromatic X-ray beam.

#### 2.2.1.2 X-ray powder diffraction

A powder sample consists of an enormous number of randomly orientated small crystallites. In such a sample, various lattice planes are present in every possible orientation. For each set of planes, therefore, at least some crystals must be oriented at the Bragg angle, to the incident beam and thus, diffraction occurs for these crystals and planes. A powder diffractogram contains information about the diffraction angles and their corresponding intensities. Factors such as crystal class, lattice type, symmetry, unit cell parameter, the distribution and type of atoms in the unit cell affects the intensity and number of reflections. As a result, nearly all crystalline

solids have a unique powder X-ray diffraction pattern in terms of position and intensities of the observed reflections. Hence, a study of X-ray diffraction is widely used for the fingerprint characterization of crystalline materials, qualitative phase analysis, sample purity and determination of crystal structure [25].

The X-ray investigation of the powder samples was performed on a STOE Stadi P diffractometer shown in figure 2.10 at room temperature as well as at low temperatures. A position sensitive detector in Debye-Scherrer geometry was used for air sensitive substances. This diffractometer is equipped with a copper anode and curved germanium (111) monochromator with Cu-$K_{\alpha 1}$ radiation of wavelength 1.5406 Å. The obtained powder X-ray pattern is analysed by using the software provided by STOE [26]. The products are identified by comparing with the well known substances, whose crystallographic data are provided by the data base PDF (Powder Diffraction Files from the Joint Committee on Powder Diffraction Standards, Sweathmore, USA). Air sensitive samples are sealed in glass capillaries of outside diameter 0.3 or 0.5 mm.
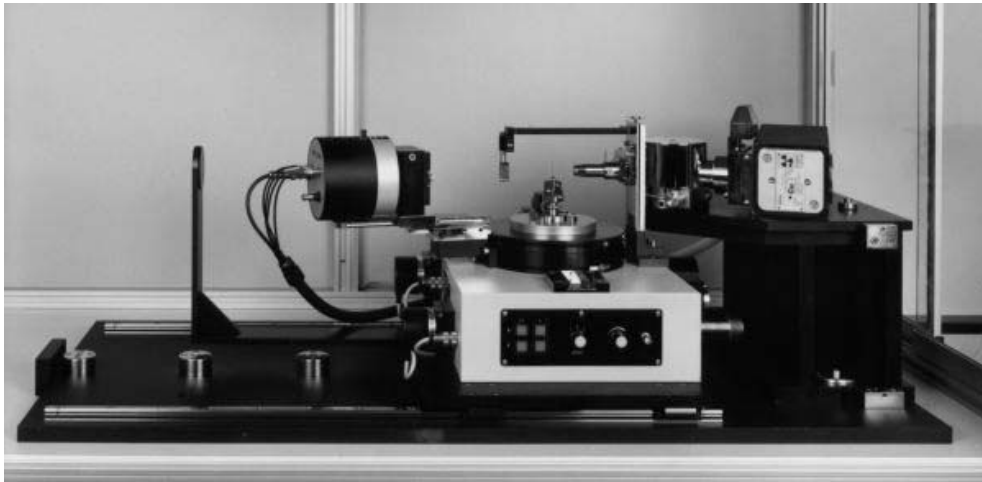


Figure 2.10: Stadi P diffractometer [26]

### 2.2.1.3 Synchrotron diffractometer

The powder X-ray investigation using synchrotron radiation was carried out at the B2-beamline of DESY-HASYLAB (Hamburg, Germany). A schematic diagram is shown in figures 2.11 and 2.12. Monochromatic radiation with a specific wavelength was selected by a double-crystal Ge(111) monochromator. Diffraction patterns were collected in Debye-Scherrer mode with a rotating capillary. The glass capillaries had

an outside diameter of 0.5 or 0.7 mm.
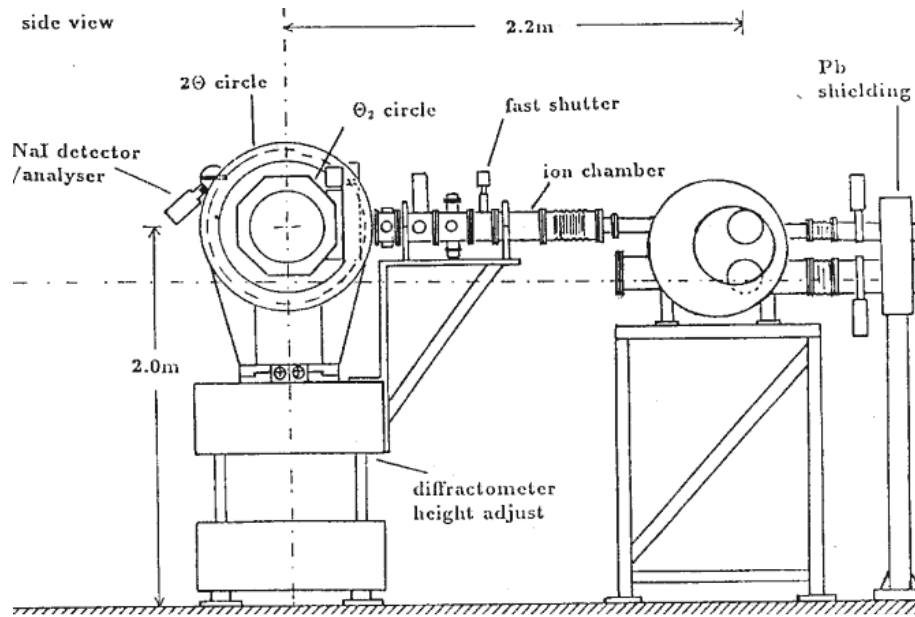


Figure 2.11: Side view of HASYLAB diffractometer
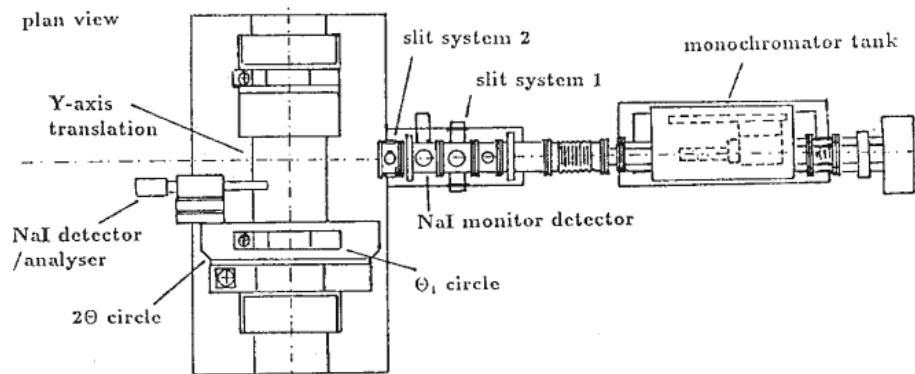


Figure 2.12: Front view of HASYLAB diffractometer

### 2.2.1.4 Structure solution and Rietveld refinement from powder data

Assigning miller indices to the various $2\theta$ values in the powder pattern is the main difficulty of structure solution and called indexing. In general the expression for $d_{hkl}$ inter-planar spacing is defined as:

$$\frac{1}{d_{hkl}^2} = \frac{1}{V^2}[h^2b^2c^2\sin^2\alpha + k^2a^2c^2\sin^2\beta + l^2a^2b^2\sin^2\gamma + 2hkabc^2(\cos\alpha\cos\beta - \cos\gamma)$$
$$+2kla^2bc(\cos\beta\cos\gamma - \cos\alpha) + 2hlab^2c(\cos\alpha\cos\gamma - \cos\beta)] \tag{2.2}$$

Where $V$ is the cell volume and is given by

$$V = abc\sqrt{1 - \cos^2\alpha - \cos^2\beta - \cos^2\gamma + 2\cos\alpha\cos\beta\cos\gamma} \tag{2.3}$$

The above equations are used in Bragg's law 2.1, which relates the diffraction angle to the miller indices. In this work, indexing has been carried out by using Werner's algorithm of the WinXPOW program supplied by STOE. Sometimes indexing is troublesome due to peak overlapping. However, if a structure model exists, the problem of overlapping of reflections can be circumvented by a method developed by Rietveld [27,28]. Despite of the structure model, following two things are required for refinement from powder data:

- Well recorded high quality data which mainly depends on purity and crystallinity of the sample, small background and a good quality diffractometer

- a profile function, which should have the same FWHM as the recorded diffractogram.

In a Rietveld refinement, not only the integrated intensities, but all the single data points of the measurement are used in the calculations. The refinement is based on the variation of profile parameters, background coefficients and structure parameters with the least squares method until the calculated profile matches with the observed powder pattern as exact as possible. GSAS+EXPGUI [29,30] was used for Rietveld refinement of X-ray data. The actual refinement begins with the adjustment of background, which is started with three background parameters and a scale factor. These can be fitted stepwise by changing the background parameters and viewing the difference between the experimental and calculated peaks. After adjustment of the background, the lattice parameters and the zero point are refined. Convergence is checked by $R$ values and simultaneously by the difference plot between calculated and experimental data. Profile parameters describe the reflection widths. Once the calculated profile and background are matched with the experimental one, then atomic co-ordinates can be refined (heavy atoms are given first preference). If the

refinement is stable, then the thermal parameters for heavy atoms can be refined. For all these steps, the following equations are used in the program.

The calculated intensity is derived as

$$Y_{ic} = Y_{ib} + \sum_{k=k1}^{k2} G_{ik}I_k \qquad (2.4)$$

where:

$Y_{ib}$ = intensity of background

$G_{ik}$ = profile function

$I_k$ = Bragg intensity

$k1 \ldots k2$ = intensities of the reflections at $i$th points

The refinement by GSAS is done using the method of least squares technique by a program GENLES. The minimization function consists of several components

$$M = \sum M_p \qquad (2.5)$$

where $M_p$ is the contribution to the minimization function for the powder diffraction data and is

$$M_p = \sum_j w_j \left| I_{j(o)} - I_{j(c)} \right|^2 \qquad (2.6)$$

where:

$I_{j(o)}$ = observed intensity at the $j$th step in the data

$I_{j(c)}$ = calculated intensity at the $j$th step in the data

$w_j$ = weight of the intensities at $j$th step in the data

The intensity at each step $j$ is determined by summing the contributions from the background and all Bragg reflections. The background intensity is affected by fluorescence of the samples, detector noise, axial divergence of the X-ray at air, etc. It is essential to accomplish a specification of the background. Therefore, the correction of the background is included in the refinement by using various functions (*e.g.* Chebyschev polynomial of the first kind, cosine Fourier series with a leading constant term etc).

The quality of least squares refinement is indicated by some residual functions. These residual functions are conventional $R$-factor ($R_{exp}$) and the weighted $R$-value ($R_{wp}$) and are defined as

$$R_{exp} = \sum \frac{\left| I_{j(o)} - I_{j(c)} \right|}{I_{j(o)}} \qquad (2.7)$$

$$R_{wp} = \sqrt{\frac{M_p}{\sum w * I_{i(o)}^2}} \qquad (2.8)$$

In general, the lower the R-values, the more likely is the structure to be correct. The "Goodness of fit" or reduced $\chi^2$ is defined by the minimization function as

$$\chi^2 = \frac{M_p}{N_{obs} - N_{var}} \qquad (2.9)$$

where:

$N_{obs}$ = number of reflections

$N_{var}$ = number of parameters

For ideal case, $\chi^2 = 1$.


A statistical measure of the serial correlation in the powder pattern differences as given by Durbin and Watson [31] is calculated from

$$D_{wd} = \frac{\sum\limits_{i=2}^{N} (\Delta_i/\sigma_i - \Delta_{i-1}/\sigma_{i-1})^2}{\sum\limits_{i=1}^{N} (\Delta_i/\sigma_i)^2} \qquad (2.10)$$

where:

$\delta = I_o - I_c$

$\sigma$ = variance of the peak


In an ideal case (where no serial correlation is present), the value of $D_{wd}$ is close to 2.

## 2.2.1.5 X-ray diffraction on single crystals

Once a suitable single crystal is available, then the structure solution of a substance is possible by the classical X-ray diffraction techniques. During the measurement, intensity assigned to every point in the reciprocal lattice (or to every reflecting plane in real space) is observed. Diffraction arises when points of the reciprocal lattice intersect the Ewald sphere. For the measurement of single crystals, a Bruker SMART APEX single crystal diffractometer (CCD detector) with nitrogen cooling was used (fig. 2.13 [32]). This is based on a three axes goniometer with fixed $\chi$ angle. The three axes ($\omega$, $\phi$ and $2\theta$) are freely movable and cut the $\chi$ axis in one point as shown in figure 2.14 [32]. The crystal is mounted on this point i.e. on a goniometer head. A fine focusing tube with Mo anode ($\lambda = 0.71073$ Å) is used as a X-ray radiation source. The radiation was monochromatized by using a graphite monochromator.
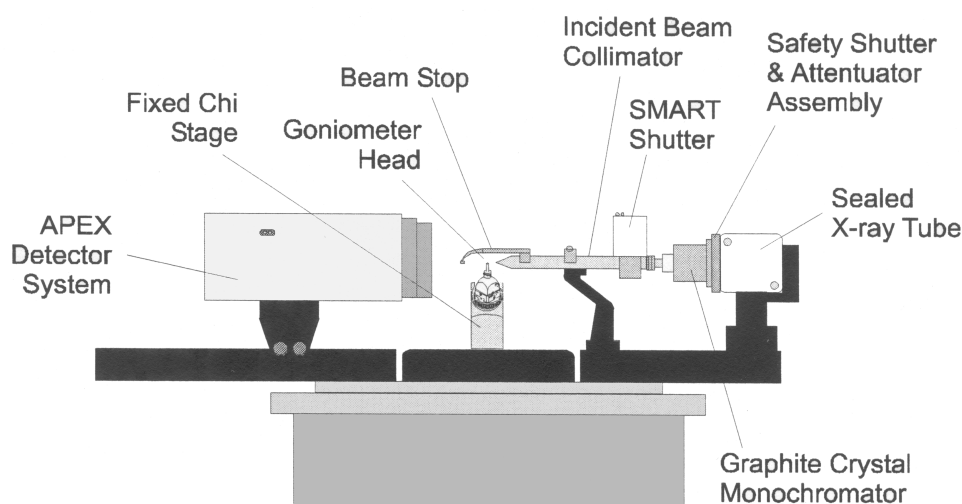


Figure 2.13: Bruker SMART APEX single crystal diffractometer [32]

## 2.2.1.6 Structure solution and refinement from single crystal diffraction

In X-ray diffraction, intensities are measured which depend on the periodic arrangement of atoms in a crystal. Different atoms produce intensities with different magnitude. The most important quantity derived from the intensities is the structure factor $f_{hkl}$, which is related to experimental observed intensities I as,
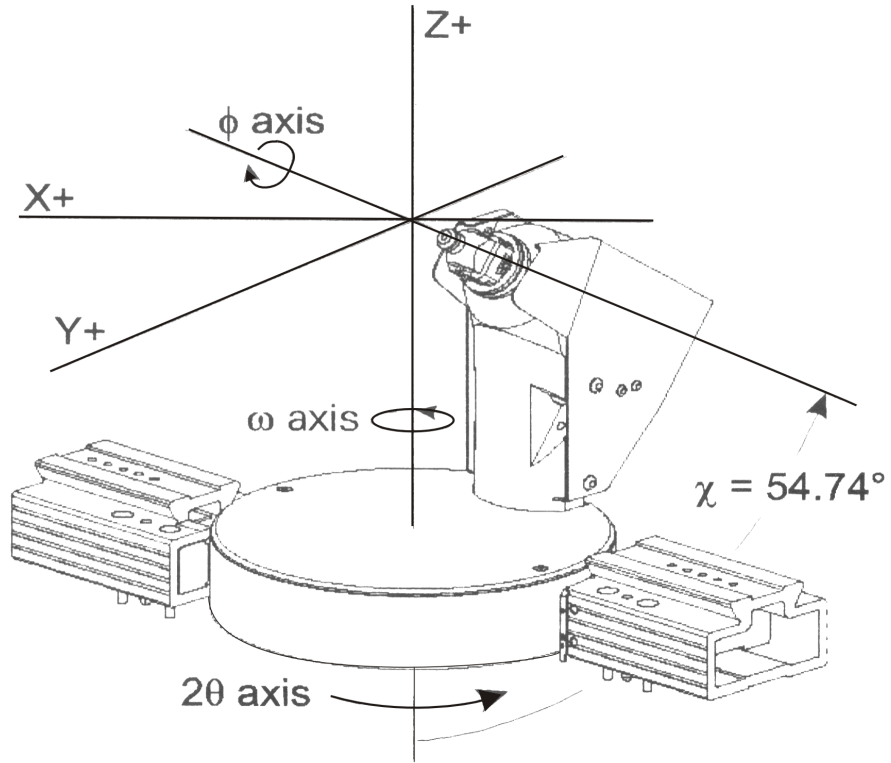
Figure 2.14: Goniometer head geometry of the single crystal diffractometer [32]

$$I \propto |f(hkl)|^2 \tag{2.11}$$

The structure factor for a system with many atoms, each with its own form factor $f_j$ and being located within the unit cell is expressed as

$$f_{hkl} = \sum_{j=1}^{N} f_j e^{[-2\pi i(hx+ky+lz)]} \tag{2.12}$$

Since the atomic form factor is a reflection of electron density, it can be written 2.13 as

$$f_{hkl} = \sum_{j=1}^{N} \rho(xyz) e^{[-2\pi i(hx+ky+lz)]} \tag{2.13}$$

The electron density $\rho(xyz)$ can be obtained through Fourier transformation of F(hkl)

24

$$\rho(xyz) = \frac{1}{V} \sum_{h,k,l} f_{hkl} e^{[-2\pi i(hx+ky+lz)]} \qquad (2.14)$$

where:

$\rho(xyz)$ = electron density at point (xyz) in the unit cell

$V$ = volume of the unit cell

The summation must be carried out on a grid of x, y, and z points as fine as possible to obtain a smooth electron density distribution in the unit cell. Where the electron density is concentrated, atoms are found. The analysis of the obtained single crystal data involve skillful extraction of the information contained within the observed intensities. The process of converting electronic measurements into usable diffraction data is called data reduction. In the data reduction different reflection-dependent parameters are taken into account by multiplying the relative intensities by suitable correction factors. These are Lorentz, polarisation and absorption corrections respectively. The polarisation correction is frequently grouped with the Lorentz correction in a single factor, the LP correction which is expressed as

$$LP = \frac{1 + \cos^2 2\theta}{2 \sin 2\theta} \qquad (2.15)$$

According to Beer's law 2.16, absorption reduces the intensity of X-ray beam travelling through a given material by an amount which depends on material and the length of the path travelled by the radiation in it. Absorption correction becomes important for crystals containing heavy elements, especially when they have plate or needle shape and can be derived as

$$I = I_0 \exp(-\mu x) \qquad (2.16)$$

where:

$\mu$ = linear absorption coefficient

$x$ = total path length

$I$ = incident X-ray intensity

$I_0$ = diffracted X-ray intensity

In this work, the integration of data was done with a computer program SAINT [33] and a numerical absorption correction was carried out with SADABS [34], whereby symmetry equivalent reflections and Friedel pairs were merged. How well the data merge together is given by the term $R_{int}$. Systematic extinctions were determined with XPREP, a part of SHELXTL package, which suggests the possible space group.

Since the experimental measurements give only the intensities, the phase information in the structure factors is lost, and only their amplitudes are known. So the solution of a structure is, in fact, solution of the phase problem. Two methods are used to solve this problem $e.g.$ the Patterson method and Direct methods. Here, for structure solution Direct methods were used. Two essential features of the crystal structure led to the development of a mathematical relation among the structure factor phases, knowing the values of the amplitudes. Two essential features are:

- The electron density of the correct model must be $\geq 0$ throughout unique volume of the unit cell (positive electron density condition given by Karle and Hauptman).

- The structure is composed of discrete atoms (discrete atom condition given by Sayre).

In this method, a few strong $I_{hkl}$ are chosen and their phases are assigned at random. Then the relationships between the phases are sought for, and the phases are constantly modified until a consistent set is obtained. This allows initial $F_c$ to be obtained. The structure was solved with the help of the SHELX-97 [35] program. This structure model is then used for refinement by the principles of least squares using the SHELXL-97 [36] program to find out new atoms from the electron density maps. Difference maps are calculated using coefficients of $(|F_o| - |F_c|)$ with the calculated phase angle. These maps tend to produce peaks where an insufficient amount of electron density has been included in the model (e.g. missing atom) and produce negative holes where too much electron density has been included in the model (e.g. too heavy of an atom for the site).

To judge how well the model fits the observed data residual or "$R$"-factors are calculated. The $R$-factors are:

$$R = \frac{\sum\limits_{hkl} ||F_o| - |F_c||}{\sum\limits_{hkl} |F_o|} \qquad (2.17)$$

$$wR_2 = \sqrt{\frac{\sum\limits_{hkl}[w(F_o^2 - F_c^2)^2]}{\sum\limits_{hkl}[w(F_o^2)^2]}} \qquad (2.18)$$

$$w = \frac{k}{\sigma^2(F_o) + g.F_o^2} \qquad (2.19)$$

where:

$R$ = conventional $R$-factor

$wR_2$ = weighted $R$-factor

$w$ = weight factor

$\sigma(F_o)$ = standard deviation from $F_o$

$\sigma^2 F_o$ = variance

Another statistic that is used to check the quality of the refinement is the "goodness of fit", S. It is strongly influenced by the weighting scheme. For a refinement on $F^2$ the goodness of fit has the form:

$$S = \frac{\sum\limits_{hkl}|w(F_o^2 - F_c^2)|}{n - p} \qquad (2.20)$$

where:

S = goodness of fit

$w$ = weight factor

$n$ = number of measured data

$p$ = number of parameter

Ideally, this value should be near 1.

The complete crystal structure must fulfill the following criteria like: chemically reasonable bond lengths and angles, low standard deviations of atomic coordinates, no peaks with strong intensities in the difference map and no atoms should have non-positive definite displacement parameters.

### 2.2.1.7 Symmetry analysis

Generally, to describe a crystal structure, one compares molecules or groups of atoms within the structure with geometrical bodies. Sometimes, atoms order themselves in these geometrical bodies in such a way that they resemble to a polyhedron. The real polyhedron and its ideal equivalent can be compared by analysing their symmetry. It is desired to know, how large the degree of distortion of a polyhedron is. In order to compare molecular structures with building units in the structure of solids, the *SYMMOL* [37] program based on a continuous symmetry measure (CSM) [38] method was used. This program helps to find out the maximum point group of the polyhedron. It gives some quantities like: the r.m.s. on the coordinates, the molecular r.m.s., the maximum deviation of the coordinates of the atom from the symmetrized ones and the continuous symmetry measure (CSM) for the whole point group and for the single elements of the point group. To compare the ideality of the polyhedra, r.m.s. values of different polyhedra are checked. The lower the r.m.s. value, the closer is the polyhedron to an ideal one. The r.m.s. value for the coordinate j of the atom i is given as:

$$r.m.s. = \sqrt{\left(\frac{1}{N_g}\right)\left[\sum_{k=1}^{N_g}\left(P_i - d_i^k\right)_j^2\right]} \tag{2.21}$$

The continuous symmetry measure is calculated as

$$S(M) = \left(\frac{100}{NN_g}\right)\left(\sum_{i=1}^{N}\sum_{k=1}^{N_g}\left\|d_i^k - P_i^l\right\|^2\right) \tag{2.22}$$

where:

$$P_i = \left(\frac{1}{N_g}\right)\left(\sum_{k=1}^{N_g} d_i^k\right) \tag{2.23}$$

$N_g$ = ordering of group of atoms
$N$ = number of atoms with the same *mol*, where *mol* is an index assigned to any atoms defining the group (the molecule) to be symmetrized
$d_i$ = inertia coordinates of the atoms

## 2.2.2 Impedance Spectroscopy

The electrical properties of materials depend on the presence of current carriers such as free electrons or ions. Depending on the current carriers materials can be divided into electronic conductors or ionic conductors. According to the values of electrical conductivities, materials can be classified as shown in figure 2.15 [39].
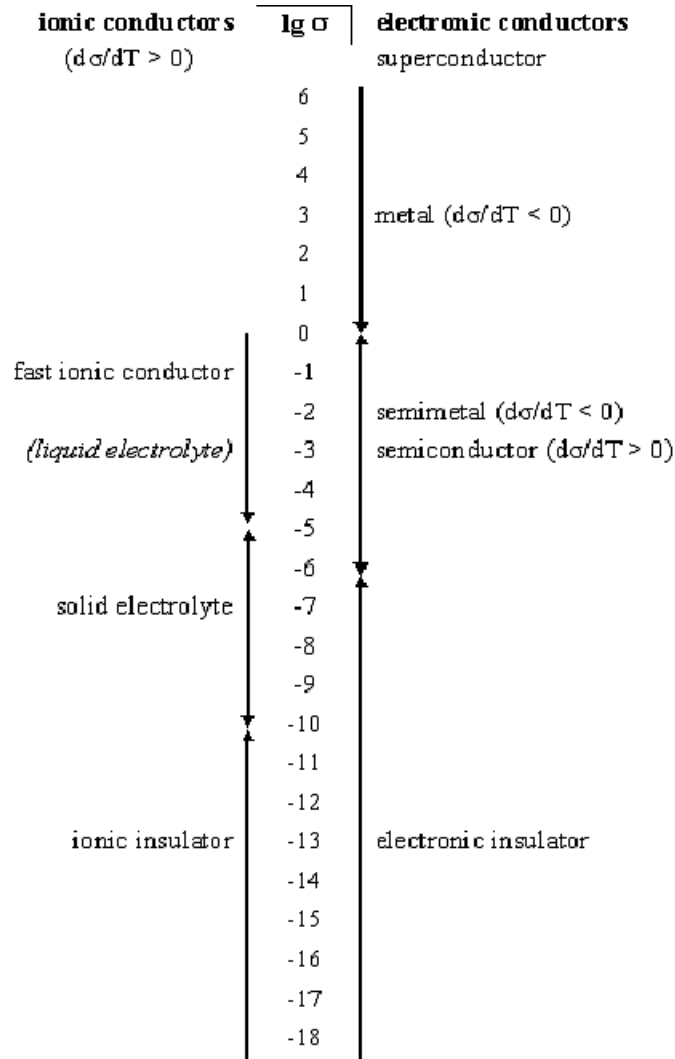


Figure 2.15: Classification of materials based on electrical conductivity [39]

Electrical conductivity usually depends on temperature. For all materials except metals and superconductors, it increases with temperature. One of the techniques to measure electrical conductivities of materials is impedance spectroscopy (IS). In impedance spectroscopy, an impedance analyzer measures the current response and phase angle of a sample when an AC voltage is applied over a range of frequencies [40,

29

41].

### 2.2.2.1 Principle

In IS, the measured current response of the sample to the applied alternating voltage contains both phase and amplitude components. For DC measurements, Ohm's law gives the relationship between the voltage (V), current (I) and resistance (R) which is given by:

$$R = \frac{V}{I} \tag{2.24}$$

But in AC-IS, when both the applied voltage and resulting current have the additional time-dependency, Ohm's law is rewritten as:

$$Z(\omega) = \frac{V(t)}{I(t)} = \frac{V_0 \cos(\omega t)}{I_0 \cos(\omega t - \theta)} = Z_0 \frac{\cos(\omega t)}{\cos(\omega t - \theta)} \tag{2.25}$$

where:
$Z(\omega)$ = impedance of the system
$V(t)$ = applied voltage at time $t$
$I(t)$ = resulting current at time $t$
$V_0$ = amplitude of the voltage signal
$I_0$ = amplitude of the current signal
$\omega$ = frequency in radians per second = $2\pi f$
$t$ = time in seconds
$\theta$ = phase shift in radians
$|Z(\omega)|$ = magnitude of impedance = $\frac{V_0}{I_0}$

Figure 2.16 shows the applied voltage and measured current with a phase difference of $(\theta)$.

The impedance data are plotted on a complex plane, where the impedance is expressed as a complex number $Z = a + jb$ with $j \equiv \sqrt{-1}$. The value of real part of $Z$ is $a$ and often written as $Re(Z)$ or $Z'$ while $b$ is the imaginary part of $Z$, written as $Im(Z)$ or $Z''$.

In polar form, $Z$ can be written as:
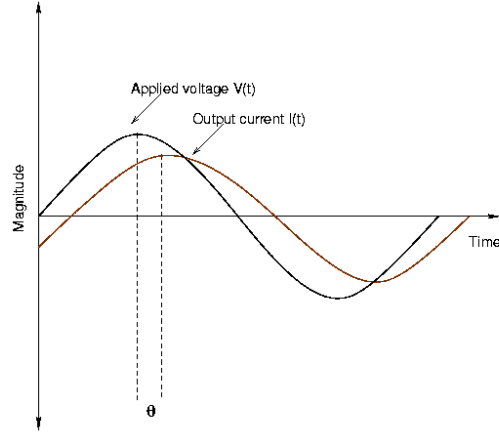
Figure 2.16: Scheme of how AC-impedance spectroscopy measures the current response of a sample when a voltage is applied. The phase difference $\theta$ is shown

$$Z(\omega) = Z_0 exp(j\theta) \tag{2.26}$$

It can be converted to rectangular form by using Euler's relationship $(\exp(j\theta) = cos\theta + jsin\theta)$ as:

$$Z(\omega) = Z_0(cos\theta + jsin\theta) = Z' + jZ'' \tag{2.27}$$

Therefore, the impedance measured at each specific frequency is plotted as a single point on a complex plane. Figure 2.17 shows the complex plane representation of $Z(\omega)$. The real and imaginary part of $Z(\omega)$ are expressed by the following [42]:

$$
\begin{aligned}
Z' &= |Z|\cos\theta \\
Z'' &= |Z|\sin\theta
\end{aligned}
\tag{2.28}
$$

where $\theta$ is the phase angle difference and is given by:

$$\theta = \tan^{-1}\left(\frac{Z''}{Z'}\right) \tag{2.29}$$

and the magnitude or modulus of $Z(\omega)$ is:

$$|Z| = \sqrt{(Z')^2 + (Z'')^2} \qquad\qquad (2.30)$$
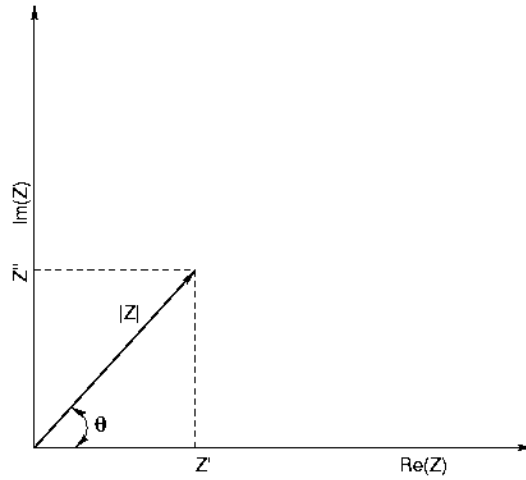


Figure 2.17: Impedance, Z, plotted on a complex plane in both Cartesian and polar
coordinates

Most materials under electrical investigation are heterogeneous systems in terms
of their electrical response, containing several components. At a minimum, the
systems consist of the response of the electrode and the bulk material. Most material
phenomena (i.e.electrode, interfaces, bulk behavior, etc.) contain both resistive
and capacitive elements, where the two contributions typically behave in parallel.
Figure 2.18 shows a typical measured data for a resistor and capacitor connected
in parallel. This is plotted on a so-called Nyquist plot (real impedance (resistive)
vs. negative imaginary (capacitive) impedance). It is common practice to plot the
negative of the imaginary impedance in the Nyquist plot representation because
most material phenomena of interest contain capacitive elements, which cause the
data to fall into the fourth quadrant of a complex plane.

A Nyquist plot provides a convenient way to view the data in the first quadrant.
As shown in figure 2.18, the resistor and capacitor in parallel produce data in the
form of a semicircular arc in the complex plane. Each point along the arc represents a
single data point taken at a different frequency, where frequency increases from right
to left (marked by an arrow). The intersection of the arc with the real impedance
axis, at lower frequencies or to the right of the Nyquist plot, indicates no contribution
from the imaginary impedance. Therefore, the intersection corresponds to the real
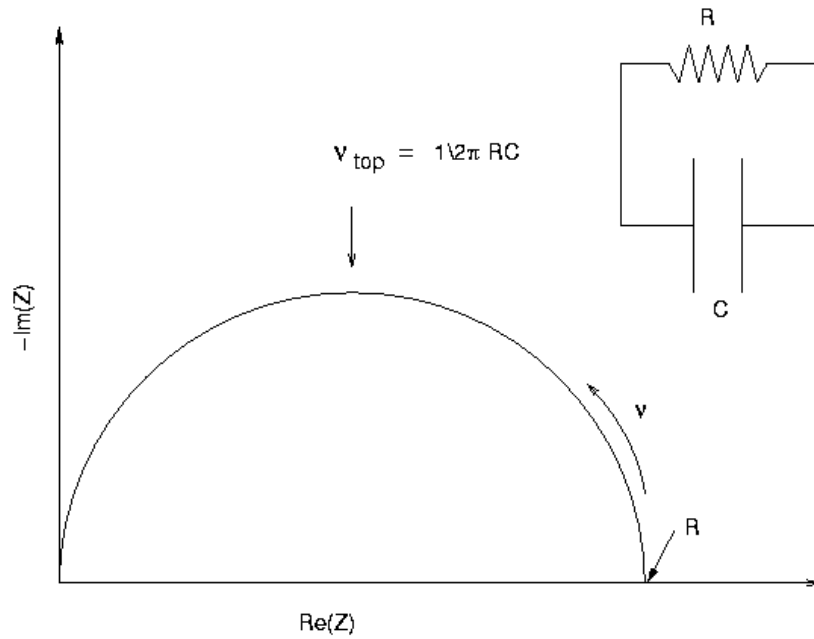
Figure 2.18: Impedance spectrum (shown as Nyquist plot) for a perfect resistor and capacitor in parallel

value i.e. resistor in the circuit element. The frequency at the top of the arc, as indicated, is given by the following relationship:

$$\nu_{top} = \frac{1}{2\pi RC} \tag{2.31}$$

The product RC is known as "time constant" and is a material parameter associated with a particular phenomenon. Resistance ($R$) is related to the resistivity ($\rho$) by the following relationship: $R = \rho l/A$, where $l$ is the length and $A$ is the cross-sectional area. Capacitance ($C$) is related to the permittivity of the medium ($\epsilon'$) by the following relationship:

$$C = \epsilon' e_0 \frac{A}{l} \tag{2.32}$$

where:

$e_0$ = permittivity of free space ($8.85 \times 10^{-12} Fm^{-1}$).

33

But, for different ionically conducting samples different spectra are observed which depend upon sample quality, measurement conditions etc. Mostly, it is required to have an appropriate working model for these spectra [43]. Ideally, a polycrystalline pellet, which lies between two ion-blocked platinum electrodes, can give rise to a spectrum similar to that shown in figure 2.19.
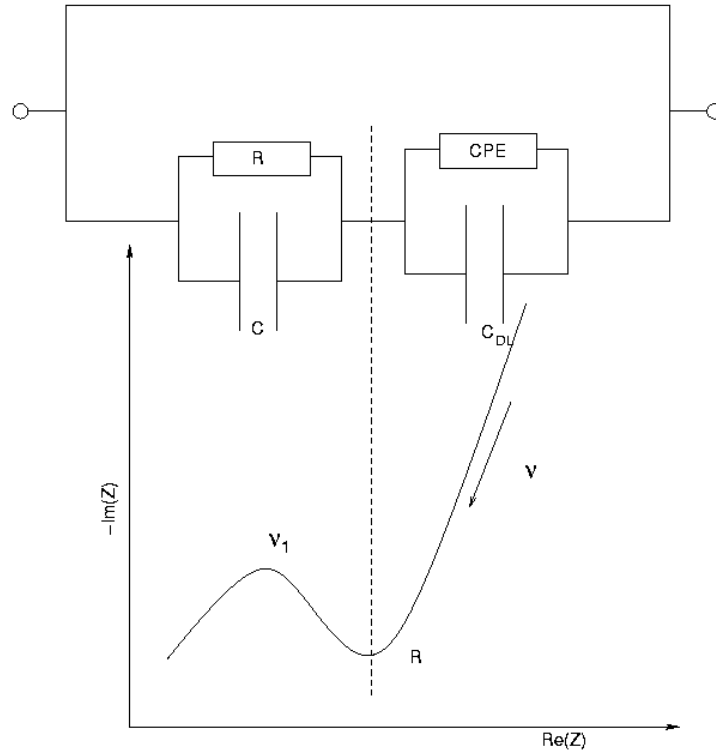


Figure 2.19: Impedance spectrum and the equivalent circuit diagram for a polycrystalline pellet lying between two ion blocked Pt electrodes

If the IS measurements are taken at a series of temperatures then an Arrhenius plot can be made from Arrhenius equation 2.33. From this plot it is possible to determine the activation energy. It is also possible to assess how different mechanisms interact and at what temperature different mechanisms become favourable.

$$\sigma = \frac{A}{T} e^{-\frac{E_a}{kT}} \qquad (2.33)$$

where:

$\sigma$ = ionic conductance

$A$ = pre-exponential factor
$T$ = temperature
$E_a$ = activation energy
$k$ = Boltzmann constant

### 2.2.2.2 Working Set Up

The IS measurements by the two-probe method were performed in the Max-Planck-Institute for Solid State Research, Stuttgart. The two-probe temperature dependent IS measurements were carried out with a HP 4192A LF (Hewlett-Packard) impedance analyser, which is capable of measuring the impedance in the frequency range of 5 Hz to 13 MHz by employing ion-blocking platinum electrodes. The dc conductivity was detected simultaneously. The measurement cell was made up of quartz glass and was connected to an inert gas line. The cell was heated using an electric oven. The temperature of the oven was controlled with a NiCr-Ni thermocouple. Data acquisition and analysis were carried out by using a computer code written by Prof. Dr. Martin Jansen's group.

In the two-probe method, resistance between contacts and sample can influence the result of the experiment. This problem can be overcome by a four-probe method [44,45].

A schematic diagram for a ac four-probe method is shown in figure 2.20. Current flows through contacts 1 and 4 and the voltage is measured between contacts 2 and 3. The resistance of the current contacts is irrelevant, because the measured current flows through the sample. The resistance of voltage contacts lie in series with the inner resistance of the voltmeter and in together lie parallel with sample resistance. As the inner resistance of the voltmeter is very high, the contact resistances can be neglected. Hence, contact resistances do not influence the result of measurement in a four-probe method.

The resistivity of spherical sample geometry, used in this measurement can be calculated as:

$$\rho = R \cdot h \cdot d/a \qquad (2.34)$$

where:
$R$ = resistance of the sample

$h$ = height of the sample
$d$ = diameter of the sample
$a$ = distance between contacts
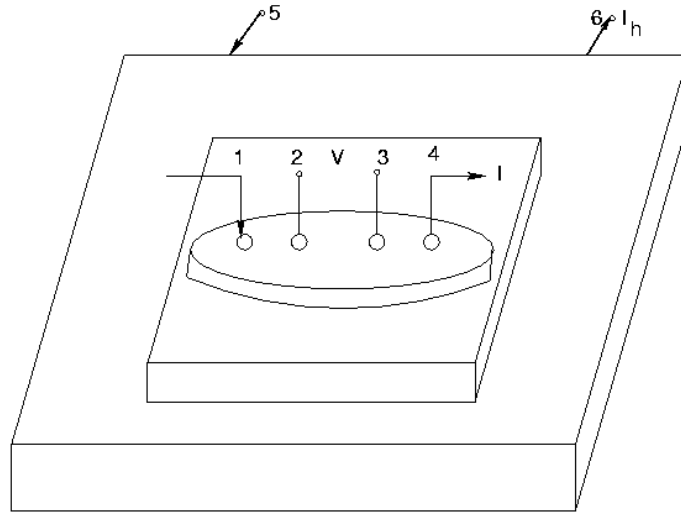
Figure 2.20: Schematic representation of linear ac four-probe method

IS measurements with the four-probe method were performed with an Alpha A (Novocontrol GmbH) Impedance analyser, which is capable of measuring impedance in the frequency range of $3\mu$Hz to 10 MHz by employing a platinum electrode. Samples were heated with direct current (Laboratory power supply EA-PS 9065-05 from EA-ELEKTRO-AUTOMATIK) flowing through a heating element (Bach Resistor Ceramics GmbH) (contacts 5 and 6) separated from the pellet with an insulator (Corundum plate). The temperature was measured with a NiCr-Ni thermocouple connected with an Eurotherm controller 2408. The measurement system shown in figure 2.21 was closed in a stainless steel housing together with the thermocouple. The cell was connected to an inert gas line in order to carry out the measurements under vacuum or argon. Data acquisition and analysis were performed by using a computer program WinDeta (Novocontrol GmbH).

## 2.2.3 Electron energy loss spectroscopy (EELS)

Electron energy loss spectroscopy is a qualitative and quantitative elemental analysis technique. In electron energy loss spectroscopy (EELS), one measures the loss

36

<center>(a)</center>



<center>(b)</center>
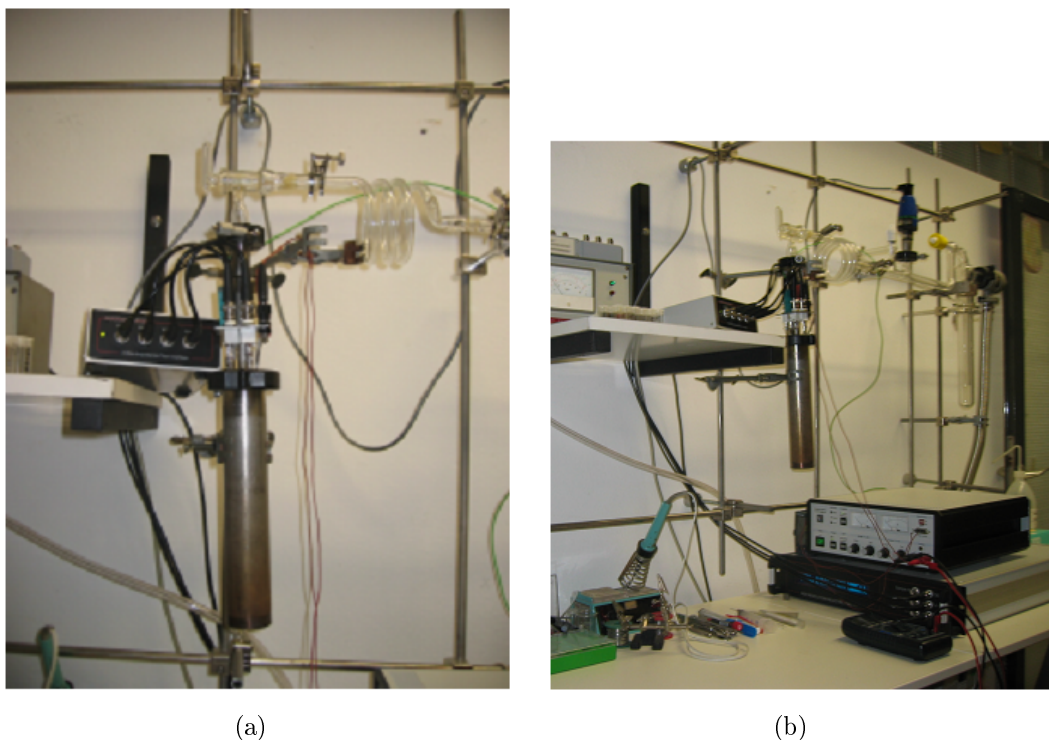
Figure 2.21: Impedance measurement cell connected to impedance analyser and to inert gas line

in energy of incident electrons. Incident electrons lose energy by inelastic scattering, which is primarily an interaction of an electron beam with an electron in the sample [46, 47].

EELS is useful particularly for light elements such as boron, carbon, oxygen and nitrogen, as the detection is reliable and exact. In addition, this method is useful to study the coordination sphere and the electronic situation of the particular atom. An electron energy loss spectrum is a plot of distribution of electrons (intensity) against the energy loss. It consists of three parts [48]:

- **Zero loss peak (0-5 eV)**: It occurs when the transmitted electrons have the original beam energy $E_0$ i.e. either electrons have only interacted elastically or not at all with the specimen. These beams are usually of high intensity, which can cause damage of the detector. Since there is no useful information in it, often it is omitted during spectrum collection.

- **Low-loss region (5-50 eV)**: In this range, the electrons have induced plasmon oscillations. Since the plasmon generation is the most frequent inelastic

<center>37</center>

interaction of electrons with the sample, the intensity in this region is relatively high. The intensity and number of plasmon peaks increase with specimen thickness.

- **High-loss region ($>$50 eV)**: In this region, the spectrum indicates the onset of excitations from the various inner atomic-shells (core) to the conduction band. This inner-shell excitation can take the form of edges, where the inner-shell intensity rises rapidly and then falls slowly with increasing energy loss. These edges correspond approximately to the energy that is required to ionise an atom. Since each element has unique inner-shell binding energies, it is possible to study a particular element (atom) in an environment of many elements (atoms) using these characteristic edges. The characteristic K shell ionization edges for boron, carbon, nitrogen and oxygen atoms appear at $\approx$ 188 eV (B), $\approx$ 284 eV (C), $\approx$ 401 eV N and $\approx$ 532 eV (O) respectively.

The ionization edge in the energy-loss spectrum shows a characteristic *fine structure*, in the form of intensity oscillations or local peaks. This can be divided into two regions:

- Energy loss near edge structure (ELNES), in the form of pronounced peaks just above an ionization-edge threshold. It is related to chemical bonding or electronic band structure (density of states). It can be used for coordination "fingerprinting", and used to to solve phase problem in complex systems [49].

- Extended energy loss fine structure (EXELFS), a weaker intensity modulation starting at 50 eV or more from the ionization edge, can be analyzed to give the distance of nearest-neighbour atoms.

EEL spectra were measured in a transmission electron microscope CM30ST (Philips) with a $LaB_6$ cathode equipped with an EEL spectrometer PEELS 666 (Gatan, software: EL/P) at the Justus-Liebig-Universität, Giessen. Samples were placed on a lacey carbon coated copper TEM grid and measured.

## 2.2.4 Infrared spectroscopy (IR)

IR spectroscopy [50] is an analytical method based on absorption of infrared radiation by the molecule. This technique is used for identifying functional groups in a molecule. The molecule absorbs the radiation, when the frequency of the specific

vibration is equal to the frequency of the IR radiation. The energy of an infrared photon can be expressed as wavenumber by the following equation:

$$E = h\nu = h\frac{c}{\lambda} = hc\widetilde{\nu} \qquad (2.35)$$

where:

$h$ = Planck's constant = $(6.626 * 10^{-34} \text{m}^2\text{kgs}^{-1})$

$c$ = Velocity of light = $3 * 10^8 \text{m s}^{-1}$

$\widetilde{\nu}$ = wavenumber in $\text{cm}^{-1}$

A polyatomic molecule of $n$ atoms has $3n$ total degrees of freedom. However, the number of fundamental vibrations for non linear molecules is $3n - 6$ (while 3 degrees of freedom are required to describe translation and 3 are required to describe rotation) and for a linear molecule it is $3n - 5$ (while only 2 degrees of freedom are required to describe rotation). Among these fundamental vibrations, those who produce a net change in dipole moment are IR active. The major type of molecular vibrations are stretching (asymmetrical or symmetrical) and bending (scissoring, wagging, twisting and rocking). Absorption in this region by a typical molecule results in the excitation of vibrational, rotational and bending modes, while the molecule itself remains in its electronic ground state. The exact frequency at which a given vibration occurs is determined by the strengths of the bonds involved. The mass of the component atoms ($m_1$, $m_2$) is described by using the following equation:

$$\widetilde{\nu} = \frac{1}{2\pi}\sqrt{\frac{k}{\mu}} \qquad (2.36)$$

where:

$\mu$ = reduced mass = $\frac{m_1 m_2}{m_1 + m_2}$

$k$ = force constant

IR absorption information is generally presented in the form of a spectrum with the wavenumber as $x$-axis and percent transmittance as the $y$-axis. The measurements were carried out in the range of 4000 - 400 cm $^{-1}$. The obtained IR bands can be correlated to the bonds of the studied compound.

In the experiments, powders were examined by mixing with Nujol, or by grinding with dried KBr. The latter is then pressed to form circular discs with a diameter of about 10 mm and a thickness of about 1-2 mm under a pressure of 10 tons. The measurement was carried out using a FT-IR 1720 (Perkin-Elmer) spectrometer.

## 2.2.5 Nuclear magnetic resonance spectroscopy (NMR)

The principle of NMR [51] is that nuclei have a spin and all nuclei are electrically charged. A spinning charge generates a magnetic field. The resulting spin-magnet has a magnetic moment ($\mu$) proportional to the spin. In the presence of a magnetic field ($H_0$), the magnetic moment ($\mu$) of an atomic nucleus (whose spin quantum number I $\neq$ 0) spins around the axis of $H_0$ with magnetic moments aligned parallel (low energy state) or antiparallel (high energy state) to the magnetic field. The difference in energy between the spin states is dependent on the external magnetic field strength. The frequency of spinning of the magnetic moments is in the RF range of the electromagnetic spectrum. In practice this can be achieved by passing an alternating current through a coil mounted perpendicular to $H_0$.

$$\Delta E = h\nu = \frac{\mu_I H_0}{I} \tag{2.37}$$

where:
$h$ = Planck's constant ($6.626 * 10^{-34}\text{m}^2\text{kgs}^{-1}$)
$\nu$ = NMR frequency
$\mu_I$ = magnetic moment of the nucleus in the field
$H_0$ = applied magnetic field
$I$ = nuclear spin quantum number

When a nucleus is located in an applied magnetic field, it is shielded by the secondary field set up by the electrons surrounding the nucleus. Thus the effective magnetic field $H_{eff}$, experienced at the nucleus is generally less than the applied field. This can be expressed as:

$$H_{eff} = H_0(1 - \sigma) \tag{2.38}$$

where:

$\sigma$ = shielding constant for the nucleus

The electron density around each nucleus in a molecule varies according to the type of nuclei and bonds in the molecule. The opposing field and therefore the effective field at each nucleus will vary. This is called chemical shift phenomenon. The quantity is reported in parts per million (ppm) and a given the symbol ($\delta$). The chemical-shift parameter $\delta_i$ for the $i$th environment is defined as:

$$\delta_i = \frac{H_i - H_r}{H_r} \times 10^6 = \frac{\nu_i - \nu_r}{\nu_0} \times 10^6 \tag{2.39}$$

where:
$H_i$ = characteristic resonance fields for the $i$th
$H_r$ = characteristic resonance fields for the reference
$\nu_i$ = resonance frequency for the $i$th
$\nu_r$ = resonance frequency of the reference
$\nu_0$ = fixed instrument frequency

Another decisive factor for the application of NMR spectroscopy is the spin-spin coupling. Nuclei experiencing the same chemical environment or chemical shift are called *equivalent*. Those nuclei experiencing different environment or having different chemical shifts are *nonequivalent*. Nuclei which are close to one another exert an influence on each other's effective magnetic field. This effect shows up in the NMR spectrum when the nuclei are nonequivalent. If the distance between nonequivalent nuclei is less than or equal to three bond lengths, this effect is observable and is called spin-spin coupling or $J$ coupling.

In this work, the $^{11}$B nuclei were used, which have a spin $I = 3/2$. The coupled $^{11}$B spectra was obtained using a Bruker Avance 400 spectrometer.

# 3 Alkali metal borides

## 3.1 Introduction

The existence of alkali metal borides was anticipated since the beginning of the nineteenth century, when the effort was made to obtain elemental boron by reduction of boron compounds (boron oxide, boron fluoride and fluoroborates) by alkali metals (Gay-Lussac and Thenard 1808, Davy 1811, Wöhler and Sainte-Claire Deville 1858, Rawson 1888) [52]. In 1892, Moissan hypothesized the existence of an alkali metal boride which was then confirmed by Kroll (1918) and by Kahlenberg (1925). After fourty years, from 1963 to 1977 Naslain and Hagenmüller were able to synthesize $KB_6$ [53, 54] and two binary sodium borides $NaB_6$, $NaB_{15}$ [17–19] and also noted the existence of lithium borides. However, later reinvestigations of the crystal structures using X-ray and neutron diffractometry, $^{23}$Na MAS-NMR spectroscopy and electron microscopy proposed the composition to be $Na_2B_{29}$ [20] instead of $NaB_{15}$ and $Na_3B_{20}$ [21, 22, 55] instead of $NaB_6$.

In the lithium-boron system, several chemical compositions were proposed for composites, alloys and compounds. However, many questions about the existence of those compounds and their crystal structures remained unexplained and the phase diagram is not known till now. In 1966, Lipp reported the first lithium boride with stoichiometry $LiB_4$ [9]. In 1967, Secrist reported $LiB_{10.85\pm0.35}$ [7]. The indexing of the diffraction pattern of this compound was reported in the tetragonal crystal system. In 1974 Rupp *et al.* proposed the existence of $LiB_6$ [56]. In 1976, James *et al.* proposed $Li_2B$ [13]. In 1978, Wang *et al.* [12, 57] proposed the preparation of this alloy and suggested the chemical composition to be $Li_5B_4$ from differential thermal analysis which was confirmed from X-ray and neutron diffraction and nuclear magnetic resonance spectroscopy. They were able to predict the crystal structure in the rhombohedral space group $R\bar{3}m$ with $a = 4.93$ Å. The compound with the composition $Li_7B_6$ was synthesized by Dalleck *et al.* [11]. They reported that electrochemical properties like standard potential and gravimetric capacity of these alloys were com-

parable with lithium, but the melting point was considerably higher (1000°C) than pure lithium. Due to this reason Li-B alloys have attracted the interest as an anode material for thermal and high power batteries [58–60].

In 1993, Li-intercalated $\alpha$-rhombohedral boron with the composition $Li_3B_{12}$ was theoretically predicted to be a superconductor [61]. In 1994, $LiB_2$ and $LiB_{10}$ were studied and reported by Serebryakova *et al.* [8] via X-ray photoelectron spectroscopy, X-ray diffraction and chemical analysis. In 1995, Meden *et al.* [14] proposed $LiB_3$ on basis of *ab initio* molecular orbital calculations and supported their results by chemical and X-ray diffraction analysis. The crystal structure was not determined for a single compound except $Li_5B_4$. In 1995, the crystal structure of $LiB_{13}$ was solved in the rhombohedral crystal system via Rietveld analysis by Kobayashi *et al.* [3].

The break-through in the Li-B system was due to the efforts of Nesper *et al.* [4,5] in 1998. They modified the synthesis procedure and for the first time were able to synthesize single crystals of three new phases $Li_3B_{14}$, $Li_{1.8}B_{14}$ and $Li_2B_6$ on the boron-rich side. Apart from this, in 1977, lithium monoboride LiB was predicted by X-ray diffraction and thermographic methods [10]. The crystal structure of this compound was proposed in 2000 by Liu *et al.* [62] as a simple hexagonal structure through X-ray diffraction analysis of a multiphase sample. At the same time, Nesper *et al.* [6] performed X-ray and neutron diffraction analysis of the pure phase $LiB_x$ ($0.82 \leq x \leq 1$) and confirmed the hexagonal structure with chains of boron atoms. Later in 2003, theoretical investigations were carried out by Picket *et al.* [63] to understand stoichiometric lithium monoboride and the mechanism of reaction synthesis was proposed by Zhijan *et al.* [64].

The main difficulties concerning the synthesis of Li-B compounds described in the literature can be summarized as:

1. Extreme difference in the melting point between starting components

2. Reaction of the starting material with crucible material at high temperatures

3. Impurities in the starting material, sensitivity of lithium and products (expected)

4. Inhomogeneous and multiphase synthesized product

Moreover, analyzing these samples by conventional methods and structurally localizing the light element makes it more difficult to establish the right formula.

(a) $(Li_6B_{18})(LiBH_4)$          (b) $Li_2B_9$
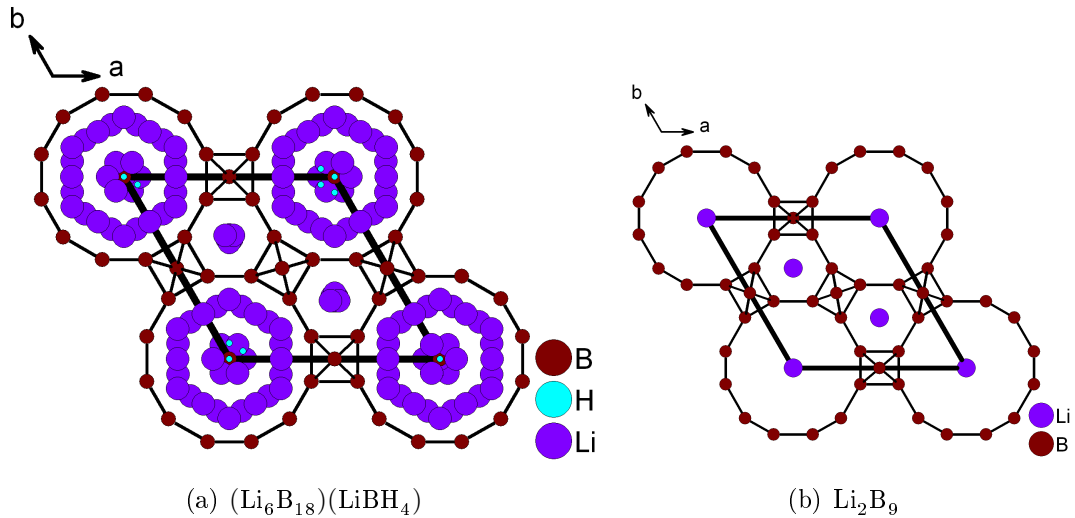
Figure 3.1: Projection of crystal structure of $(Li_6B_{18})(LiBH_4)$ and $Li_2B_9$ along $c$-axis

Due to the above mentioned problems, one compound has been found in the Li-B system that was described with different formulas in two different theses without final conclusions. Based on chemical analysis and X-ray investigations Wörle *et al.* [15] proposed a composition "$Li_6B_{19}$" or "$Li_6B_{18}X$" (X = $BH_3$ or $Li_2O$). The crystal structure was described in the hexagonal crystal system in space group $P6/mmm$ (no. 191). In 1997, Schmitt *et al.* [16] synthesized a similar compound and described the crystal structure in same space group, suggesting the approximate formula "$Li_2B_9$". Both the structural models of the compound are shown in figure 3.1. The structure consists of a three-dimensionally interconnected framework of boron atom octahedra forming two kinds of channels. The larger channel is believed to be filled with either $[BH_4]^-$ unit or $Li_2O$ for "$Li_6B_{18}X$" and with Li for "$Li_2B_9$". The smaller channel was filled with Li in both cases. Moreover, it was mentioned in the introduction of [5], oxygen is essential for stability of this compound.

The crystal structure refinements of these compounds were not satisfactory and the purity of the samples was not ensured. This has stimulated our investigations of this compound. Moreover, the open channel framework of boron suggests a possible lithium ion mobility which might result in ionic conductivity. An exciting application of compounds which exhibit lithium ion mobility is the use as an electrode and solid electrolyte in battery technology [65–68].

## 3.2 Synthesis and characterization of Li$_2$B$_9$

### 3.2.1 Synthesis

The synthesis of Li$_2$B$_9$ was carried out in three different routes.

**Route 1**: Li$_2$B$_9$ was synthesized from elemental lithium and boron. Commercial amorphous boron (1 micron, 99.99 %, Chempur) was heated at 1273 K for 12 to 16 hours under vacuum of $6 \times 10^{-3}$ mbar to separate volatile impurities. About 0.162 g (15 mmol) of boron and 0.041 g (6 mmol) of lithium were filled in an iron tube. The tube was sealed by arc welding under argon. The sealed iron tube was then placed in a sealed evacuated quartz ampoule. The ampoule was placed in an oven and heated up to 1073 K with a rate of 5 K/min, kept at this temperature for 7 days and cooled down slowly to room temperature. The powder obtained was always inhomogeneous and was carefully separated in the glove box according to the colour of the samples *i.e.* gray or brown. The separated products were sealed in glass ampoules under argon for further investigations.

It was observed during the synthesis that the product phase was highly sensitive to the amount of reactants and the temperature. A slight variation in the quantity of the reactants affected the intensities of the reflections in the X-ray diffraction pattern. An excess amount of boron leads to the less crystalline phase. Multiple product phases were obtained when the temperature of the reaction deviated slightly ($\pm$ 10 K) from 1073 K. Due to these difficulties several attempts were made during the syntheses to reproduce the result with precise control of the experimental parameters.

**Route 2**: To obtain a more homogeneous distribution of lithium a different synthesis method (*i.e.* reactants were mixed in liquid ammonia before the heat treatment) was adopted. Boron (0.310 g, 28 mmol) and lithium (0.1 g, 14 mmol) were put in a Schlenk tube and liquid ammonia was distilled over it. It was mixed properly for 1 h by a magnetic stirrer. Then liquid ammonia was evaporated through the mercury valve and the powder was collected in an iron tube. The iron tube was sealed by arc-welding under argon. The tube was then sealed into a quartz ampoule under vacuum. The ampoule was placed in an oven and heated up to 1073 K with a heating rate 10 K/min, kept at this temperature for 10 days and then cooled down to room temperature with a rate 2 K/min.

**Route 3**: A precursor route for synthesizing Li$_2$B$_9$ was carried out for the first time in this study using Li$_2$[B$_{10}$H$_{10}$] as a precursor material. A detailed description

of this route is given in the section 3.4.

## 3.2.2 Characterization

### 3.2.2.1 Powder diffraction analysis at room temperature

X-ray powder diffraction experiments were carried out for all the products (separated according to the colour) as initial characterization. It was observed from the diffractogram that the product obtained via **Route 1** was a mixture containing byproducts like $Li_2B_6$ or $Li_5B_4$ or a mixture of both except for two samples. These two samples were used for washing with liquid ammonia and EEL spectroscopy. The diffractograms of the monophasic gray and brown samples are shown in figure 3.2. The gray sample was found to be more crystalline and less air-sensitive than the brown one.
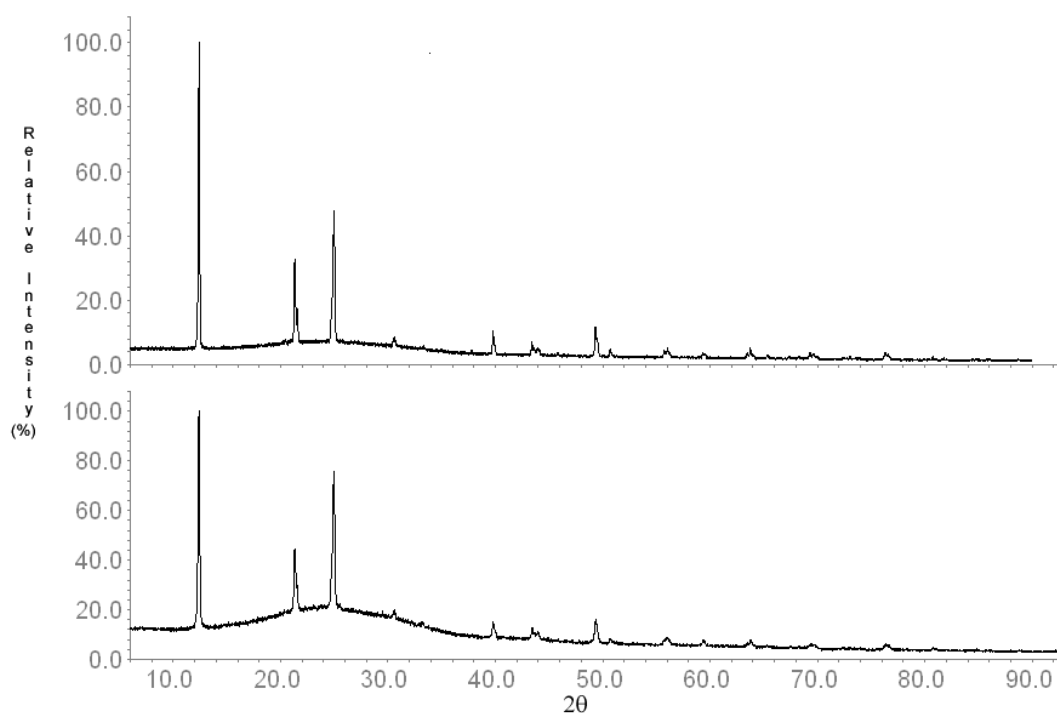


Figure 3.2: Measured X-ray patterns of $Li_2B_9$. Gray sample (top) and brown sample (bottom)

In order to understand the difference between gray and brown samples, they were treated separately in liquid ammonia. The liquid ammonia turned blue for the brown powder. Therefore, it was washed by using a H-tube till a colourless solution was obtained. The liquid ammonia did not change its color for the gray

(a) Gray portion of sample      (b) Brown portion of sample
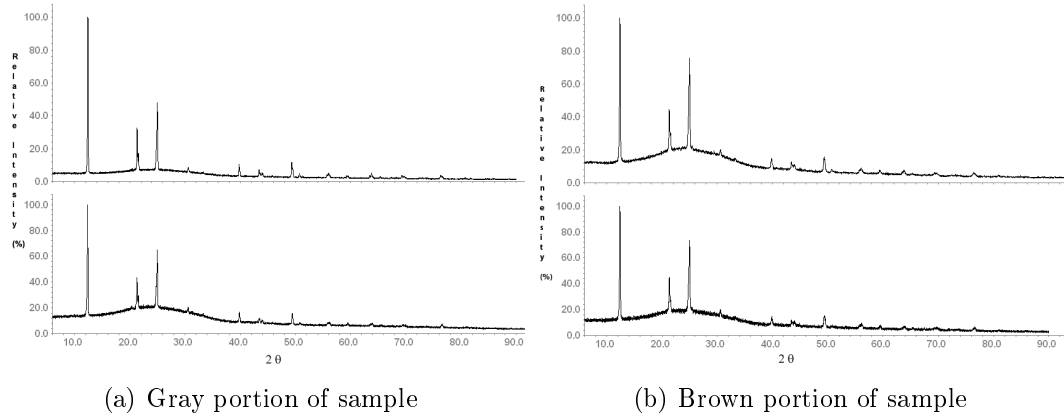
Figure 3.3: Measured X-ray pattern of the gray and brown parts of $Li_2B_9$ before and after washing with liquid ammonia. Left (gray portion of sample) top (before washing), bottom (after washing), right (brown portion of sample) top (before washing), bottom (after washing)

powder. Therefore, it can be concluded that the brown part of the sample contains an excess of lithium. The diffractogram of gray and brown powder before and after washing are shown in figure 3.3. There is no remarkable difference observed in the diffractogram before and after washing of the sample.

Due to better crystallinity and stability against moisture and air the gray part of the sample was used for further characterization.

The product obtained via **Route 2** was always found to contain a nitride phase either as $Li_3BN_2$ [69, 70] or BN [71]. A powder diffractogram exhibiting a mixture of two phases ($Li_2B_9$ and $Li_3BN_2$) is shown in figure 3.4.
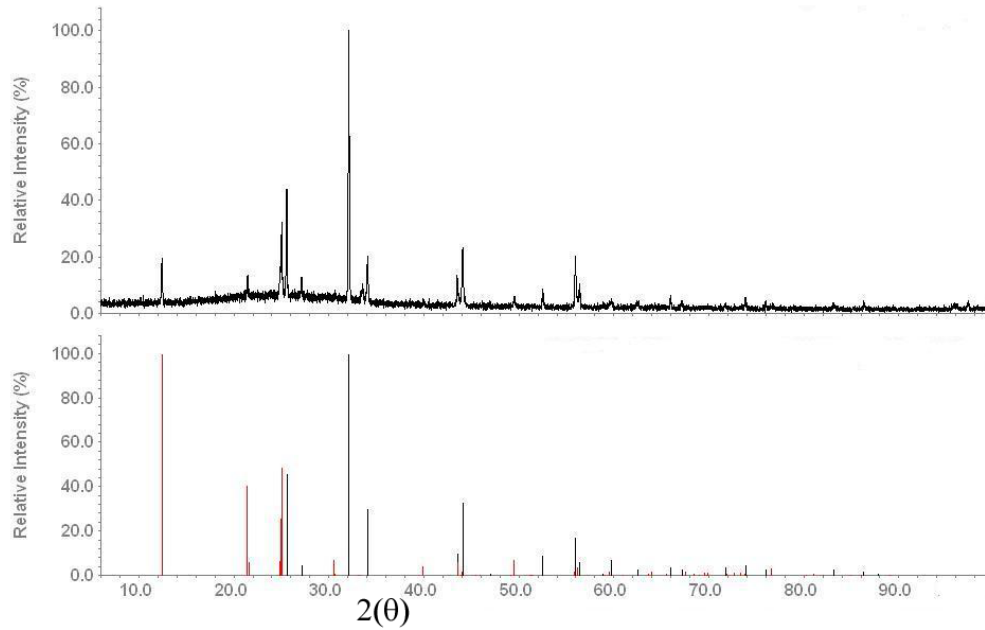
Figure 3.4: Comparison between measured X-ray powder pattern (top) and the reflection positions (bottom) of $Li_2B_9$ (red) and $Li_3BN_2$ (black)

### 3.2.2.2 Electron energy loss spectroscopy

EEL spectroscopy was used to characterize the sample. EEL spectra were recorded for several samples. In most of the samples except for the $B_K$ ionization edge, the spectrum does not exhibit any features between 200 and 800 eV, which shows that the samples are free from impurities like oxygen, nitrogen and carbon. The $Li_K$ ionization edge (55 eV) was not measured as it falls in the vicinity of the intense plasmon peak. A typical EEL spectrum is shown in figure 3.5.

The fine structure of the $B_K$-ionisation edge is highly sensitive to the co-ordination and electronic situation of the boron atoms. For a number of boron-rich borides Albert *et al.* have reported that the building unit can be identified by using characteristic ELNES spectra of boron atoms [72]. It is well known that hexaborides such as $CaB_6$, $SrB_6$, $BaB_6$ [73–76] consist of three-dimensionally interconnected boron atom octahedra. The comparison of the $B_K$ ELNES edge of $Li_2B_9$ and $CaB_6$ is shown in figure 3.6. They are similar to each other at least in the near-edge range.

Therefore, a binary lithium boride with the presence of boron atom octahedra is highly probable from the fine edge structure of the $Li_2B_9$ sample.
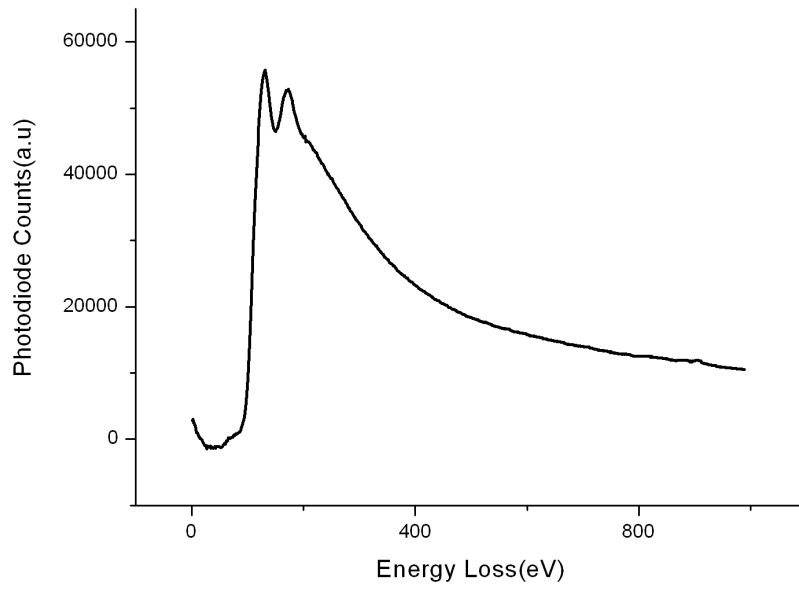
Figure 3.5: Electron energy loss spectrum of $Li_2B_9$ sample showing the $B_K$ edge
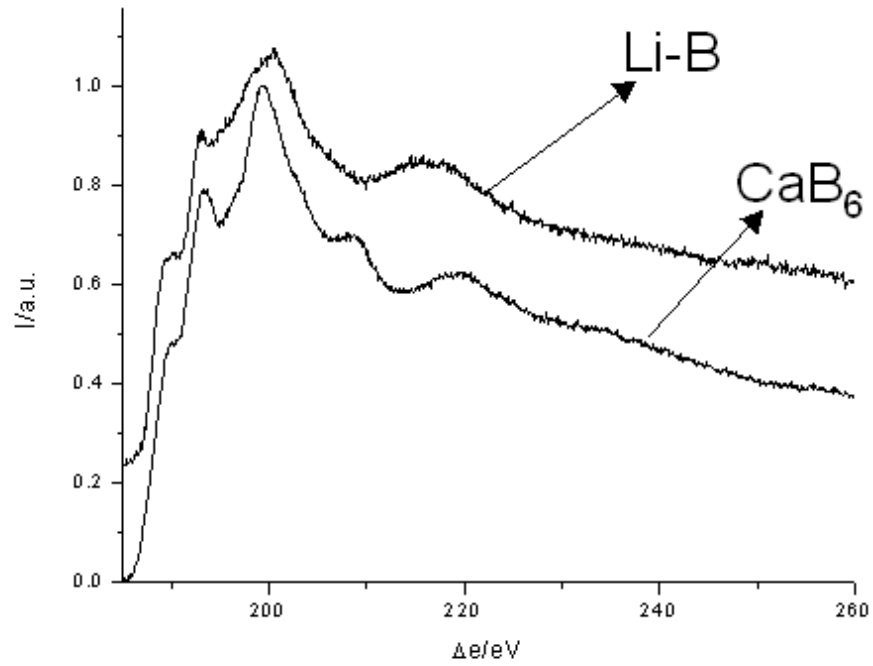


Figure 3.6: Comparison of $B_K$ ELNES between $Li_2B_9$ (top) and $CaB_6$ (bottom)

### 3.2.3 "New" Structural description

#### 3.2.3.1 Indexing of the powder diffractogram

To determine the crystal system and refine the lattice constants, indexing of the observed reflections from the laboratory data of the gray sample was performed with the program WinXPOW [77]. It was not possible to index the diffractogram in the hexagonal crystal system suggested by Schmitt *et al.* and Wörle *et al.* with $a = 8.2474$ Å and $c = 4.1620$ Å.

To obtain a better resolved pattern synchrotron X-ray measurement was carried out at B2-beamline of DESY-HASYLAB with a wavelength of 0.499694 Å. This diffraction pattern is compared with the laboratory data and is shown in figure 3.7. The powder pattern obtained at DESY-HASYLAB has one extra reflection at 0.236 (1/D) which could be assigned to $Li_2B_6$. The reflection at 0.28(1/D) is more resolved in synchrotron data and could not be described in the space group $P6/mmm$ [16]. This compels for the reduction of symmetry. However, the synchrotron X-ray diffractogram could not be used for indexing due to high noise to intensity ratio at higher angles.

A low temperature X-ray powder diffraction experiment in the laboratory was carried out at 100 K assuming the Li atom to be localized based on [16] structural model. This diffraction pattern was compared with the room temperature diffractogram and found to be identical as shown in figure 3.8. This low temperature data was used for indexing and further refinement.

Indexing is possible in the orthorhombic and monoclinic crystal systems. However, the orthorhombic crystal system was preferred based on the smaller number of unindexed lines. The cell was refined for 53 accepted peaks with cell parameters $a = 14.221(6)$Å, $b = 8.330(2)$Å, $c = 8.250(2)$Å and volume = $977.4(4)$Å$^3$. There were 20 single indexed lines and 7 unindexed lines after refinement. The maximum intensity of the unindexed line lies in $2\theta$ value of 4.2. The indexing results were shown in table 3.1.
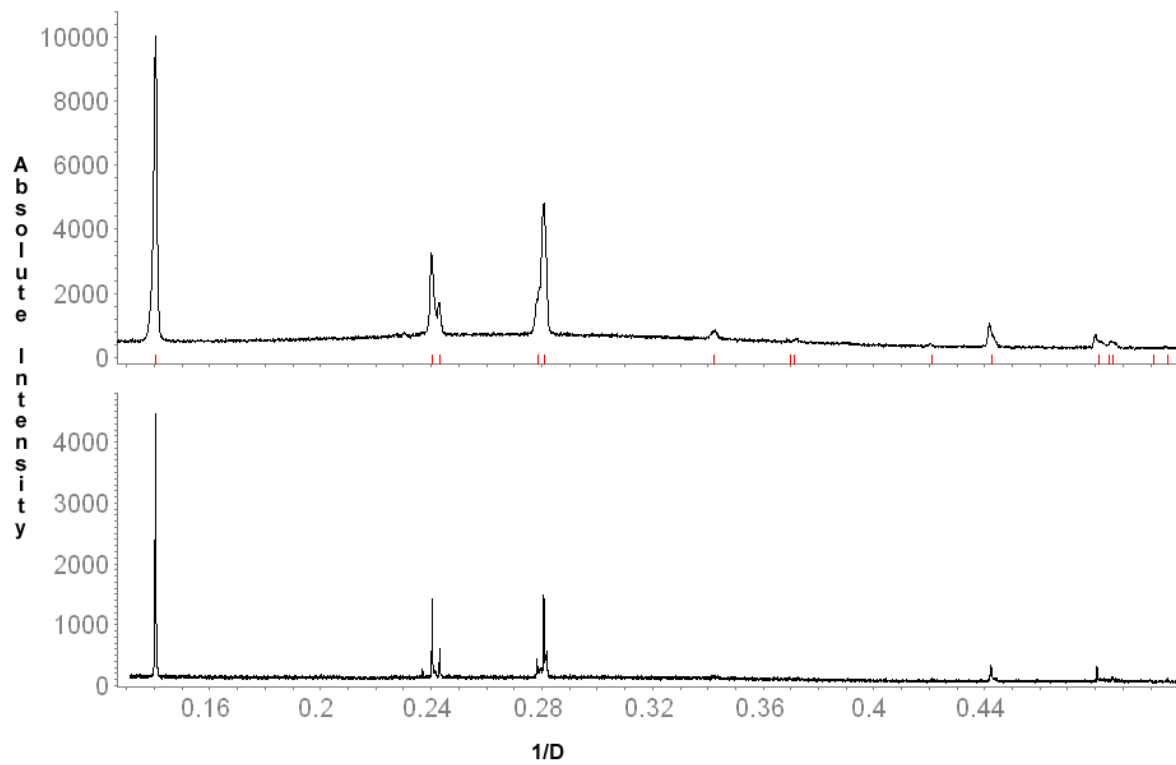
Figure 3.7: Comparison between laboratory diffractogram (top) and synchrotron powder diffractogram (bottom). The vertical red lines indicate the position of the reflections in $P6/mmm$ (top)
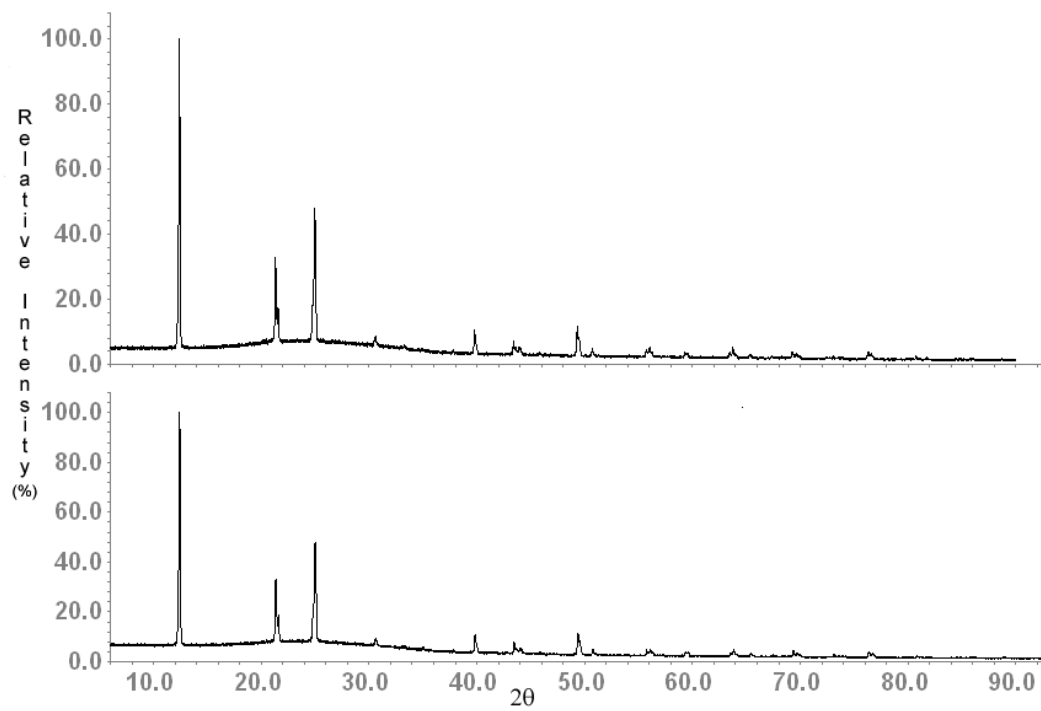
Figure 3.8: Measured X-ray pattern of $Li_2B_9$ at room temperature (top) and 100 K (bottom)

| N | $2\theta$ (obs) | $h$ | $k$ | $l$ | $2\theta$ (calc) | obs-calc | Int. | d (obs) | d (calc) |
|---|---|---|---|---|---|---|---|---|---|
| 1 | 12.402 | 1 | 0 | 1 | 12.393 | 0.0093 | 100.0 | 7.1311 | 7.1364 |
| | | 2 | 0 | 0 | 12.438 | -0.0360 | | | 7.1105 |
| 2 | 21.331 | 0 | 2 | 0 | 21.315 | 0.0159 | 26.7 | 4.1620 | 4.1651 |
| 3 | 21.560 | 0 | 0 | 2 | 21.524 | 0.0362 | 10.2 | 4.1184 | 4.1252 |
| | | 3 | 1 | 0 | 21.552 | 0.0084 | | | 4.1200 |
| | | 3 | 0 | 1 | 21.603 | -0.0433 | | | 4.1102 |
| 4 | 24.784 | 2 | 2 | 0 | 24.753 | 0.0310 | 13.0 | 3.5895 | 3.5939 |
| 5 | 24.977 | 2 | 0 | 2 | 24.934 | 0.0426 | 48.5 | 3.5622 | 3.5682 |
| | | 4 | 0 | 0 | 25.026 | -0.0497 | | | 3.5553 |
| 6 | 30.508 | 0 | 2 | 2 | 30.474 | 0.0340 | 1.7 | 2.9278 | 2.9310 |
| | | 3 | 2 | 1 | 30.532 | -0.0235 | | | 2.9256 |
| 7 | 30.621 | 3 | 1 | 2 | 30.644 | -0.0234 | 2.2 | 2.9173 | 2.9151 |
| 8 | 33.018 | 2 | 2 | 2 | 33.030 | -0.0116 | 0.4 | 2.7107 | 2.7098 |
| 9 | 33.301 | 5 | 1 | 0 | 33.259 | 0.0420 | 1.0 | 2.6883 | 2.6916 |
| | | 5 | 0 | 1 | 33.294 | 0.0073 | | | 2.6889 |
| 10 | 34.975 | 2 | 0 | 3 | 34.953 | 0.0218 | 0.6 | 2.5634 | 2.5650 |
| | | 4 | 1 | 2 | 34.988 | -0.0130 | | | 2.5625 |
| 11 | 37.797 | 3 | 0 | 3 | 37.788 | 0.0089 | 0.7 | 2.3783 | 2.3788 |
| 12 | 39.803 | 4 | 2 | 2 | 39.828 | -0.0246 | 7.0 | 2.2629 | 2.2615 |
| 13 | 39.962 | 5 | 1 | 2 | 39.963 | -0.0003 | 1.7 | 2.2542 | 2.2542 |
| 14 | 43.421 | 0 | 4 | 0 | 43.417 | 0.0046 | 3.8 | 2.0823 | 2.0825 |
| 15 | 43.633 | 3 | 3 | 2 | 43.653 | -0.0197 | 1.8 | 2.0727 | 2.0718 |
| 16 | 43.929 | 1 | 4 | 0 | 43.904 | 0.0256 | 1.9 | 2.0594 | 2.0606 |
| | | 6 | 2 | 0 | 43.917 | 0.0126 | | | 2.0600 |
| 17 | 44.081 | | — not indexed — | | | | | 1.3 | 2.0527 |
| 18 | 45.824 | 5 | 0 | 3 | 45.861 | -0.0376 | 0.6 | 1.9786 | 1.9771 |
| 19 | 49.332 | 3 | 1 | 4 | 49.372 | -0.0398 | 8.4 | 1.8458 | 1.8444 |
| 20 | 49.514 | | — not indexed — | | | | | 4.2 | 1.8394 |
| 21 | 50.715 | 2 | 4 | 2 | 50.716 | -0.0007 | 1.9 | 1.7986 | 1.7986 |
| 22 | 50.917 | | — not indexed — | | | | | 0.3 | 1.7920 |
| 23 | 55.738 | 1 | 4 | 3 | 55.695 | 0.0431 | 1.8 | 1.6479 | 1.6490 |
| | | 6 | 2 | 3 | 55.706 | 0.0321 | | | 1.6487 |
| | | 4 | 4 | 2 | 55.754 | -0.0159 | | | 1.6474 |
| 24 | 56.023 | 4 | 2 | 4 | 56.030 | -0.0068 | 2.6 | 1.6402 | 1.6400 |
| | | 7 | 3 | 0 | 56.044 | -0.0214 | | | 1.6396 |
| | | 1 | 0 | 5 | 56.063 | -0.0399 | | | 1.6391 |
| 25 | 56.250 | 8 | 2 | 0 | 56.217 | 0.0324 | 1.0 | 1.6341 | 1.6350 |
| | | 7 | 0 | 3 | 56.250 | -0.0005 | | | 1.6341 |
| | | 0 | 5 | 1 | 56.288 | -0.0380 | | | 1.6331 |
| 26 | 59.317 | 5 | 4 | 2 | 59.340 | -0.0228 | 1.1 | 1.5567 | 1.5561 |
| | | 6 | 0 | 4 | 59.349 | -0.0312 | | | 1.5559 |

Table 3.1: Indexing of $Li_2B_9$ in orthorhombic crystal system

| N | $2\theta$ (obs) | $h$ | $k$ | $l$ | $2\theta$ (calc) | obs-calc | Int. | d (obs) | d (calc) |
|---|---|---|---|---|---|---|---|---|---|
| 27 | 59.527 | 9 | 1 | 0 | 59.496 | 0.0304 | 1.1 | 1.5517 | 1.5524 |
|  |  | 9 | 0 | 1 | 59.518 | 0.0083 |  |  | 1.5519 |
| 28 | 63.459 | 0 | 4 | 4 | 63.421 | 0.0378 | 1.2 | 1.4647 | 1.4655 |
| 29 | 63.763 | 1 | 4 | 4 | 63.796 | -0.0333 | 2.7 | 1.4584 | 1.4578 |
|  | 6 | 2 | 4 | 63.806 | -0.0433 |  |  | 1.4576 |  |
| 30 | 64.001 | 9 | 2 | 1 | 63.969 | 0.0316 | 0.8 | 1.4536 | 1.4542 |
|  | 7 | 4 | 0 | 63.970 | 0.0308 |  |  | 1.4542 |  |
|  | 9 | 1 | 2 | 64.033 | -0.0319 |  |  | 1.4530 |  |

Table 3.1: Indexing of $Li_2B_9$ in orthorhombic crystal system

### 3.2.3.2 Possible space groups

The symmetry reduction from the hexagonal to the orthorhombic crystal system was carried out using group-subgroup relationships. Bärnighausen *et al.* [78, 79] introduce a comprehensive and compact view of the group-subgroup relationships. A *Bärnighausen* tree of $Li_2B_9$ was made with the help of the *International Tables for Crystallography* [80, 81] and is shown in figure 3.9. In the case of a *translationengleiche* (t) reduction, translational symmetry is not lost (*i.e.* the translation vector does not change) but the crystal class is changed. In contrast, for *klassengleiche* (k) reduction the crystal class remains the same. Based on this principle, the suggested orthorhombic unit cell can be derived from the hexagonal $Li_2B_9$ [16]. The symmetry is reduced by a *translationengleiche* reduction of index 3 (t3) leading to the orthorhombic space group *Cmmm*. A doubling of the c-axis by *klassengleiche* transition of index 2 (k2) results the space group to be *Cmcm, Cccm, Immm, Ibam* and *Ibmm*. Due to multiple indexing of some reflections, one can not be sure about the systematic absences *i.e.* $h+k = 2n$ refers to $C$-centering type of cell and $h+k+l = 2n$ refers to $I$- centering type of cell. Therefore, refinement was tried in all the above space groups. Among all the above mentioned space groups, best results were obtained in the space group *Ibmm* in terms of being able to refine freely the lithium atom positions and in terms of the $R$ values. The allowed *translationengleiche* reduction of index 2 of *Ibmm* leads to the subgroup *I2mb*. Rietveld refinement was also tried with this noncentrosymmetric space group, but did not lead to a better result. Therefore, the refinement and crystal structure is finally described in *Ibmm*.

$P6/\text{m } 2/\text{m } 2/\text{m}$

t3
**a, a+2b, c**
x-1/2y, 1/2y, z

$C2/\text{m } 2/\text{m } 2/\text{m}$

k2
**a, b, 2c**
x, y, 1/2z; +(0, 0, ½)

*C* 2/m 2/c 2₁/m, *C* 2/c 2/c 2/m, *I* 2/m 2/m 2/m, *I* 2/b 2/a 2/m, *I* 2₁/b 2₁/m 2₁/m

t2
**b, c, a**
y, z, x

*I* 2mb
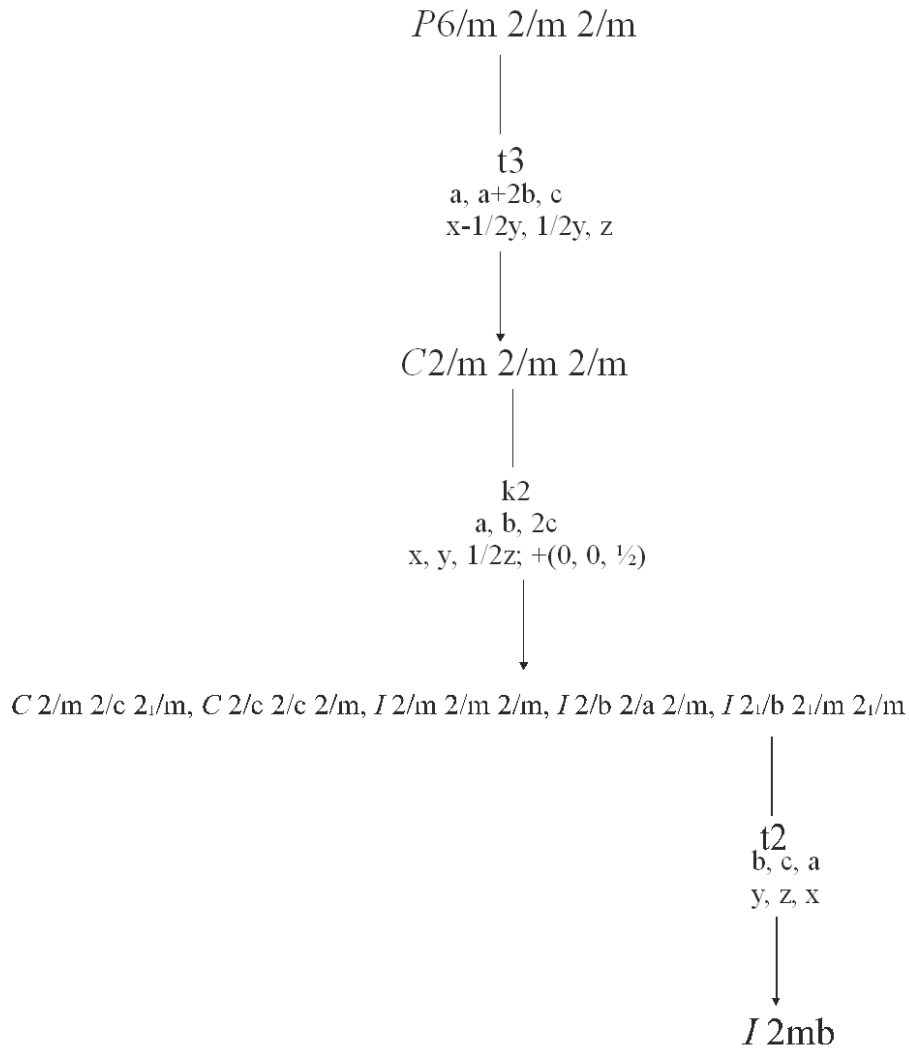
Figure 3.9: *Bärnighausen* tree of the group-subgroup relationship for $\text{Li}_2\text{B}_9$. The indices of the *klassengleiche* (k), the *translationengleiche* (t) transitions, as well as the unit cell transformations are given. The numbers after t and k indicate the index of the reduction in symmetry

## 3.2.4 Rietveld refinement

The structural refinement was performed using low temperature (100 K) X-ray diffraction data. First, a Le Bail fit was performed for the background and profile parameters (fundamental parameters approach) and the lattice constants. The background was fitted with a sixteen term cosine Fourier series type 2 background function. The agreement factors of the Le Bail fit were $R_{wp} = 7.78$, $\chi^2 = 2.415$. After that, these parameters were fixed and used as input for the structure refinement process by the Rietveld method using the GSAS program.

An initial model for atomic coordinates was derived in the space group *Ibmm* (as discussed in 3.2.3.2) from the program POWDERCELL [82]. The B-B bond length (1.7 Å) constraints were included to refine boron atom positions. For the boron atoms a common displacement parameter was used. The atomic positions of the lithium atoms were refined freely and displacement parameters were refined isotropically. The details of the refinement are listed in table 3.2. The observed and calculated powder pattern is shown in figure 3.10.

| | |
|---|---|
| Diffractometer | STOE Transmission Diffractometer (STADI-P) |
| Empirical formula | $Li_2B_9$ |
| Formula weight /g/mol | 111.18 |
| Crystal system | Orthorhombic |
| Space group | *Ibmm* (no. 74) |
| $a$ /Å | 8.218(3) |
| $b$ /Å | 14.230(6) |
| $c$ /Å | 8.309(3) |
| $V$ /Å$^3$ | 971.51(2) |
| X-ray source | $CuK_\alpha$ |
| Wave length /Å | 1.54056 |
| $2\theta$-range /° | 6 -100 |
| Temperature /K | 100 |
| Estimated reflections | 796 |
| Total no. of reflections | 634 |
| No. of background parameters | 16 |
| $R_p$ | 0.0558 |
| $R_{wp}$ | 0.0820 |
| $D_{wd}$ | 0.435 |
| $\chi^2$ | 4.072 |

Table 3.2: Crystal data and structure refinement parameters for $Li_2B_9$
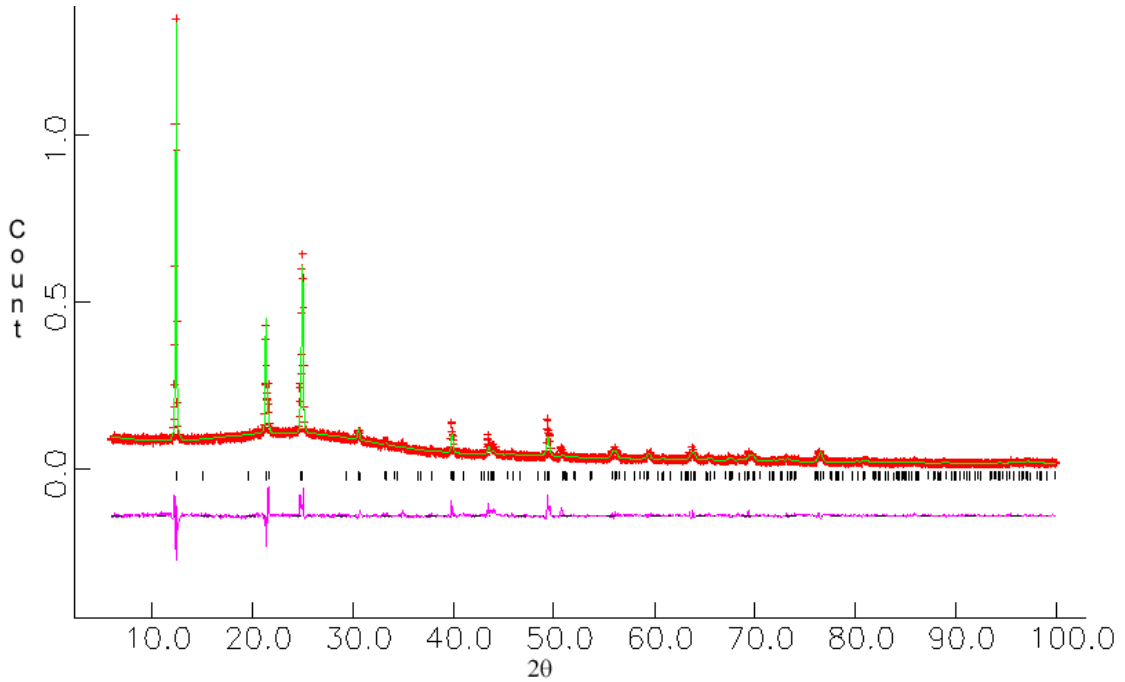
Figure 3.10: Rietveld refinement plot of $Li_2B_9$. Shown are the observed pattern (+), the calculated pattern (solid line) and the difference plot. The vertical dashes indicate the position of the reflections

### 3.2.4.1 Description of the crystal structure

The positional, thermal displacement parameters and site occupancies are given in table 3.3. There are three lithium atoms observed during the refinement. Among three lithium atom positions, the lithium atom situated at Wyckoff position $8f$ is fully occupied and the other two situated at $4a$ and $4e$ are partially occupied by 50 %. The selected boron-boron and lithium-lithium bond distances are shown in table 3.4. The lithium-lithium distances 2.13056(9)Å among the zig-zag chains are comparable to the Li-Li distance reported for $Li_2B_6$ [5]. The intra-polyhedral B-B bond lengths vary from 1.6702(6)Å to 1.8038(3)Å. The inter-polyhedral bond lengths vary from 1.53472(6)Å to 1.8026(8)Å. The shortest bond length 1.53472(6)Å can be compared to the average boron-boron distances in $LiB_x$ (0.82≤ x ≤ 1) [6] and the longest boron-boron bond distance 1.8038(3)Å can be compared to that found for $Na_3B_{20}$ [22]. The boron atoms are arranged as distorted octahedra as shown in figure 3.11. The octahedra are connected to form two different kinds of channels parallel to the $c$-axis. In one plane the small channel is made up of 3 interconnected boron atom octahedra and the big channel is made up of 6 interconnected boron

atom octahedra. The smaller channels contain lithium atoms on fully occupied positions and are responsible for building vertices of the hexagon. The bigger channel was believed to be filled with either $[BH_4]^-$ unit by Wörle *et al.* [15] or with Li by Schmitt *et al.* [16]. In this work the bigger channels could be better described by zig-zag chains of lithium atoms as shown in figure 3.12. We believe that the lithium atoms in the channels play an important role for symmetry reduction.

| Atom | Wyck. | $x/a$ | $y/b$ | $z/c$ | $U_{iso}$ | SOF |
|------|-------|-------|-------|-------|-----------|-----|
| B1 | 8i | 0.297(4) | 0.828(2) | 0.2500 | 0.018 | 1 |
| B2 | 8i | 0.737(4) | 0.166(2) | 0.2500 | 0.018 | 1 |
| B3 | 8i | 0.610(4) | 0.939(1) | 0.2500 | 0.018 | 1 |
| B4 | 8i | 0.399(5) | 0.058(1) | 0.2500 | 0.018 | 1 |
| B5 | 8i | 0.608(3) | 0.728(2) | 0.2500 | 0.018 | 1 |
| B6 | 8i | 0.385(3) | 0.289(2) | 0.2500 | 0.018 | 1 |
| B7 | 8h | 0.496(5) | 0.0000 | 0.913(2) | 0.018 | 1 |
| B8 | 8g | 0.2500 | 0.2500 | 0.915(3) | 0.018 | 1 |
| B9 | 8g | 0.2500 | 0.2500 | 0.416(3) | 0.018 | 1 |
| Li1 | 4a | 0 | 0 | 0 | 0.031(3) | 0.5 |
| Li2 | 4e | -0.057(4) | 0.000 | 0.2500 | 0.022(4) | 0.5 |
| Li3 | 8f | 0 | 0.318(2) | 0 | 0.077(5) | 1 |

Table 3.3: Positional, displacement parameters and site occupancies (SOF) for $Li_2B_9$

| Bond | Length /Å | Bond | Length /Å |
|------|-----------|------|-----------|
| B(1)-B(4) | 1.7421(6) | B(4)-B(4) | 1.7098(7) |
| B(1)-B(6) | 1.6702(6) | B(4)-B(7) | 1.7543(3) |
| B(1)-B(9) | 1.7681(3) | B(5)-B(6) | 1.8036(8) |
| B(2)-B(3) | 1.7660(6) | B(5)-B(8) | 1.7951(3) |
| B(2)-B(5) | 1.6718(6) | B(6)-B(9) | 1.8038(3) |
| B(2)-B(8) | 1.7820(3) | B(7)-B(7) | 1.64285(6) |
| B(3)-B(3) | 1.7266(7) | B(8)-B(9) | 1.53472(6) |
| B(3)-B(4) | 1.7721(8) | Li(1)-Li(3) | 2.13056(9) |
| B(3)-B(7) | 1.7709(3) | | |

Table 3.4: Selected bond lengths of $Li_2B_9$. Standard deviations are shown in bracket
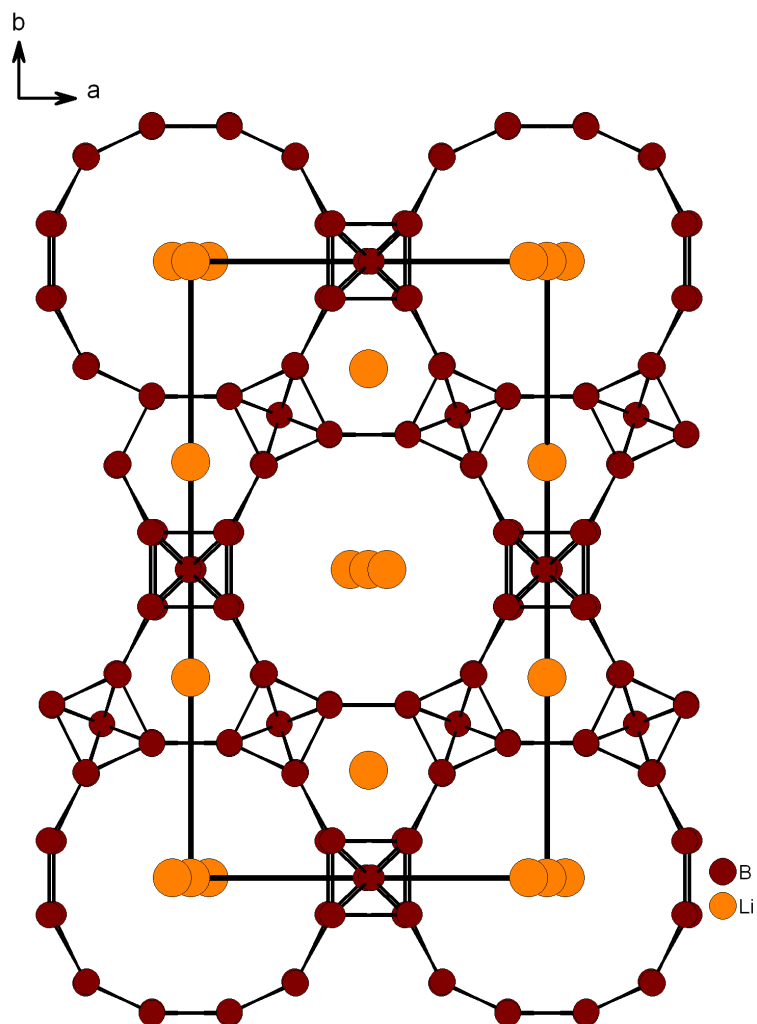
Figure 3.11: Projection of the structure of $Li_2B_9$. View along the $c$-axis
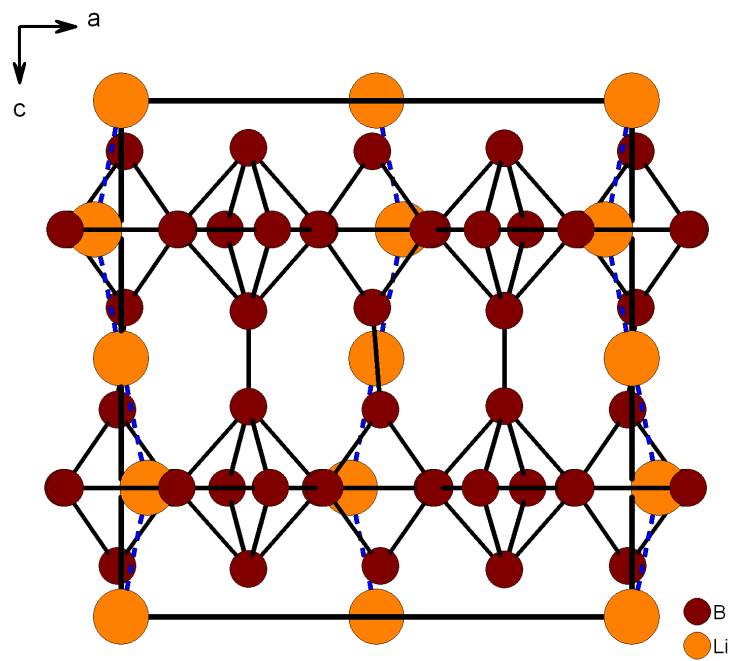
Figure 3.12: Projection of the structure of $Li_2B_9$ along the $b$-axis showing the zig-zag chains of lithium

## 3.2.5 Impedance spectroscopy

Approximately 100 mg of the powder sample containing $Li_2B_6$ as a byproduct phase were pressed using a 5 mm dia pellet-press inside the glove box. The impedance data were collected for four subsequent heating and cooling cycles between 298 K and 923 K. The first two cycles of heating and cooling did not give any reproducible results whereas, the third and fourth cycle results were reproducible. Therefore, only results of the fourth cycle measurements are discussed here. Two sets of the AC data, in the form of complex impedance plane plots (Nyquist plot) are shown in figure 3.13. The data collected at 312 K shows no spikes whereas, at 503 K contains a semicircle at the high frequency region and a spike at the low frequency region. This indicates that the sample is semiconducting at low temperatures and ionic conducting at high temperatures.

An Arrhenius plot for the temperature dependence of the electrical conductivity for is shown in figure 3.14. The AC and DC cooling curves are equivalent till 323 K. At higher temperatures, they deviate from each other. This establishes that the sample is semiconducting at low temperatures and ionic conducting at high temperatures. The humps above 423 K in the AC and DC heating curves may be assigned to a phase transition in the compound. The average activation energy computed from the figure 3.14 is 38.5 kJ/mol.
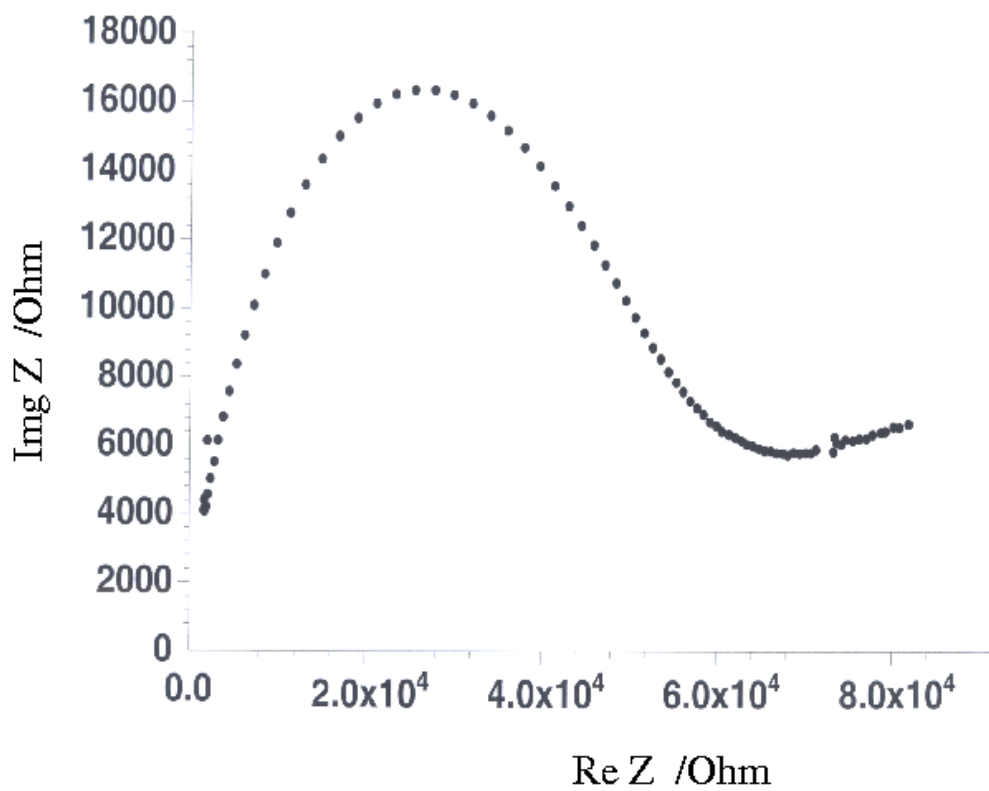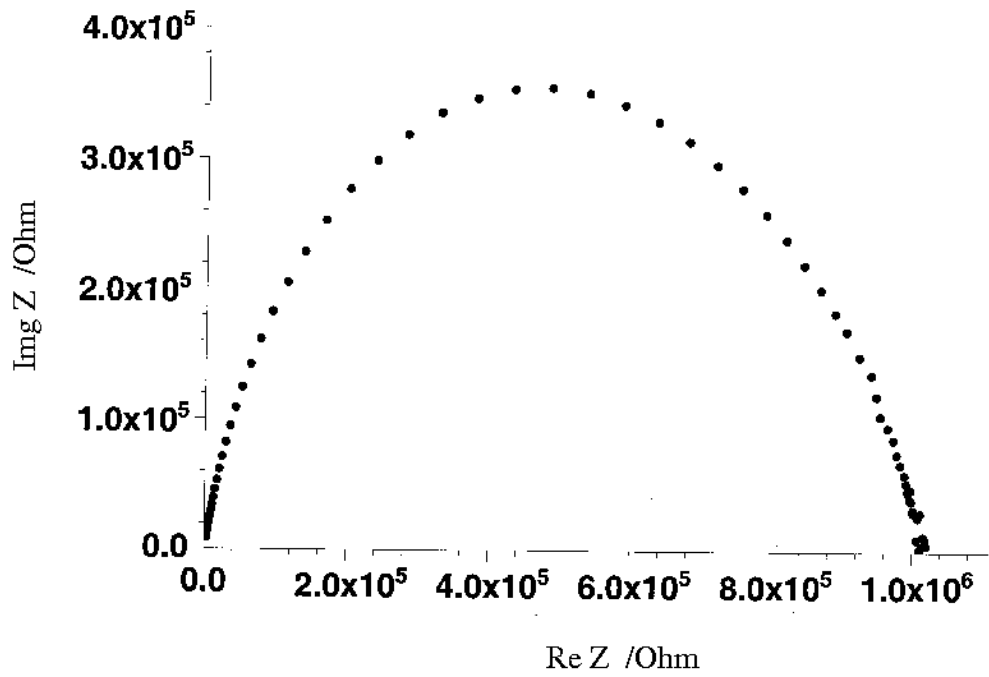
Figure 3.13: Nyquist plot for a $Li_2B_9$ pellet lying between two ion-blocked Pt electrodes at 312 K (top) and 503 K (bottom)
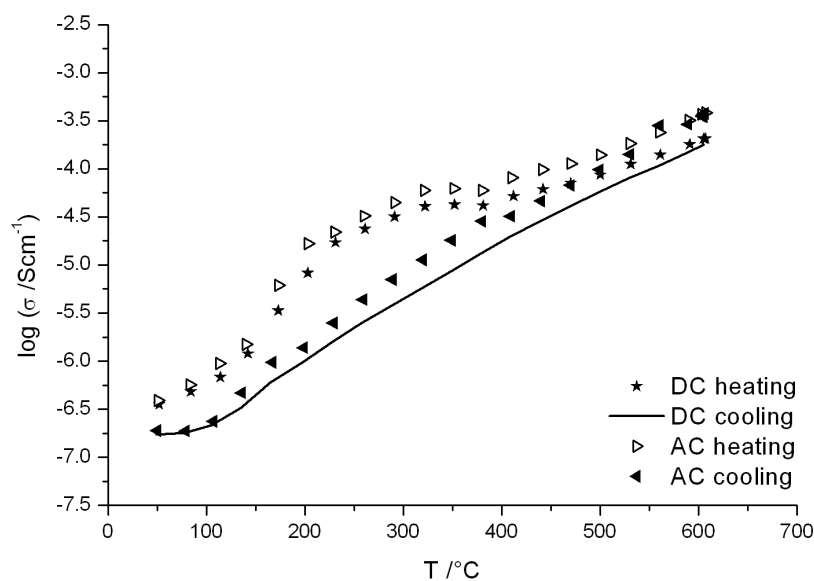
Figure 3.14: Temperature dependant electrical conductivity of $Li_2B_9$ as Arrhenius plot

## 3.2.6 Discussion

The goal was to synthesize single phase, homogeneous and ultrapure binary lithium boride with the expected chemical formula $Li_2B_9$, to solve the crystal structure and to determine its ionic conductivity. To obtain the required product three different synthesis routes (as described in 3.2.1) were adopted. In spite of a lot of trials, it seems to be difficult to obtain a single phase, homogeneous product. Only for two times the product was synthesized without any second phase. The inhomogeneous products can be separated by seeing the colour differences (gray or brown). From X-ray diffraction measurements, the gray part is shown to be more crystalline than the brown part. Washing the products with ammonia proved that the gray part of the sample does not contain any elemental lithium whereas the brown part does. Therefore, the gray part of the sample is used for most of the characterization techniques. EEL spectroscopy was carried out for several samples and most of the studied sample were proved to be pure $i$.e. without presence of oxygen.

The crystal structure of the required compound was described before in space group $P6/mmm$ with an three-dimensionally interconnected framework of boron atom octahedra forming two kinds of channels. The analysis of ELNES supports

the probability of octahedral B-atom co-ordination at the short range. Indexing of the diffractogram of the required product was not possible in the hexagonal crystal system. Analysis of synchrotron X-ray measurements suggests the symmetry reduction. Indexing of all the reflections of diffractogram was not possible. Indexing of the low temperature diffractogram was possible in either orthorhombic or monoclinic crystal systems. The orthorhombic crystal system having $a = 14.221(6)$Å, $b = 8.330(2)$Å and $c = 8.250(2)$Å was chosen based on less number of unindexed line. The structure model was reduced from $P6/mmm$ to $Cmcm$, $Cccm$, $Immm$, $Ibam$ and $Ibmm$ using Bärnighausen group-subgroup relationships. Refinement was tried in all the above space groups. Finally, the crystal structure was described in the space group $Ibmm$. The refinement in this space group is also not fully satisfactory as can be seen from the following results. The difference plot was not found to be minimum. The values of $D_{wd}$ and $\chi^2$ were not satisfactory. The boron atom positions were not freely refinable. Though B-B bond length constraints were used, the B-B bond length vary from 1.53472(6)Å to 1.8038(3)Å. It can be imagined that a proper structure description using X-ray powder method might not be easy because of presence of only light elements. A proper structure description might be possible using a higher dimensional space group with additional characterization techniques like solid state NMR and neutron diffraction.

The impedance data show this compound exhibits ionic conductivity at elevated temperature. The average activation energy computed from the graph is 38.5 kJ/mol.

# 3.3 Modified synthesis route and structure confirmation of LiB$_{13}$ using Rietveld refinement

The aim was to verify the crystal structure of LiB$_{13}$. The lithium containing boron-rich compound LiB$_{13}$ was described by Kobayashi *et al.* [3] as an intercalation compound of lithium into $\beta$-rhombohedral boron. In [3], the synthesis was performed from the elements in a tantalum boat, enclosed in an evacuated quartz tube. During the Rietveld refinement, Kobayashi *et al.* excluded eleven small peaks (which might result from oxidation of the substance). This pattern had a highly undulated background and the occupation factor of one of the boron atoms was described as 0.1. In this study a modified synthesis route was followed to synthesize LiB$_{13}$ and the structure model was then verified.

## 3.3.1 Synthesis

$\beta$-rhombohedral boron (0.157 g, 0.14 mol) and lithium (0.013 g, 0.002 mol) were filled inside a tantalum tube. For a modified synthesis compared to literature a closed tantalum tube was used. The tantalum tube was sealed under argon by arc-welding. The tube was then sealed into a quartz ampoule under vacuum. The ampoule was placed in an oven and heated up to 1273 K with a rate of 2 K/min, kept at this temperature for 12 h and then quenched to room temperature.

## 3.3.2 Rietveld refinement

Rietveld refinement was performed using the LiB$_{13}$ model as the initial model. A pseudo-Voigt peak shape was used with a sixteen term cosine fourier series background function. The background parameters, profile and lattice constants were fitted first. After that, these parameters were fixed and used as input for the structure refinement process. Rather than eleven here just one experimental reflection ($2\theta = 20.9°$) was excluded. The boron-boron bond distances and angles are comparable to the reported structure model. The thermal parameters for B9, B13 and B14 were refined with 9 damping factors. The final refinement parameters are given in the table 3.5. Figure 3.15 shows the Rietveld fit and difference profile. The position of the atoms and isotropic displacement parameters are shown in the table 3.6.
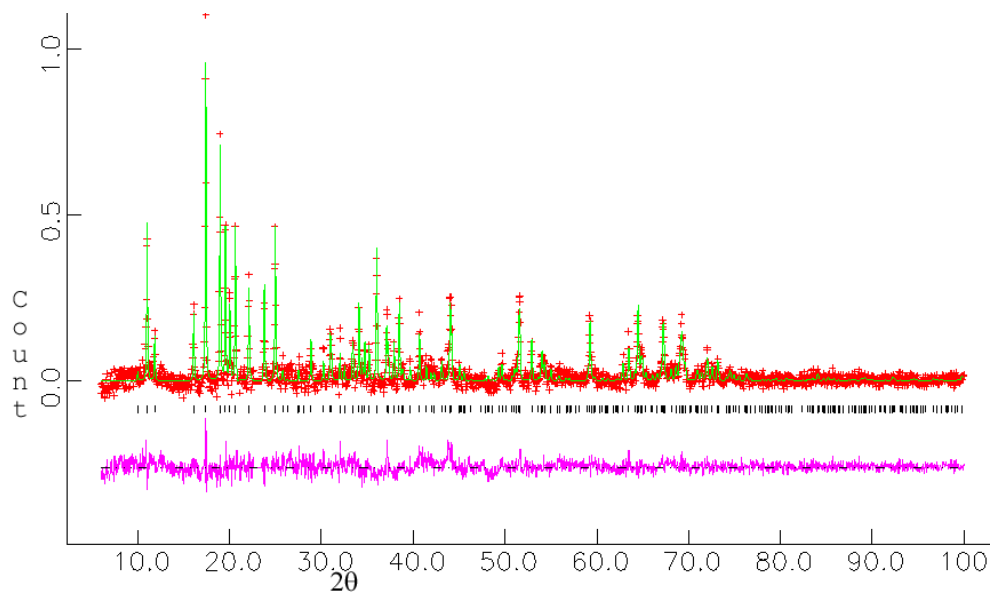
Figure 3.15: Observed (+) and calculated (solid line) powder diffraction pattern (corrected for the background) with the difference curve (bottom). The vertical dashes indicate the position of reflection

| | |
|---|---|
| Diffractometer | STOE Transmission Diffractometer (STADI-P) |
| Empirical formula | $LiB_{12.85}$ |
| Formula weight /g/mol | 149.91 |
| Crystal system | Trigonal |
| Space group | $R\bar{3}m$ (No.166) |
| $a$ /Å | 11.0079(3) |
| $c$ /Å | 24.1226(9) |
| $V$ /Å$^3$ | 2531.43(2) |
| X-ray source | $CuK_\alpha$ |
| Wave length /Å | 1.54056 |
| $2\theta$-Range /° | 6 -100 |
| Temperature /K | 298 |
| Estimated reflections | 476 |
| Generated reflections | 378 |
| Parameters | 54 |
| No. of background parameters | 16 |
| $R_p$ | 0.0564 |
| $R_wp$ | 0.0732 |
| D$wd$ | 1.206 |
| $\chi^2$ | 1.278 |

Table 3.5: Crystal data and structure refinement parameters for $LiB_{13}$

66
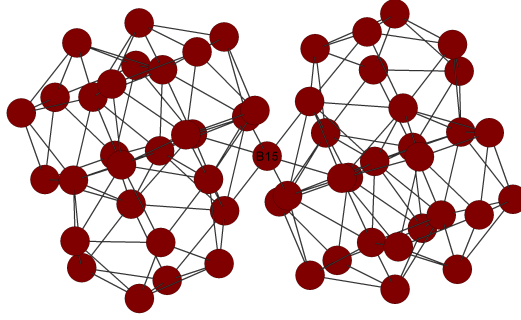
Figure 3.16: Part of the boron framework showing the arrangement of boron icosa-
hedra

| Atom | Wyck. | $x/a$ | $y/b$ | $z/c$ | $U_{iso}$ |
|------|-------|-------|-------|-------|-----------|
| B1 | 36i | 0.1684(7) | 0.1667(8) | 0.1753(3) | 0.029(4) |
| B2 | 36i | 0.3132(9) | 0.2925(8) | 0.1288(3) | 0.012(4) |
| B3 | 36i | 0.2616(9) | 0.2164(9) | 0.4202(4) | 0.022(1) |
| B4 | 36i | 0.2338(1) | 0.2580(9) | 0.3475(4) | 0.007(2) |
| B5 | 18h | 0.0549(6) | -0.0549(6) | -0.0636(5) | 0.023(1) |
| B6 | 18h | 0.0815(6) | -0.0815(6) | 0.0092(7) | 0.015(1) |
| B7 | 18h | 0.1160(7) | 0.8839(7) | 0.8941(5) | 0.042(2) |
| B8 | 18h | 0.1686(6) | 0.8314(6) | 0.0257(7) | 0.031(4) |
| B9 | 18h | 0.1245(7) | 0.8755(7) | 0.7696(5) | 0.016(1) |
| B10 | 18h | 0.1063(7) | 0.8937(7) | 0.6989(6) | 0.022(1) |
| B11 | 18h | 0.0588(5) | -0.0588(5) | 0.3289(6) | 0.026(1) |
| B12 | 18h | 0.0847(7) | -0.0847(7) | 0.3976(6) | 0.018(2) |
| B13 | 18h | 0.0617(9) | -0.0617(9) | 0.5529(8) | 0.008(1) |
| B14 | 6c | 0 | 0 | 0.3850(1) | 0.015(1) |
| B15 | 3b | 0 | 0 | 0.5 | 0.054(1) |
| Li1 | 18h | 0.1976(8) | 0.8023(8) | 0.181(1) | 0.011(1) |
| Li2 | 6c | 0 | 0 | 0.228(2) | 0.027(2) |

Table 3.6: Atomic co-ordinates and isotropic displacement parameters for $LiB_{13}$

The unit cell of $LiB_{13}$ contains 308.52 B-atoms and 24 Li atoms. Each lithium
atom is surrounded by 15 boron atoms. The structure consists of $B_{12}$-icosahedra. In
each case three $B_{12}$-icosahedra are linked over faces with one another to a polyhedron
as shown in figure 3.16. The polyhedra are linked further with one another through
B15. The boron atom B16 with an occupancy factor of 0.1 was removed from
the model which improved the goodness factor. The position B13 is only partially
occupied (occupation factor 0.64) as in the Kobayashi *et al.* model. One finds
similar partial occupation also in $\beta$-rhombohedral boron structure.

## 3.4 Precursor route to synthesize alkali metal borides

### 3.4.1 Introduction

The conventional method of preparation of alkali metal borides is based on direct reactions between elements *i.e.* alkali metals and boron. As described in section 3.1, the starting materials are often difficult to handle and purify and their reactions do not always provide homogeneous products. Therefore, it is required to establish a new method for the preparation of pure and homogeneous borides. It is known that the metal borides can be synthesized by thermal decomposition of tetrahydroborates [83, 84]. Itoh *et al.* synthesized cerium and gadolinium borides by reacting the boron cage compound $M_2[B_{10}H_{10}]_3 \cdot xH_2O$ (M = Ce and Gd) with metal hydrides [85]. Hence, metal borides were synthesized by thermal decomposition of *closo*-hydroborates with the anions $[B_nH_n]^{2-}$ (n = 6-12) [86]. In the present work, $Li_2B_9$ and $Na_3B_{20}$ were synthesized using $M_2[B_{10}H_{10}]$ (M = Li and Na).

Sodium azide $NaN_3$ was used as another precursor material for synthesizing sodium boride. The *"Azide route"* was used by Jansen *et al.* for synthesizing oxides [87–90] and oxynitride compounds [91]. In this study this route was used for synthesizing borides and $Na_2B_{29}$ was obtained without using elemental sodium. It is described in the literature [20] that an excess of sodium is always required for the synthesis of sodium borides such as $Na_2B_{29}$. However, here we received this compound without adding elemental sodium to the starting mixture.

### 3.4.2 $Li_2[B_{10}H_{10}]$ as a precursor to synthesize $Li_2B_9$

The precursor material of $Li_2[B_{10}H_{10}]$ was prepared by cation exchange of bis-(triethylammonium) decahydrodecaborate $[(C_2H_5)_3NH]_2[B_{10}H_{10}]$ and $LiOH \cdot H_2O$ (Fluka) [92, 93]. $[(C_2H_5)_3NH]_2[B_{10}H_{10}]$ was prepared by reaction between decaborane $B_{10}H_{14}$ and triethylamine $Et_3N$ in xylene [94]. The product $Li_2[B_{10}H_{10}]$ is hygroscopic in nature. To obtain dry powder, it was dried at high vaccum at $6 \times 10^{-5}$ mbar or washed with liquid ammonia. The comparison of X-ray powder diffractogram and reflection position from Johnson *et al.* [92] is shown in figure 3.17. The crystal structure of this compound is not known.

An empty boron nitride crucible was heated at 1273 K in a quartz tube under vacuum of $6 \times 10^{-3}$ mbar for 16 hours. Approximately 0.2 g of $Li_2[B_{10}H_{10}]$ powder
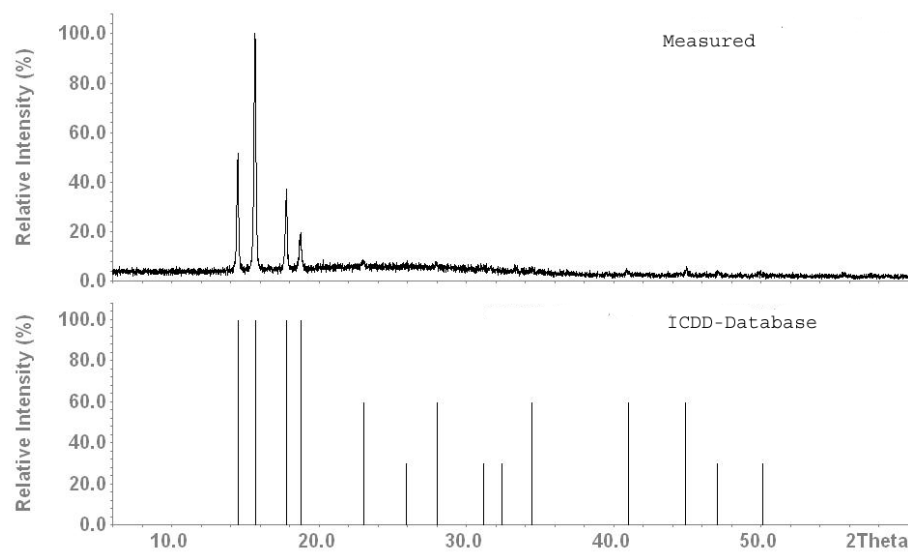
Figure 3.17: Comparison between measured X-ray powder diffractogram (top) and reflection positions from literature [92] (bottom)

was put in this crucible and thermally treated at 973 K for 1 hour under vacuum of $8 \times 10^{-3}$ mbar. The heating rate was initially 2 K/min till 573 K followed by 5 K/min till 973 K. It was then cooled to room temperature within 1 hour. A brown powder was obtained in the above reaction process. To 0.144 g (13 mmol) of the brown powder, 0.039 g (5 mmol) of Li was added into the boron nitride crucible. The crucible was put inside a tantalum tube and the tantalum tube was sealed under argon by arc-welding. The sealed tantalum tube was placed in a sealed evacuated quartz ampoule. The ampoule was then placed in an oven at 1073 K, with heating rate of 5 K/min. It was kept at this temperature for 8 days and then cooled to room temperature, with a rate of 5 K/min. A brown/gray powder was obtained which was then characterized by x-ray diffraction. The measured x-ray diffractogram was compared to the diffractogram obtained via elemental route and are shown in figure 3.18.

### 3.4.3 $Na_2[B_{10}H_{10}]$ as a precursor to synthesize $Na_3B_{20}$

The starting material $Na_2[B_{10}H_{10}]$ was prepared by cation exchange of bis (triethy-lammonium) decahydrodecaborate $[(C_2H_5)_3NH]_2[B_{10}H_{10}]$ and NaOH (Fluka). Approximately 0.2 g of $Na_2[B_{10}H_{10}]$ powder was put in a previously heated boron nitride crucible and thermally treated at 973 K for 1 hour under vacuum of $6 \times 10^{-3}$ mbar.
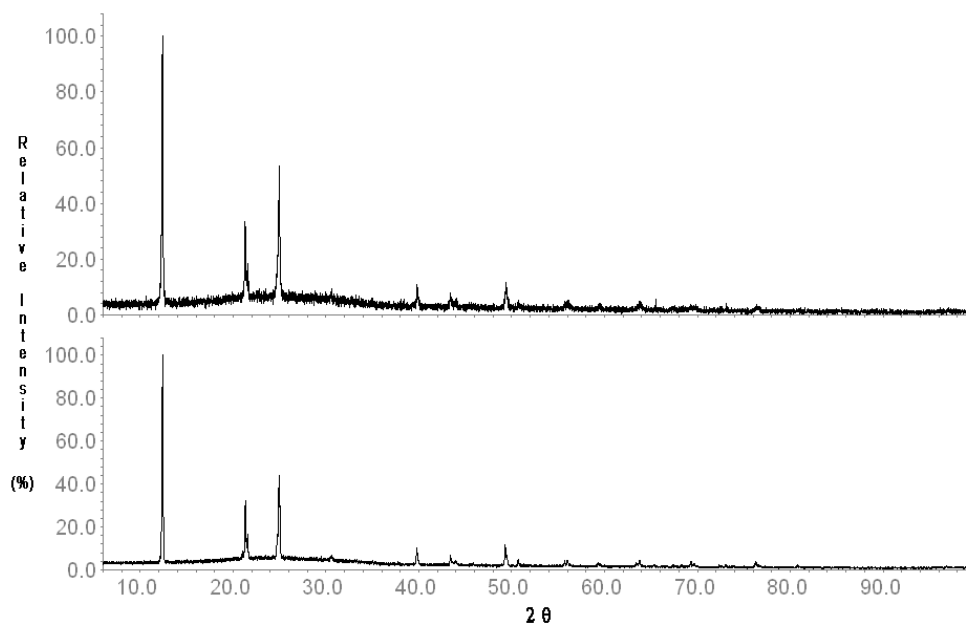
Figure 3.18: Comparison of the X-ray powder diffractograms of the products $Li_2B_9$ from the precursor route (top) and elemental route(bottom)

The heating rate was initially 2 K/min till 573 K followed by 5 K/min till 973 K. It was cooled to room temperature within 1 hour. A black powder was obtained in the above reaction process. To 0.103 g of the black powder, 0.2 g of Na was added into the boron nitride crucible. The crucible was put inside a tantalum tube and the tantalum tube was sealed under argon by arc-welding. The sealed tantalum tube was placed in a sealed quartz ampoule under vacuum. The ampoule was placed in an oven at 1273 K, kept at this temperature for 3 h and quenched to room temperature. After the reaction, the excess of sodium was removed by distillation at $6 \times 10^{-3}$ mbar at 623 K. A bluish black powder was obtained which was later characterized by x-ray diffraction.

### 3.4.4 X-ray diffraction of $Na_3B_{20}$

The obtained powders were characterized by the powder X-ray method. The X-ray diffraction data were collected at room temperature in the laboratory.

A Rietveld refinement was performed using the laboratory data. A pseudo-Voigt peak shape was used with a nineteen term cosine fourier series background function. Structural refinement was performed using the $Na_3B_{20}$ model as the initial model. Three experimental reflections ($2\theta = 30.66°$, $37.85°$, $43.26°$) were excluded as the re-

flections of the model do not agree with those of the experiment. Figure 3.19 shows the Rietveld fit and difference profile. The boron-boron bond distances and angles are also comparable to the reported structure model. The final refinement parameters are given in the table 3.7. The position and thermal displacement parameters of the atoms are shown in the table 3.8.

| | |
|---|---|
| Diffractometer | STOE Transmission Diffractometer (STADI-P) |
| Empirical formula | $Na_3B_{20}$ |
| Formula weight /g/mol | 285.37 |
| Crystal system | Orthorhombic |
| Space group | $Cmmm$ (No. 65) |
| $a$ /Å | 18.6782(5) |
| $b$ /Å | 5.6975(1) |
| $c$ /Å | 4.1457(1) |
| $V$ /Å$^3$ | 441.19(3) |
| X-ray source | $CuK_\alpha$ |
| Wave length /Å | 1.54056 |
| $2\theta$-Range /° | 6 -100 |
| Temperature /K | 298 |
| Estimated reflections | 422 |
| Generated reflections | 354 |
| Parameter | 43 |
| No. of background parameters | 19 |
| $R_p$ | 0.0610 |
| $R_{wp}$ | 0.0786 |
| $D_{wd}$ | 0.949 |
| $\chi^2$ | 1.737 |

Table 3.7: Crystal data and structure refinement parameters for $Na_3B_{20}$
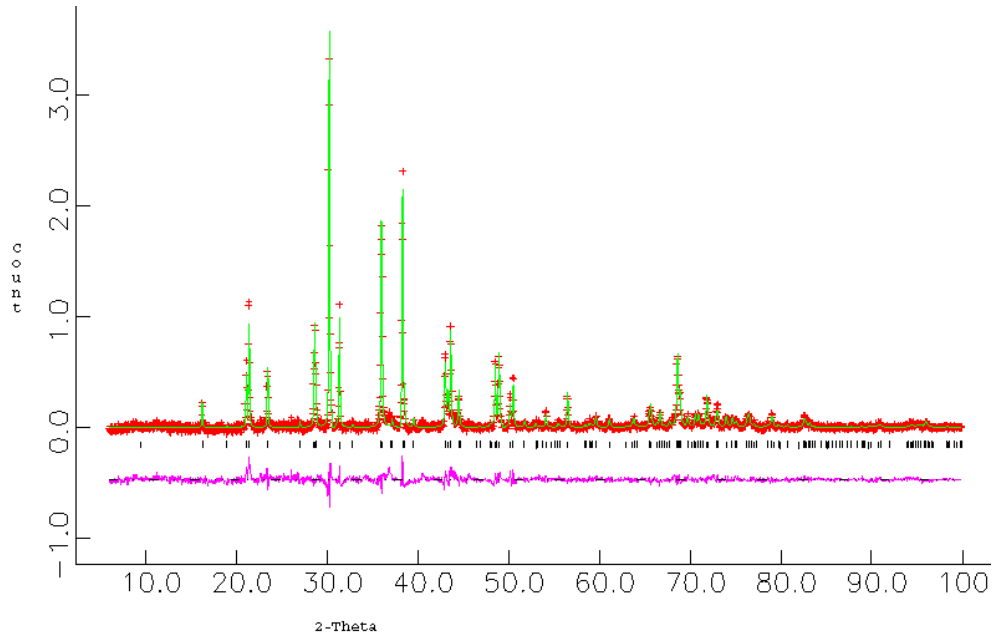
Figure 3.19: Observed (+) and calculated (solid line) powder diffraction pattern (corrected for the background) with the difference curve (bottom). The vertical dashes indicate the position of reflection

| Atom | Wyck. | $x/a$ | $y/b$ | $z/c$ | $U_{iso}$ |
|------|-------|-------|-------|-------|-----------|
| Na1 | 2a | 0 | 0 | 0 | 0.055(2) |
| Na2 | 4g | 0.8630(1) | 0.5 | 0 | 0.038(1) |
| B1 | 8o | 0.8263(3) | 0 | 0.2079(8) | 0.018(1) |
| B2 | 4l | 0 | 0.5 | 0.1980(2) | 0.016(3) |
| B3 | 8q | 0.9540(2) | 0.3427(7) | 0.5 | 0.016(2) |
| B4 | 8q | 0.8868(3) | 0.1491(7) | 0.5 | 0.015(2) |
| B5 | 8q | 0.7983(2) | 0.2245(9) | 0.5 | 0.016(2) |
| B6 | 4h | 0.7442(4) | 0 | 0.5 | 0.029(3) |

Table 3.8: Atomic co-ordinates, Wyckoff positions (Wyck.) and isotropic displacement parameters for $Na_3B_{20}$

### 3.4.5 Sodium azide NaN$_3$ as a precursor to synthesize Na$_2$B$_{29}$

Na$_2$B$_{29}$ was synthesized from 3 mmol (0.195 g) sodium azide NaN$_3$ (99.99 %, Sigma Aldrich) and 15 mmol amorphous boron (0.162 g) (1 micron, 99.99 %, Chempur). The powders were ground thoroughly, pressed into pellets measuring 10 mm diameter and 2-3 mm in height. The pellet was then dried under vaccum ($3 \times 10^{-3}$ mbar) at 423 K for 12 h and placed under argon in a tightly closed steel container described in 2.1.5.4. In flow of dry argon the following temperature treatment was applied : 298 K $\rightarrow$ 523 K (230 K/h) $\rightarrow$ 653 K (5 K/h) $\rightarrow$ 923 K (300 K/h). It was kept for 72 hours at 923 K and then cooled to 300 K following the temperature treatment 353 K/h. The product obtained was characterized using powder X-ray method. The product is an X-ray amorphous solid which is shown in figure 3.20
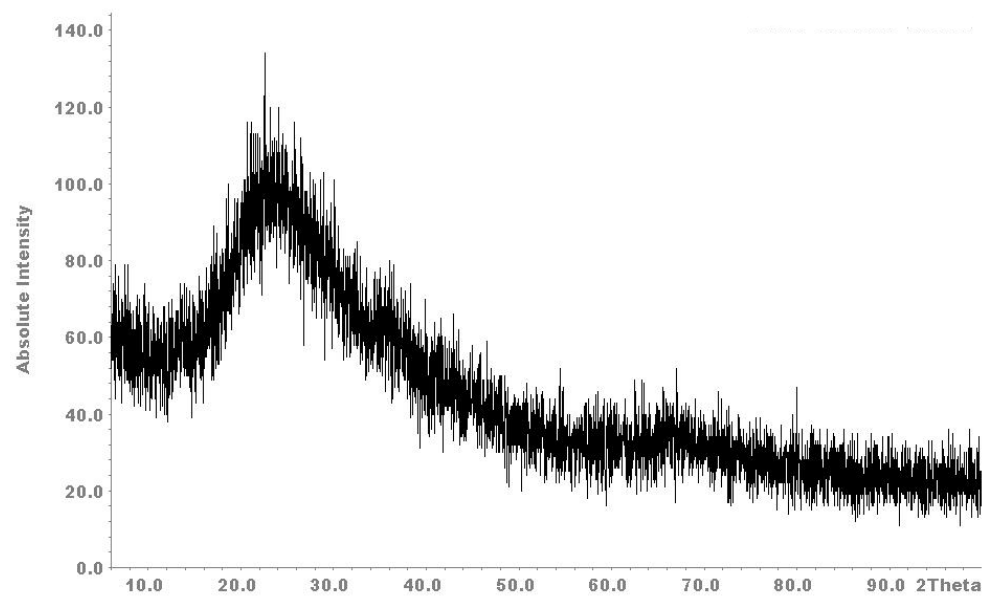


Figure 3.20: Powder pattern of a product of NaN$_3$ and B

The obtained X-ray amorphous solid was then further sintered in a sealed preboronated tantalum tube at 1673 K with a heating rate of 10 K/min and held at the reaction temperature for 2 hours. The reaction was carried out under constant argon flow. At the end of the heating period, the tube was cooled to room temperature following the temperature treatment of 10 K/min. The obtained product was characterized using powder X-ray diffraction. Figure 3.21 displays the crystalline Na$_2$B$_{29}$.
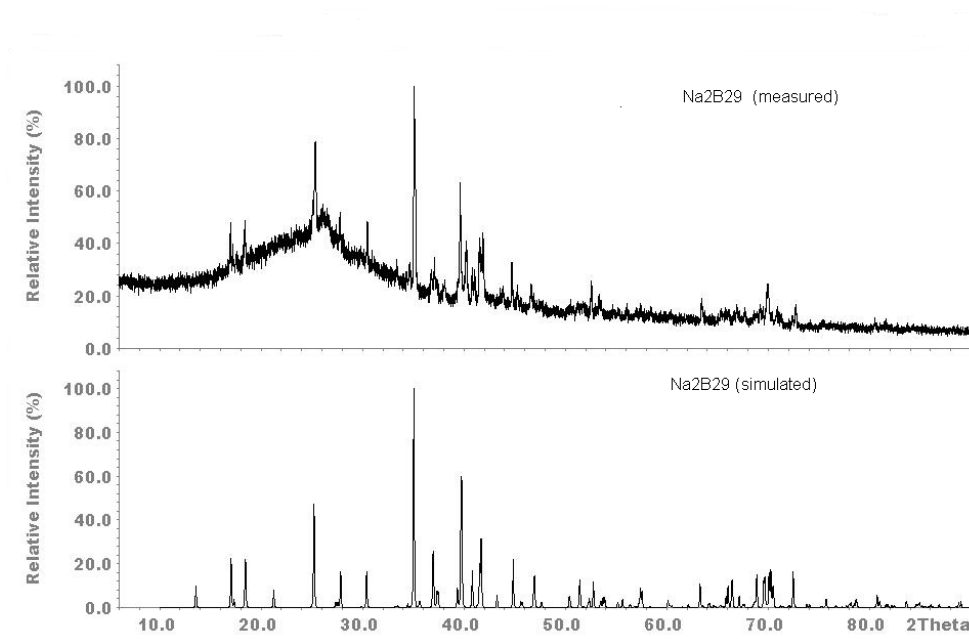
Figure 3.21: Powder XRD of measured $Na_2B_{29}$ (top) and simulated $Na_2B_{29}$ (bottom)

## 3.5 Concluding remark

The goal was to synthesize a single phase, homogeneous and ultrapure binary boron-rich boride with expected chemical formula $Li_2B_9$ and to solve the crystal structure (previously described in $P6/mmm$). The required compound was successfully synthesized from the elements as well as from a precursor such as $Li_2B_{10}H_{10}$. The product was always inhomogeneous and could be separated mechanically by colour difference of the sample (*i.e.* gray and brown). The gray part of the product was proved to be more crystalline than the brown part. Washing the products with ammonia proved that the gray part of the sample does not contain any elemental lithium whereas the brown part does. EEL spectroscopy was carried out for several samples and most of the studied sample were proved to be pure (*i.e.* in the absence of oxygen). The ELNES supports the probability of B-atom octahedra from the near-edge range analysis. Analysis of the synchrotron X-ray diffraction measurement and indexing of the powder diffractogram suggests the reduction of symmetry and was successfull in the orthorhombic crystal system with $a = 14.221(6)$ Å, $b = 8.330(2)$ Å and $c = 8.250(2)$ Å. Bärnighausen group-subgroup relationships help to reduce the structure model from $P6/mmm$ to *Cmcm, Cccm, Immm, Ibam* or *Ibmm.* The crystal structure was described in the space group *Ibmm* as it gives best results

74

in terms of the localization of the lithium atoms and $R$ values. According to the impedance data this compound exhibits ionic mobility at elevated temperature. The average activation energy of the compound was found to be 38.5 kJ/mol. $LiB_{13}$ was synthesized and the crystal structure was verified in the space group $R\bar{3}m$.

Sodium borides such as $Na_2B_{29}$ and $Na_3B_{20}$ were synthesized from precursors such as sodium azide and sodium decahydro-*closo*-decaborate, respectively.

# 4 *Closo*-Hydroborate chemistry in liquid ammonia

## 4.1 Literature survey and motivation

The history of *closo*-hydroborates $[B_nH_n]^{2-}$ (n = 5 to 12) is almost half a century old. MO-LCAO calculations by Higgins *et al.* in 1955 [95] predicted *closo*-hydroborates to be stable only as dianions. Among these series of boronates, the smallest stable unit was experimentally found to be the $[B_6H_6]^{2-}$ cluster, when the compound $[N(CH_3)_4]_2[B_6H_6]$ [96] was synthesized in 1964. Though several decades have been passed, crystal structures of only few compounds containing the $[B_6H_6]^{2-}$ anion are known such as $M_2[B_6H_6]$ ( M = Cs, K) [97]. The largest unit in the $[B_nH_n]^{2-}$ series is the dodecahydro-*closo*-dodecaborate anion $[B_{12}H_{12}]^{2-}$, which was experimentally verified by Hawthorne and Pitochelli in 1960, when this anion was prepared as the side product of the reaction of 2-iododecaborane and triethylamine in refluxing benzene [96]. Up to now the crystal structure of compounds like $M_2[B_{12}H_{12}]$ ( M = K, Rb, Cs) [98–100], $M_2[B_{12}H_{12}]\cdot xH_2O$ ( M = Ca, Sr, Ba) (x = 6, 7, 8) [101, 102], $Na_2[B_{12}H_{12}]\cdot 4\,H_2O$ [103], $K_2[B_{12}H_{12}]\cdot KBr$ [104] $[(C_2H_5)_2NH]_2[B_{12}H_{12}]$ [105], $[(CH_3)_2NH]_2[B_{12}H_{12}]\cdot 2\,DMF$ [106] are known. In between these two units there is one more popular and stable unit, the $[B_{10}H_{10}]^{2-}$ cluster, which is known since 1959, when bis(tetramethylammonium)-decahydrodecaborate $[N(CH_3)_4]_2[B_{10}H_{10}]$ [107] was synthesized. In this case the crystal structure of the following compounds are known: $[(C_5H_5)Fe(C_5H_4CH_2N(CH_3)_3]_2[B_{10}H_{10}]$ [108], $[C_{10}H_9N_2]_2[B_{10}H_{10}]$ [109, 110], $C_{10}H_{10}N_2[B_{10}H_{10}]$ [109, 110], $[(CH_3)_3NH]_2[B_{10}H_{10}]$ [106], $[(C_5H_5N)_2NH_2]_2[B_{10}H_{10}]$ [111], $[(C_2H_5)_3NH]_2[B_{10}H_{10}]$ [112], $[P(C_2H_5)_3NH_2]_2[B_{10}H_{10}]$ [113], $M_2[B_{10}H_{10}]$( M = Na, K, Rb) [114], $[(C_5H_5)_2NH_2]_2[B_{10}H_{10}]\cdot 2\,H_2O$ [115], $[Rb_2[B_{10}H_{10}]\cdot 1\cdot 5\,H_2O$ [116] $[(C_6H_5)_3P)_2Cu]_2[B_{10}H_{10}]\cdot CHCl_3$ [117]. In this work compounds of these three anions were synthesized.

Although *closo*-hydroborate chemistry has been known for a long period, crystal

structures of very few compounds were known containing alkali metal cations. Most of the structurally known solvent-free hydroborates are stabilized by large organic or heavy alkali metal cations. Up to now there is no compound reported with a light element like lithium.

In this work, for the first time liquid ammonia was used both as a solvent and reactant to explore the chemistry of *closo*-hydroborates. The objective of this study is to synthesize and characterize *closo*-hydroborates as ammoniates like $M_2[B_nH_n] \cdot xNH_3$ (single/multi cationic compound). So far only one multi cationic alkali metal compound $Cs[Na(NH_3)_6][B_{10}H_{10}] \cdot NH_3$ [118] had been successfully synthesized and characterized. Further a careful removal of ammonia might lead to new solvent free, crystalline hydroborates which can be used as precursors for metal borides. These *closo*-hydroborate compounds contain the same kind of polyhedron found in borides such as $Na_2B_{29}$ [20], $Li_2B_6$ [5], $Na_3B_{20}$ [18], $Li_3B_{14}$ [3].

## 4.2 Alkali metal compounds containing the $[B_6H_6]^{2-}$ anion

As described in the literature [119], the synthesis of compounds with the $[B_6H_6]^{2-}$ anion is extremely difficult due to low yields and the instability of the salts in acidic media. $[N(C_4H_9)_4][B_6H_6H^{fac}]$ was synthesized from $NaBH_4$ and $BF_3 \cdot O(C_2H_5)_2$ in diglyme according to literaure procedure [120]. In this work, $[N(C_4H_9)_4][B_6H_6H^{fac}]$ was used as starting materials.

$[B_6H_6]^{2-}$ is a regular octahedron with point symmetry $O_h$ (see in fig. 4.1). It consists of six boron atoms surrounded by a larger octahedron of six hydrogen atoms. Earlier, the octahedral structure has been confirmed by X-ray diffraction of its salts, as well as by NMR and vibrational spectroscopy for the solution state. The localization of $H^{fac}$ for the protonated $[B_6H_6H^{fac}]$ form has also been confirmed by X-ray analysis of its salt $[Ni(bipy)_3][B_6H_6H^{fac}]$ [121] and $[N(C_4H_9)_4][B_6H_6H^{fac}]$ [122] and NMR analysis of the solution. In the solid state the $H^{fac}$ atom is located above one of the octahedron's facets and in solution it fluctuates across the octahedron's surface via the edges.
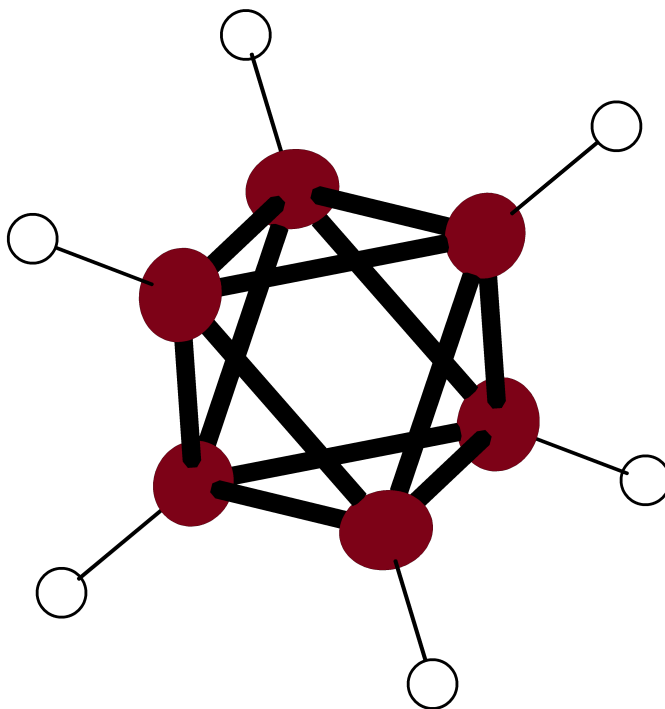


Figure 4.1: $[B_6H_6]^{2-}$ unit

Using ammonia as a solvent, it was possible to synthesize and structurally characterize ammoniates of lithium and sodium containing *closo*-hydroborates such as $[Li(NH_3)_4]_2[B_6H_6] \cdot 2\,NH_3$ and $[Na(NH_3)_4]_2[B_6H_6] \cdot 2\,NH_3$. It was also possible to obtain a single crystal of $[N(C_4H_9)_4]_2[B_6H_6]$. The crystal structures of all these compounds are described here.

## 4.2.1 Synthesis and characterization of Bis-(tetraamminelithium)-hexahydro-*closo*-hexa--borate- ammonia (1/2) $[Li(NH_3)_4]_2[B_6H_6] \cdot 2\,NH_3$

### 4.2.1.1 Synthesis

All the synthetic work was performed using Schlenk glassware and techniques. $[Li(NH_3)_4]_2[B_6H_6] \cdot 2\,NH_3$ was synthesized from dry $[N(C_4H_9)_4][B_6H_6H^{fac}]$ and distilled lithium. $[N(C_4H_9)_4][B_6H_6H^{fac}]$ was dried at room temperature for 18 h at $3 \times 10^{-3}$ mbar. 0.012 g (1.6 mmol) of distilled lithium and 0.092 g (1.6 mmol) of $[N(C_4H_9)_4][B_6H_6H^{fac}]$ were placed in a Schlenk tube and the evacuated vessel was cooled by a dry ice/ isopropanol slush. Approximately 20 mL of liquid ammonia was condensed into the tube through a vacuum line, yielding a blue solution of alkali metal. It was then stored at 235 K for 10 days resulting in colorless crystals in the shape of cubes. A crystal (0.22 mm × 0.17 mm × 0.14 mm) was measured on the diffractometer.

### 4.2.1.2 X-ray investigation

Single crystals were handled in perfluorinated inert oils and diffraction data were collected at 123 K. Numerical absorption correction was carried out in the Laue class $2/m$. Systematic extinctions were determined and suggested the possible space group as $P2_1/c$. The structure was solved by direct methods in this space group and refined against $F^2$. All the atoms (including hydrogen) were localized by Fourier cycling methods and their thermal displacement parameters were refined isotropically, those of the non-hydrogen atoms could also be refined anisotropically. To verify the selection of the space group $P2_1/c$, searches for additional symmetry were performed using the structure model without hydrogen atoms by the program PLATON [123], which stated the correctness of the assignment. Crystallographic data and details of data collection are given in table 4.1.

| | |
|---|---|
| Empirical formula | $H_{36}B_6Li_2\,N_{10}$ |
| Formula weight /g/mol | 255.10 |
| Crystal system | Monoclinic |
| Space group | $P2_1/c$ (No. 14) |
| $a$ /Å | 7.4793(8) |
| $b$ /Å | 11.864(1) |
| $c$ /Å | 10.596(1) |
| $\beta$ /° | 95.371(2) |
| $V$ /Å$^3$ | 936.1(2) |
| $Z$ | 2 |
| $\rho_c$ /g/cm$^3$ | 0.905 |
| Wave length /Å | 0.71073 |
| Detector distance /mm | 60 |
| $\omega$- Increment | 0.3° |
| Temperature /K | 123 |
| $F(000)$ | 284 |
| $\mu(\mathrm{MoK}_\alpha)$ /mm$^{-1}$ | 0.06 |
| $\theta$-Range | 2.37° to 28.02° |
| Collected reflections | 11260 |
| Unique reflections | 2211 |
| Reflections with I $>4\sigma$ (I) | 1213 |
| $R_{int}$ | 0.0608 |
| $h$ | -9 to 9 |
| $k$ | -15 to 15 |
| $l$ | -13 to 13 |
| Refinement method | Full-matrix least-squares on F$^2$ |
| Final $R$ indices [I>4$\sigma$(I)] | $R_1 = 0.0453$ |
| $R$ indices (all data) | $R_1 = 0.0878$, $wR_2 = 0.0903$ |
| Goodness-of-fit (S) | 0.814 |
| Number of parameters | 154 |
| $w=1/[\sigma^2(\mathrm{Fo}^2)+(0.0285\mathrm{P})^2+0.0000\mathrm{P}]$ | |
| P=(Fo$^2$+2Fc$^2$)/3 | |
| $\Delta\rho_{max}$ /eÅ$^{-3}$ | 0.23 |
| $\Delta\rho_{min}$ /eÅ$^{-3}$ | -0.12 |

Table 4.1: Crystal data and structure refinement for $[\mathrm{Li(NH_3)_4}]_2[\mathrm{B_6H_6}]\cdot 2\,\mathrm{NH_3}$

### 4.2.1.3 Description of the crystal structure

$[\mathrm{Li(NH_3)_4}]_2[\mathrm{B_6H_6}]\cdot 2\,\mathrm{NH_3}$ crystallizes in a monoclinic crystal system with two formula units per unit cell. The asymmetric unit contains one lithium atom, three boron atoms, three hydrogen atoms and five ammonia molecules. All atoms are situated at general positions $4e$. All the atomic co-ordinates and thermal displacement parameters are shown in tables 4.2 and 4.3. The asymmetric unit is shown in figure 4.2.
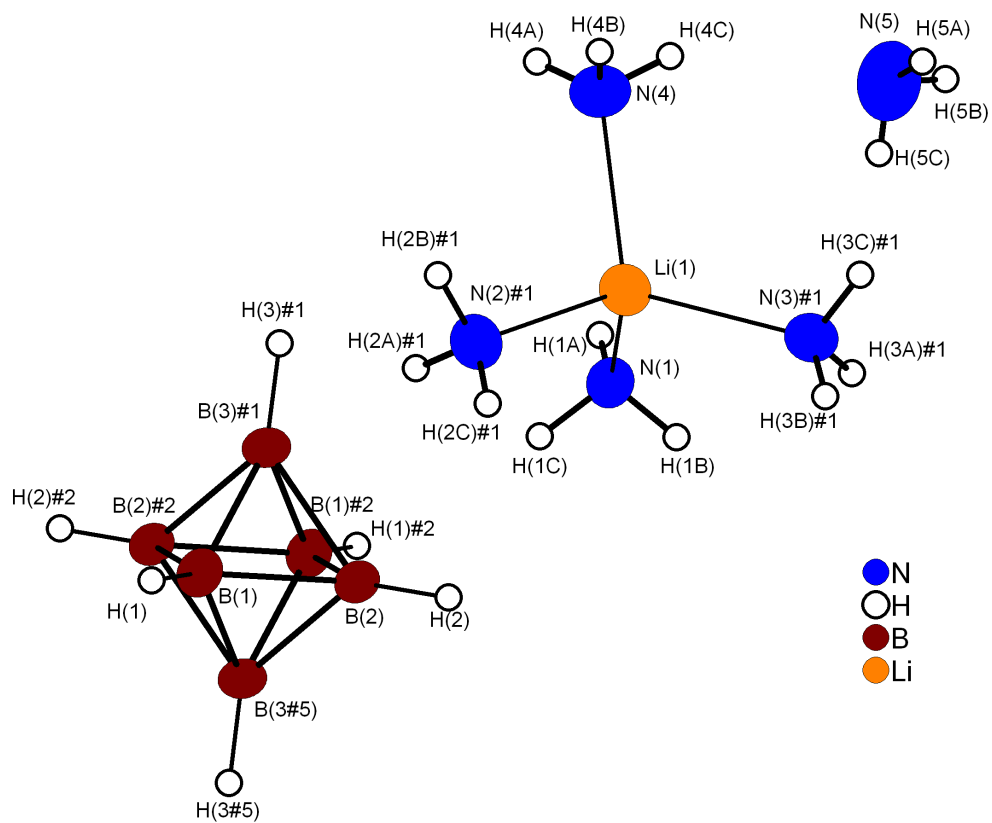
Figure 4.2: Asymmetric unit of $[\text{Li}(\text{NH}_3)_4]_2[\text{B}_6\text{H}_6] \cdot 2\,\text{NH}_3$. Ellipsoids of the thermal displacement parameters are drawn at 70 % probability

| Atom | Wyck. | x /a | y /b | z /b | $U_{eq}$ |
|------|-------|------|------|------|------|
| N1 | 4e | 0.4938(2) | 0.1618(1) | 0.0342(2) | 0.0274(3) |
| H1A | 4e | 0.491(2) | 0.200(1) | - 0.034(1) | 0.047(6) |
| H1B | 4e | 0.589(2) | 0.114(2) | 0.035(1) | 0.057(6) |
| H1C | 4e | 0.396(2) | 0.114(1) | 0.029(1) | 0.066(6) |
| N2 | 4e | 0.2531(2) | 0.2914(1) | -0.2102(1) | 0.0313(4) |
| H2A | 4e | 0.181(2) | 0.318(1) | -0.274(1) | 0.043(5) |
| H2B | 4e | 0.192(2) | 0.232(2) | -0.182(1) | 0.062(6) |
| H2C | 4e | 0.260(2) | 0.342(1) | -0.148(2) | 0.069(7) |
| N3 | 4e | 0.7268(1) | 0.2848(1) | -0.1997(1) | 0.0327(4) |
| H3A | 4e | 0.797(2) | 0.3189(1) | -0.256(2) | 0.063(6) |
| H3B | 4e | 0.737(2) | 0.333(2) | -0.136(2) | 0.068(7) |
| H3C | 4e | 0.788(2) | 0.228(2) | -0.166(1) | 0.052(5) |
| N4 | 4e | 0.4480(2) | 0.4221(1) | 0.1567(2) | 0.0385(4) |
| H4A | 4e | 0.369(2) | 0.448(1) | 0.098(2) | 0.056(6) |
| H4B | 4e | 0.434(3) | 0.459(2) | 0.222(2) | 0.086(8) |
| H4C | 4e | 0.550(3) | 0.452(2) | 0.134(2) | 0.100(9) |
| N5 | 4e | 0.8705(3) | 0.4296(2) | 0.0890(2) | 0.0503(5) |
| H5A | 4e | 0.903(2) | 0.450(2) | 0.164(2) | 0.065(7) |
| H5B | 4e | 0.957(5) | 0.430(3) | 0.054(3) | 0.212(2) |
| H5C | 4e | 0.859(4) | 0.366(2) | 0.087(3) | 0.147(2) |
| B1 | 4e | -0.0938(2) | -0.0046(1) | 0.0872(2) | 0.0243(4) |
| H1 | 4e | -0.1770(2) | -0.0079(2) | 0.1678(1) | 0.033(4) |
| B2 | 4e | 0.1321(2) | -0.0122(1) | 0.0738(1) | 0.0219(4) |
| H2 | 4e | 0.249(2) | -0.0221(9) | 0.140(1) | 0.027(4) |
| B3 | 4e | 0.0114(2) | 0.3984(1) | -0.4873(2) | 0.0239(4) |
| H3 | 4e | 0.0246(2) | 0.3067(2) | -0.4739(1) | 0.032(4) |
| Li | 4e | 0.4809(3) | 0.2508(2) | 0.1983(2) | 0.0299(6) |

Table 4.2: Atomic co-ordinates and equivalent thermal displacement parameters for
$[\mathrm{Li(NH_3)_4}]_2[\mathrm{B_6H_6}] \cdot 2\,\mathrm{NH_3}$

| Atom | U11 | U22 | U33 | U23 | U13 | U12 |
|------|-----|-----|-----|-----|-----|-----|
| N1 | 0.0257(8) | 0.0300(8) | 0.0266(8) | 0.0008(6) | 0.0027(6) | 0.0017(7) |
| N2 | 0.0310(8) | 0.0346(8) | 0.0282(9) | 0.0080(7) | 0.0016(7) | 0.0017(7) |
| N3 | 0.0350(9) | 0.0265(8) | 0.0351(9) | 0.0060(7) | -0.0047(7) | 0.0012(7) |
| N4 | 0.044(1) | 0.0312(8) | 0.039(1) | -0.0008(8) | -0.0018(8) | 0.0010(8) |
| N5 | 0.046(1) | 0.0719(1) | 0.033(1) | -0.0104(9) | 0.0046(8) | 0.0052(9) |
| B1 | 0.0234(9) | 0.0274(9) | 0.0225(9) | 0.0005(7) | -0.0007(7) | 0.0025(7) |
| B2 | 0.0239(9) | 0.0204(9) | 0.0207(9) | -0.0005(7) | 0.0063(8) | -0.0030(8) |
| B3 | 0.0280(9) | 0.0182(8) | 0.0247(9) | -0.0002(7) | -0.0011(7) | -0.0013(7) |
| Li | 0.0305(1) | 0.0300(1) | 0.0292(1) | -0.0034(1) | 0.0028(1) | -0.0011(1) |

Table 4.3: Anisotropic thermal displacement parameters for
$[\mathrm{Li(NH_3)_4}]_2[\mathrm{B_6H_6}] \cdot 2\,\mathrm{NH_3}$
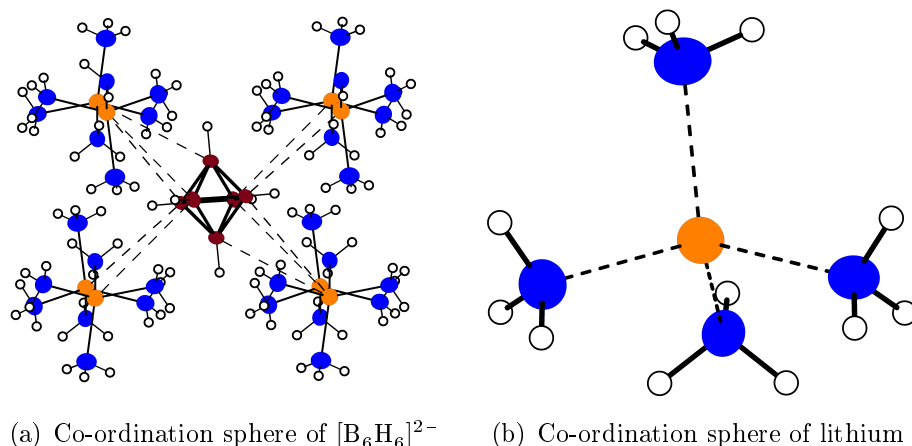
(a) Co-ordination sphere of $[B_6H_6]^{2-}$  (b) Co-ordination sphere of lithium

Figure 4.3: Co-ordination sphere of the $[B_6H_6]$ anion and the lithium cation. Ellipsoids of the thermal displacement parameters are drawn at 70 % probability

The hexahydro-*closo*-hexaborate cage is built up by three boron and three hydrogen atoms and their symmetry equivalents respectively, forming the well-known shape of $[B_6H_6]^{2-}$ similar to an octahedron. The bond lengths of B-B and B-H are shown in the table 4.4. B-B-B bond angles vary between 89.8(1)° and 90.2(1)° in the boron square plane and between 59.78(8)° and 60.2(1)° in the boron triangle of the octahedron cage. All the apical boron atoms are centered within 0.2° and located about 1.214 Å above a r.m.s. plane through their corresponding boron square plane. The $[B_6H_6]^{2-}$ cluster is surrounded by eight symmetry equivalent tetraammine lithium complexes with Li-B distances in the range from 4.25 to 4.82 Å. The lithium cation is coordinated by four molecules of ammonia yielding almost a tetrahedron, shown in figure 4.3. The Li-N bond lengths extend from 2.045(3) to 2.098(3) Å in the range of the sum of the covalent radii (2.09 Å) [124] indicating the presence of covalent Li-N bonding. Three types of N-H···N hydrogen bonds are found in an asymmetric unit. The N(1)-H(1A)···N(2) hydrogen bond is formed by two symmetry equivalent tetraammine lithium ions, and is responsible for a zig-zag chain running along the *c*-axis as shown in figure 4.4. The N(4)-H(4C)···N(5) hydrogen bond connects an isolated ammonia molecule with one of the nitrogen atom of a tetraammine lithium cation. The third type of N-H···N bond is formed between two isolated ammonia molecules. These latter type of hydrogen bond is responsible for the cross linking of the zig-zag chains. Selected bond lengths (in Å) and angles (in °) responsible for hydrogen bonds are as follows:

(a) Hydrogen bonding in asymmetric unit     (b) Projection of chains in *bc*-plane
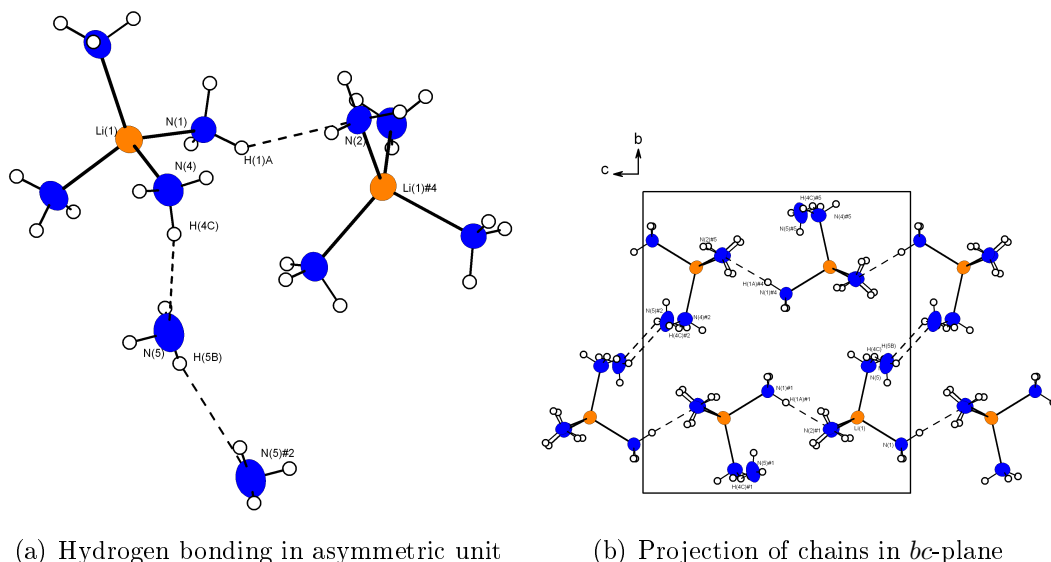
Figure 4.4: Hydrogen bonded zig-zag chains of $[\mathrm{Li(NH_3)_4}]$. Symmetry transformations to generate equivalent atoms: $\#2 = -x, -y, -z$. Thermal ellipsoids at 70 % probability

N(1)-H(1A) 0.85(2), N(2)$\cdots$ H(1A) 2.687, N(1)-H(1A)$\cdots$ N(2) 140.17; N(4)-H(4c) 0.90(2), N(5)$\cdots$ H(4c) 2.499, N(4)-H(4c)$\cdots$ N(5) 149.85 and N(5)-H(5B) 0.78(3), N(5)#2 $\cdots$H(5B) 2.663, N(5)-H(5B)$\cdots$N(5)#2 138.37. The primitive unit cell of $[\mathrm{Li(NH_3)_4}]_2[\mathrm{B_6H_6}] \cdot 2\,\mathrm{NH_3}$ is shown in figure 4.5, where $[\mathrm{B_6H_6}]^{2-}$ clusters are located in the center of the *bc*-plane as well as at the corners of the unit cell. The rest of the unit cell is occupied by tetraammine lithium ions and ammonia molecules.

| Bond | Length /Å | Bond | Length /Å |
|------|-----------|------|-----------|
| B(1)-B(2) | 1.711(2) | B(3)-B(2)#3 | 1.717(2) |
| B(1)-B(2)#2 | 1.715(2) | B(3)-B(1)#3 | 1.716(2) |
| B(1)-B(3)#5 | 1.716(2) | B(3)-B(2)#4 | 1.716(2) |
| B(1)-B(3)#1 | 1.717(2) | B(3)-B(1)#4 | 1.717(2) |
| B(2)-B(3)#5 | 1.712(2) | B(1)-H(1) | 1.103(1) |
| B(2)-B(1)#2 | 1.715(2) | B(2)-H(2) | 1.079(1) |
| B(2)-B(3)#1 | 1.716(2) | B(3)#1 -H(3)#1 | 1.102(1) |

Table 4.4: Bond lengths in $[\mathrm{B_6H_6}]^{2-}$
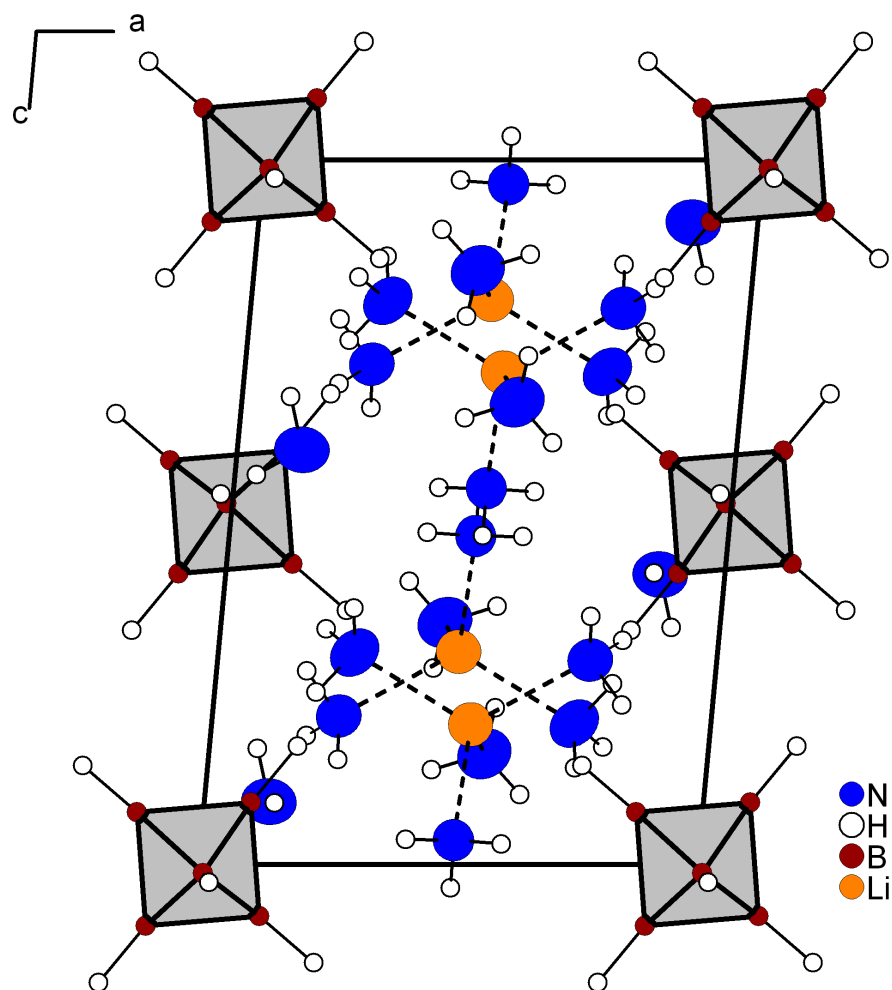
Figure 4.5: Crystal structure of $[\mathrm{Li(NH_3)_4}]_2[\mathrm{B_6H_6}] \cdot 2\,\mathrm{NH_3}$. The arrangement of the boron atoms is shown as polyhedrons. Ellipsoids of the thermal displacement parameters are drawn at 70 % probability

## 4.2.2 Synthesis and characterization of Bis-(tetraamminesodium)-hexahydro-*closo*-hexaborate- ammonia (1/2) $[\mathrm{Na(NH_3)_4}]_2[\mathrm{B_6H_6}] \cdot 2\,\mathrm{NH_3}$

### 4.2.2.1 Synthesis

The synthetic work was carried out using Schlenk glassware and inert gas techniques. $[\mathrm{Na(NH_3)_4}]_2[\mathrm{B_6H_6}] \cdot 2\,\mathrm{NH_3}$ was synthesized from dry $[(\mathrm{N(C_4H_9)_4})][\mathrm{B_6H_6H^{fac}}]$ and distilled sodium. $[(\mathrm{N(C_4H_9)_4})][\mathrm{B_6H_6H^{fac}}]$ was dried at room temperature for 18 h in $3\times10^{-3}$ mbar. 0.277 g (0.05 mmol) of $[(\mathrm{N(C_4H_9)_4})][\mathrm{B_6H_6H^{fac}}]$ and 0.057 g (2.5 mmol) of distilled sodium were placed in a prepared Schlenk tube and the evacuated vessel was cooled by a dry ice/isopropanol slush. Approximately 20 mL of liquid ammonia was condensed into the tube through a vacuum line yielding a blue solution of alkali metal. It was then stored at 235 K for 25 days resulting colorless crystals in the form of thin plates. Compare to all the discussed crystals, these crystals are more sensitive to air, moisture and temperature. Above the temperature of liquid ammonia, the crystals loose ammonia and decompose. Therefore, it was not possible to measure more than one crystal. The main problem behind not being able to measure more than one crystal is the shape and sensitivity of these crystal. Though it is possible to see the nice crystals under the microscope, during the process of transfer to the goniometer head, it falls apart. Therefore, an improved technique for crystal handling might be necessary. Though not a very good crystal, but for a single time it was possible to measure a crystal (0.41 mm × 0.19 mm × 0.17 mm) on the diffractometer.

### 4.2.2.2 X-ray investigation

Crystallographic details of data collection and refinement parameters are given in table 4.5. Systematic extinctions of the data led to the possible space groups as $P2_1$ or $P2_1/m$ . The structure was solved by direct methods in the non-centrosymmetric space group $P2_1$. It was refined in this space group by a full-matrix least-squares procedure, which yielded a chemically reasonable structure. All the non-hydrogen atoms were localized by Fourier cycling methods and refined anisotropically in the asymmetric unit. The positions of hydrogen atoms of the isolated ammonia molecules were refined freely and their thermal displacement parameter were refined isotropically, whereas the hydrogen atoms of the boron cluster and of the co-ordinating

ammonia molecules were placed on calculated positions using a "riding" model. The $R$ values obtained in this space group are not satisfactory. It was not possible to refine the structure in the space group $P2_1/m$ or $P2_1/c$ (isotypic with $[\mathrm{Li(NH_3)_4}]_2\mathrm{B_6H_6} \cdot 2\,\mathrm{NH_3}$). To confirm the selection of the space group $P2_1$, searches for additional symmetry were performed, which did not indicate further symmetries. Therefore, a preliminary structure model is described here in the space group $P2_1$.

It was observed that the structure appears as a superposition of two molecules, one at x, y, z and the other one at x+0.5, y, z. The contribution of the molecule at x+0.5, y, z is not big but influences two peaks in the difference map, that appears with incorrect intensities. To all reflections with h = 2n, the scale factor 1 was applied and to all reflections with h = 2n+1 the scale factor 2 was applied in the *hkl* file by a program developed by Michael Bolte (J. W. Goethe-Universität, Frankfurt). The scale factor 2 downweigths the structure factors with h = 2n+1. Then to the instruction file, the BASF (batch scale factor) 0.5 command was added.

| | |
|---|---|
| Empirical formula | $H_{36}B_6Na_2\,N_{10}$ |
| Formula weight /g/mol | 287.19 |
| Crystal system | Monoclinic |
| Space group | $P2_1$(No. 4) |
| $a$ /Å | 7.615(3) |
| $b$ /Å | 11.851(5) |
| $c$ /Å | 10.749(4) |
| $\beta$ /° | 100.28(1) |
| $V$ /Å$^3$ | 954.49(1) |
| $Z$ | 2 |
| $\rho_c$ /g/cm$^3$ | 1.536 |
| Wave length /Å | 0.71073 |
| Detector distance /mm | 60 |
| $\omega$- Increment | 0.3° |
| Temperature /K | 123 |
| $F(000)$ | 462 |
| $\mu(\mathrm{MoK}_\alpha)$ /mm$^{-1}$ | 0.12 |
| $\theta$-Range | 2.37° to 28.15° |
| Collected reflections | 8971 |
| Unique reflections | 2342 |
| Reflections with I >4$\sigma$ (I) | 1229 |
| $R_{int}$ | 0.0530 |
| $h$ | -10 to 9 |
| $k$ | 0 to 15 |
| $l$ | 0 to 14 |
| Refinement method | Full-matrix least-squares on F$^2$ |
| Final $R$ indices [I>4$\sigma$(I)] | $R_1 = 0.1006$ |
| $R$ indices (all data) | $R_1 = 0.1694$, $wR_2 = 0.3053$ |
| Goodness-of-fit (S) | 1.061 |
| Number of parameters | 196 |
| $w=1/[\sigma^2(\mathrm{Fo}^2)+(0.0285\mathrm{P})^2+0.0000\mathrm{P}]$ | |
| P=(Fo$^2$+2Fc$^2$)/3 | |
| $\Delta\rho_{max}$ /eÅ$^{-3}$ | 0.87 |
| $\Delta\rho_{min}$ /eÅ$^{-3}$ | -0.41 |

Table 4.5: Crystal data and structure refinement for $[\mathrm{Na(NH_3)_4}]_2[\mathrm{B_6H_6}]\cdot 2\,\mathrm{NH_3}$

### 4.2.2.3 Description of the crystal structure

$[\mathrm{Na(NH_3)_4}]_2[\mathrm{B_6H_6}]\cdot 2\,\mathrm{NH_3}$ crystallizes in a monoclinic crystal system with two formula units per unit cell. The asymmetric unit contains two sodium atoms, one hexahydro-*closo*-hexaborate unit and ten ammonia molecules. All atoms are situated at general positions 2*a*. All the atomic co-ordinates, isotropic and anisotropic thermal parameters are given in tables 4.6 and 4.7. The asymmetric unit is shown in the figure 4.6.
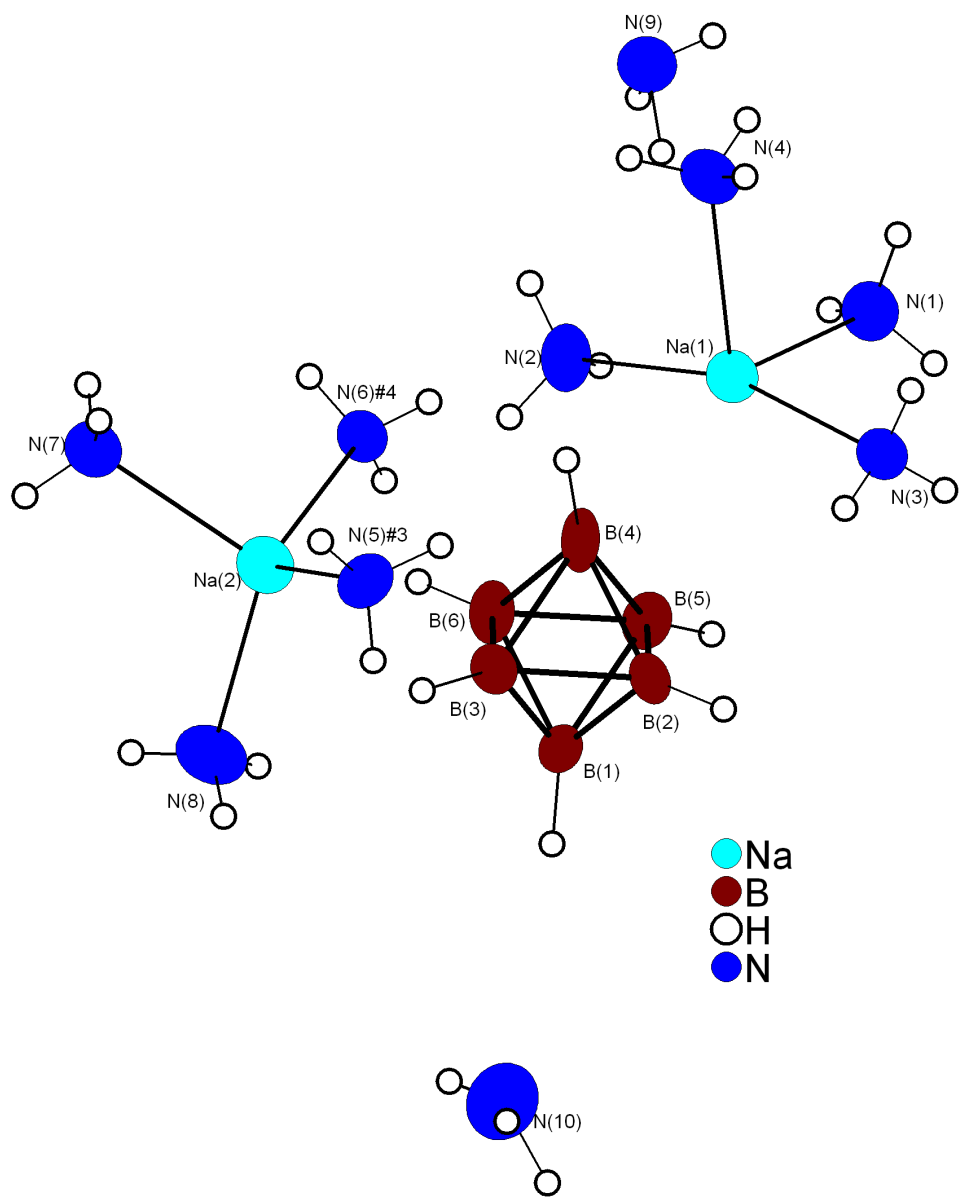
Figure 4.6: Asymmetric unit of $[\text{Na}(\text{NH}_3)_4]_2[\text{B}_6\text{H}_6] \cdot 2\,\text{NH}_3$. Ellipsoids of the thermal displacement parameters are drawn at 50 % probability. Symmetry transformations to generate equivalent atoms: $\#3 = -x+2, y+0.5, -z+2$, $\#4 = -x+1, y+0.5, -z+2$

| Atom | Wyck. | x /a | y /b | z /c | $U_{eq}$ |
|------|-------|------|------|------|----------|
| Na1 | 2a | 0.1321(5) | 0.4754(3) | 0.5740(3) | 0.0366(9) |
| Na2 | 2a | 1.0194(5) | 0.5032(3) | 1.0671(3) | 0.038(1) |
| B1 | 2a | 0.4499(2) | 0.1782(9) | 0.7619(9) | 0.031(1) |
| H1 | 2a | 0.45923 | 0.08431 | 0.77288 | 0.03669 |
| B2 | 2a | 0.5301(2) | 0.2746(9) | 0.6681(8) | 0.029(2) |
| H2 | 2a | 0.61440 | 0.26941 | 0.59292 | 0.03469 |
| B3 | 2a | 0.5709(2) | 0.2878(9) | 0.8304(9) | 0.028(2) |
| H3 | 2a | 0.69278 | 0.29563 | 0.90547 | 0.03347 |
| B4 | 2a | 0.4314(2) | 0.3841(1) | 0.7364(9) | 0.028(2) |
| H4 | 2a | 0.47079 | 0.47501 | 0.74897 | 0.03395 |
| B5 | 2a | 0.3049(2) | 0.2718(1) | 0.6688(9) | 0.030(2) |
| H5 | 2a | 0.19388 | 0.23107 | 0.60137 | 0.03552 |
| B6 | 2a | 0.3481(3) | 0.285(1) | 0.8301(9) | 0.031(2) |
| H6 | 2a | 0.26290 | 0.28938 | 0.90468 | 0.03681 |
| N1 | 2a | -0.1509(1) | 0.4710(9) | 0.4279(7) | 0.0412(2) |
| H1A | 2a | -0.23832 | 0.44662 | 0.46912 | 0.06298 |
| H1B | 2a | -0.14254 | 0.42326 | 0.36294 | 0.06298 |
| H1C | 2a | -0.17796 | 0.54161 | 0.39691 | 0.06298 |
| N2 | 2a | -0.0550(2) | 0.4364(8) | 0.7446(7) | 0.041(2) |
| H2A | 2a | -0.08034 | 0.50268 | 0.78028 | 0.06149 |
| H2B | 2a | 0.00728 | 0.39088 | 0.80505 | 0.06149 |
| H2C | 2a | -0.15850 | 0.40171 | 0.70916 | 0.06149 |
| N3 | 2a | 0.3423(2) | 0.4608(8) | 0.4215(7) | 0.043(2) |
| H3A | 2a | 0.44845 | 0.43246 | 0.46167 | 0.06414 |
| H3B | 2a | 0.35988 | 0.53044 | 0.39021 | 0.06414 |
| H3C | 2a | 0.29534 | 0.41411 | 0.35680 | 0.06414 |
| N4 | 2a | 0.2689(9) | 0.0598(7) | 1.0378(7) | 0.0312(2) |
| H4A | 2a | 0.25867 | 0.10013 | 1.10818 | 0.04679 |
| H4B | 2a | 0.32121 | 0.10330 | 0.98494 | 0.04679 |
| H4C | 2a | 0.33722 | -0.00243 | 1.06043 | 0.04679 |
| N5 | 2a | 0.7411(1) | 0.0561(7) | 1.0350(7) | 0.038(2) |
| H5A | 2a | 0.78542 | 0.08272 | 1.11377 | 0.05702 |
| H5B | 2a | 0.67093 | -0.00512 | 1.04131 | 0.05702 |
| H5C | 2a | 0.67504 | 0.11080 | 0.98921 | 0.05702 |
| N6 | 2a | 0.1483(2) | 0.6798(7) | 0.5923(8) | 0.040(2) |
| H6A | 2a | 0.24062 | 0.70568 | 0.55654 | 0.06007 |
| H6B | 2a | 0.16660 | 0.69963 | 0.67542 | 0.06007 |
| H6C | 2a | 0.04420 | 0.71060 | 0.55184 | 0.06007 |
| N7 | 2a | 1.0585(1) | 0.6229(7) | 1.2429(7) | 0.038(2) |
| H7A | 2a | 1.09152 | 0.58155 | 1.31462 | 0.05687 |
| H7B | 2a | 0.95428 | 0.65935 | 1.24626 | 0.05687 |
| H7C | 2a | 1.14500 | 0.67443 | 1.23631 | 0.05687 |
| N8 | 2a | 1.0141(1) | 0.3083(7) | 1.1274(9) | 0.049(2) |
| H8A | 2a | 1.11734 | 0.27431 | 1.11631 | 0.07406 |
| H8B | 2a | 0.91987 | 0.27321 | 1.07861 | 0.07406 |
| H8C | 2a | 1.00298 | 0.30342 | 1.21014 | 0.07406 |
| N9 | 2a | -0.3311(4) | 0.6606(8) | 0.6524(9) | 0.045(2) |

Table 4.6: Atomic co-ordinates and equivalent thermal displacement parameters for $[Na(NH_3)_4]_2[B_6H_6] \cdot 2\,NH_3$

| Atom | Wyck. | x /a | y /b | z /c | U$_{eq}$ |
|------|-------|------|------|------|------|
| H9A | 2a | -0.359(2) | 0.685(7) | 0.583(7) | 0.01(2) |
| H9B | 2a | -0.443(2) | 0.597(2) | 0.661(1) | 0.08(4) |
| H9C | 2a | -0.232(3) | 0.599(7) | 0.639(7) | 0.02(2) |
| N10 | 2a | 0.4195(2) | -0.187(1) | 0.831(1) | 0.062(3) |
| H10A | 2a | 0.416(2) | -0.268(9) | 0.785(8) | 0.02(2) |
| H10B | 2a | 0.383(3) | -0.180(2) | 0.885(2) | 0.16(2) |
| H10C | 2a | 0.513(1) | -0.182(7) | 0.827(7) | 0.01(2) |

Table 4.6: Atomic co-ordinates and equivalent thermal displacement parameters for $[Na(NH_3)_4]_2[B_6H_6] \cdot 2\,NH_3$

| Atom | U11 | U22 | U33 | U23 | U13 | U12 |
|------|-----|-----|-----|-----|-----|-----|
| Na1 | 0.040(2) | 0.035(2) | 0.034(1) | 0.001(2) | 0.006(1) | 0.0007(2) |
| Na2 | 0.026(1) | 0.046(3) | 0.042(2) | 0.002(1) | 0.005(2) | 0.038(1) |
| B1 | 0.030(5) | 0.037(6) | 0.025(4) | -0.003(4) | 0.006(4) | 0.008(5) |
| B2 | 0.031(5) | 0.031(5) | 0.022(5) | 0.002(4) | -0.005(4) | 0.003(4) |
| B3 | 0.017(4) | 0.036(6) | 0.028(4) | -0.001(4) | -0.003(3) | 0.001(4) |
| B4 | 0.018(5) | 0.047(7) | 0.019(4) | -0.004(4) | 0.002(4) | -0.015(4) |
| B5 | 0.015(4) | 0.041(6) | 0.032(5) | -0.008(5) | -0.001(4) | -0.030(2) |
| B6 | 0.024(5) | 0.041(6) | 0.026(4) | -0.003(4) | 0.004(4) | -0.018(5) |
| N1 | 0.048(5) | 0.034(5) | 0.041(4) | -0.002(4) | 0.001(4) | -0.012(4) |
| N2 | 0.041(5) | 0.050(6) | 0.031(4) | -0.001(4) | 0.008(4) | -0.013(4) |
| N3 | 0.056(6) | 0.037(5) | 0.033(4) | 0.002(4) | 0.003(4) | 0.010(4) |
| N4 | 0.021(4) | 0.039(5) | 0.032(4) | -0.001(4) | 0.001(3) | -0.003(3) |
| N5 | 0.033(4) | 0.039(5) | 0.040(4) | 0.010(4) | 0.002(3) | 0.038(2) |
| N6 | 0.034(4) | 0.037(5) | 0.044(5) | 0.003(4) | -0.006(4) | -0.001(4) |
| N7 | 0.029(4) | 0.045(5) | 0.041(4) | 0.005(4) | 0.009(4) | 0.038(2) |
| N8 | 0.036(5) | 0.038(5) | 0.063(6) | -0.001(4) | -0.020(4) | 0.009(4) |
| N9 | 0.052(6) | 0.038(6) | 0.045(5) | 0.001(4) | 0.006(5) | -0.001(5) |
| N10 | 0.052(7) | 0.070(9) | 0.068(8) | -0.006(6) | 0.017(6) | -0.013(6) |

Table 4.7: Anisotropic thermal displacement parameters for $[Na(NH_3)_4]_2[B_6H_6] \cdot 2\,NH_3$

The hexahydro-*closo*-hexaborate cage consists of six boron and six hydrogen atoms forming the well-known shape of $[B_6H_6]^{2-}$ similar to an octahedron. The bond lengths between boron atoms are given in table 4.8. B-B-B bond angles vary from 88.6(7)° to 91.2(7)° in the boron square plane and from 58.2(6)° to 61.4(6)° in the boron triangle of the octahedron cage. All the apical boron atoms are centered within 2° and located about 1.244 Å above a r.m.s. plane through their corresponding boron square plane. The $[B_6H_6]^{2-}$ cage is surrounded by five tetraammine sodium ions with Na-B distances in the range from 2.83 to 4.76 Å. The smallest Na-B distance is comparable to that reported for $Na_2[B_{10}H_{10}]$ [114]. One sodium cation is

coordinated by four molecules of ammonia yielding nearly a tetrahedron. The Na-N bond lengths extend from 2.339(9) Å to 2.401(9) Å and N-Na-N angle vary from 100.7(3)° to 115.5(4)°. The second sodium cation is co-ordinated by four ammonia molecules and the $[B_6H_6]^{2-}$ unit with Na-B distances of 2.83 Å forming a distorted trigonal bipyramid geometry as shown in figure 4.7. The Na-N bond lengths vary from 2.430(9) Å to 2.557(8) Å and the N-Na-N angles vary from 85.2(3)° to 164.6(6)°. The later kind of geometry, bond lengths and angles is similar to that observed for $[Na(NH_3)_5]_2As_4 \cdot 3\,NH_3$ [125]. All the Na-N bond distances and bond angles are shown in 4.9. A very weak interaction between $[Na(NH_3)_4]^+$ and $[B_6H_6]^{2-}$ is responsible for shortest Na-B distance 2.83 Å and for the distorted trigonal bipyramid geometry. Whenever this distorted tetrammine sodium complex is present between two $[B_6H_6]^{2-}$ octahedra, the octahedra shift from their position. On the reverse, there is no such effect found whenever a tetrahedral sodium tetrammine complex is present between two octahedra. Due to this reason octahedra are running in zig-zag fashion along b-axis of $[Na(NH_3)_4]_2[B_6H_6] \cdot 2\,NH_3$ as shown in figure 4.8. In contrast distortion of octahedra is not observed in $[Li(NH_3)_4]_2[B_6H_6] \cdot 2\,NH_3$ compound as the $[Li(NH_3)_4]^+$ complex is very stable and always found in tetrahedral geometry.

| Bond | Length /Å | Bond | Length /Å |
|------|-----------|------|-----------|
| B(1)-B(3) | 1.68(2) | B(2)-B(4) | 1.73(2) |
| B(1)-B(2) | 1.71(2) | B(3)-B(6) | 1.70(1) |
| B(1)-B(6) | 1.71(2) | B(3)-B(4) | 1.75(1) |
| B(1)-B(5) | 1.75(2) | B(4)-B(5) | 1.73(1) |
| B(2)-B(5) | 1.72(1) | B(4)-B(6) | 1.74(1) |
| B(2)-B(3) | 1.72(1) | B(5)-B(6) | 1.71(1) |

Table 4.8: Bond lengths in $[B_6H_6]^{2-}$

| Bond | Length /Å | Bond | Angle /° |
|------|-----------|------|----------|
| Na(1)-N(1) | 2.430(9) | N1-Na1-N4 | 95.7(3) |
| Na(1)-N(2) | 2.557(8) | N2-Na1-N3 | 164.6(3) |
| Na(1)-N(3) | 2.494(9) | N2-Na1-N1 | 85.19(3) |
| Na(1)-N(4) | 2.431(9) | N3-Na1-N4 | 95.35(3) |
| Na(2)-N(5)#3 | 2.375(8) | N(5)#3-Na2-N(6)#4 | 115.2(3) |
| Na(2)-N(6)#4 | 2.379(8) | N(6)#4-Na(2)-N7 | 100.7(3) |
| Na(2)-N(7) | 2.339(9) | N(7)-Na(2)-N(8) | 102.5(3) |
| Na(2)-N(8) | 2.401(9) | N(8)-Na(2)-N(5)#3 | 115.5(3) |

Table 4.9: Bond lengths of two independent $[Na(NH_3)_4]^+$ entities

(a) Co-ordination sphere of $[B_6H_6]^{2-}$

(b) Co-ordination sphere of sodium
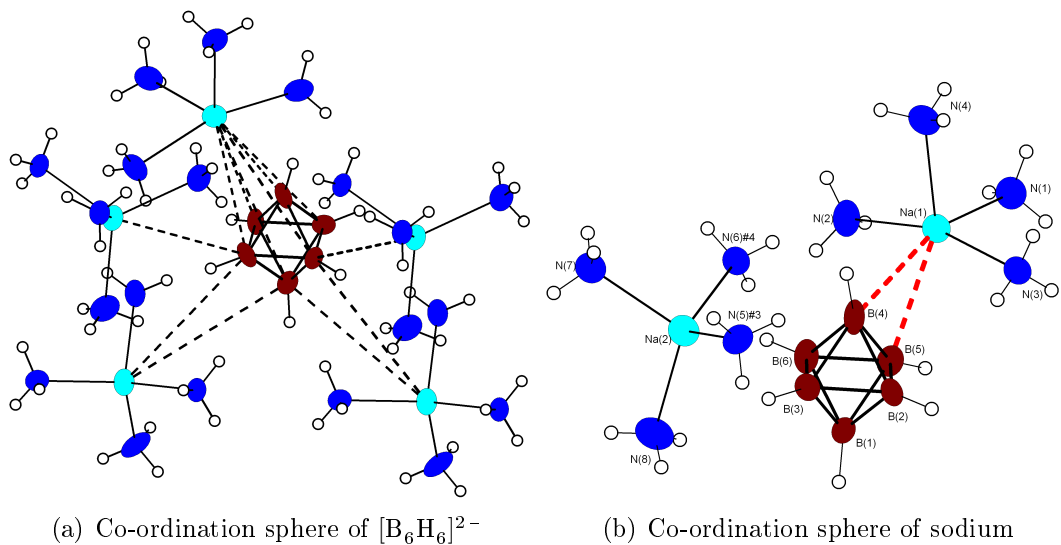
Figure 4.7: Co-ordination sphere of both anion and cation. Ellipsoids of the thermal displacement parameters are drawn at 50 % probability
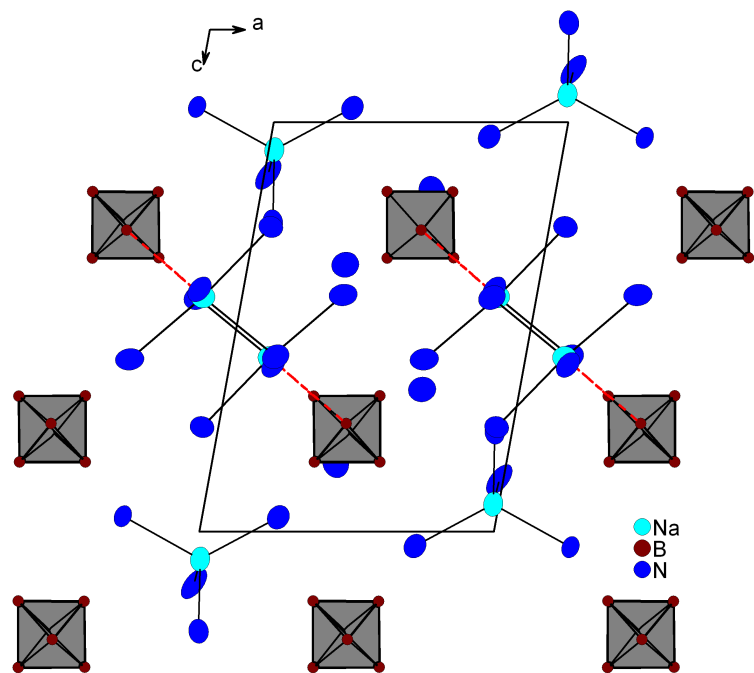


Figure 4.8: The crystal structure of $[Na(NH_3)_4]_2[B_6H_6] \cdot 2NH_3$. The boron atoms of *closo*-hexahydroborates are shown as polyhedrons. Hydrogen atoms are omitted for clarity. Ellipsoids of the thermal displacement parameters are drawn at 50 % probability

### 4.2.3 Crystallization and characterization of Bis-(tetra-n-butylammonium)-hexahydro-*closo*-hexaborate [N(C$_4$H$_9$)$_4$]$_2$[B$_6$H$_6$]
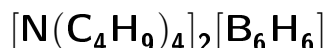
#### 4.2.3.1 Crystallization

A single crystal of [N(C$_4$H$_9$)$_4$]$_2$[B$_6$H$_6$] was obtained by storing 0.092 g (1.6 mmol) of the crystalline [N(C$_4$H$_9$)$_4$][B$_6$H$_6$H$^{\text{fac}}$] powder in approximately 20 mL of liquid ammonia. It was stored at 235 K for 10 days resulting in colourless crystals in the form of cuboids. A crystal (0.6 mm × 0.19 mm × 0.14 mm) was measured on the diffractometer.

#### 4.2.3.2 X-ray investigation

Details of the data collection and refinement parameters are given in table 4.10, and selected bond distances and angles are given in table 4.13. Analysis of the crystallographic data suggested the space group as $P2_1/c$. The structure was solved by direct methods and refined in this space group by the full-matrix least-squares procedure, which yielded a chemically reasonable structure model. All the non-hydrogen atoms were localized by Fourier cycling methods and refined anisotropically in the asymmetric unit. The positions of hydrogen atoms of the boron cluster were refined freely, whereas, the hydrogen atoms of the [N(C$_4$H$_9$)$_4$] cations were placed on calculated positions using a "riding" model. Although in this space group the $R$ values were not satisfactory, no additional symmetry was found.

| | |
|---|---|
| Empirical formula | $H_{78}B_6N_2C_{32}$ |
| Formula weight /g/mol | 555.68 |
| Crystal system | Monoclinic |
| Space group | $P2_1/c$ (No. 14) |
| $a$ /Å | 10.2672(7) |
| $b$ /Å | 22.931(2) |
| $c$ /Å | 16.699(1) |
| $\beta$ /° | 96.827(1) |
| $V$ /Å$^3$ | 3903.9(7) |
| $Z$ | 4 |
| $\rho_c$ /g/cm$^3$ | 1.107 |
| Wave length /Å | 0.71073 |
| Detector distance /mm | 60 |
| $\omega$- Increment | 0.3° |
| Temperature /K | 123 |
| $F(000)$ | 1440 |
| $\mu(\text{MoK}_\alpha)$ /mm$^{-1}$ | 0.06 |
| $\theta$-Range | 2.37° to 22.5° |
| Collected reflections | 47765 |
| Unique reflections | 5084 |
| Reflections with I $>4\sigma$ (I) | 2730 |
| $R_{int}$ | 0.0747 |
| $h$ | -11 to 11 |
| $k$ | -24 to 24 |
| $l$ | -17 to 17 |
| Refinement method | Full-matrix least-squares on F$^2$ |
| Final $R$ indices [I$>4\sigma$(I)] | $R_1 = 0.0905$ |
| $R$ indices (all data) | $R_1 = 0.1456$, $wR_2 = 0.2625$ |
| Goodness-of-fit (S) | 1.373 |
| Number of parameters | 393 |
| $w=1/[\sigma^2(\text{Fo}^2)+(0.0285\text{P})^2+0.0000\text{P}]$ | |
| P=(Fo$^2$+2Fc$^2$)/3 | |
| $\Delta\rho_{max}$ /eÅ$^{-3}$ | 0.70 |
| $\Delta\rho_{min}$ /eÅ$^{-3}$ | -0.36 |

Table 4.10: Crystal data and structure refinement for $[N(C_4H_9)_4]_2[B_6H_6]$

### 4.2.3.3 Description of the crystal structure

$[(N(C_4H_9)_4)]_2[B_6H_6]$ crystallizes in the monoclinic crystal system with four formula units per unit cell. The asymmetric unit contains two $[N(C_4H_9)_4]$ cations and one hexahydro-*closo*-hexaborate unit. All atoms are situated at general positions 4$e$. All the atomic co-ordinates, isotropic and anisotropic thermal displacement parameters are shown in tables 4.11 and 4.12. The asymmetric unit is shown in the figure 4.9.
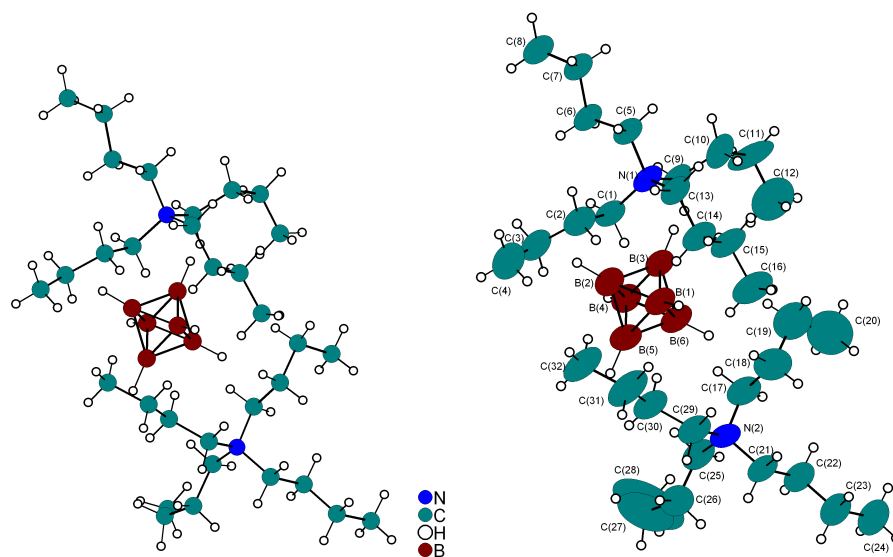
Figure 4.9: Asymmetric unit of $[N(C_4H_9)_4]_2[B_6H_6]$ without thermal displacement parameters (left) and with anisotropically refined thermal displacement parameted (right). Ellipsoids of the thermal displacement parameters are drawn at 50 % probability (right)

| Atom | Wyck. | x /a | y /b | z /c | $U_{eq}$ |
|------|-------|------|------|------|------|
| N1 | 4e | 0.2856(3) | 0.5758(2) | 0.5896(2) | 0.054(1) |
| N2 | 4e | -0.1711(3) | 0.6841(2) | 0.9181(2) | 0.062(1) |
| C1 | 4e | 0.2264(4) | 0.6359(2) | 0.5775(3) | 0.059(1) |
| H1A | 4e | 0.16771 | 0.64258 | 0.61957 | 0.07067 |
| H1B | 4e | 0.17165 | 0.63681 | 0.52461 | 0.07067 |
| C2 | 4e | 0.3243(4) | 0.6857(2) | 0.5805(3) | 0.069(1) |
| H2A | 4e | 0.36018 | 0.69326 | 0.63725 | 0.08321 |
| H2B | 4e | 0.39807 | 0.67457 | 0.55052 | 0.08321 |
| C3 | 4e | 0.2606(5) | 0.7405(3) | 0.5443(3) | 0.081(2) |
| H3A | 4e | 0.17756 | 0.74734 | 0.56740 | 0.09671 |
| H3B | 4e | 0.23910 | 0.73499 | 0.48537 | 0.09671 |
| C4 | 4e | 0.3483(7) | 0.7936(3) | 0.5596(4) | 0.108(2) |
| H4A | 4e | 0.37130 | 0.79876 | 0.61783 | 0.16217 |
| H4B | 4e | 0.30178 | 0.82823 | 0.53695 | 0.16217 |
| H4C | 4e | 0.42845 | 0.78798 | 0.53399 | 0.16217 |
| C5 | 4e | 0.3649(4) | 0.5602(2) | 0.5212(4) | 0.055(2) |
| H5A | 4e | 0.45168 | 0.57931 | 0.53197 | 0.06614 |
| H5B | 4e | 0.38009 | 0.51756 | 0.52278 | 0.06614 |
| C6 | 4e | 0.3065(4) | 0.5763(2) | 0.4369(2) | 0.055(1) |
| H6A | 4e | 0.30675 | 0.61922 | 0.43047 | 0.06611 |
| H6B | 4e | 0.21450 | 0.56259 | 0.42733 | 0.06611 |
| C7 | 4e | 0.3867(4) | 0.5483(2) | 0.3765(2) | 0.058(1) |
| H7A | 4e | 0.47869 | 0.56165 | 0.38765 | 0.06926 |
| H7B | 4e | 0.38599 | 0.50543 | 0.38395 | 0.06926 |
| C8 | 4e | 0.3364(5) | 0.5623(2) | 0.2902(3) | 0.073(2) |
| H8A | 4e | 0.24913 | 0.54504 | 0.27679 | 0.10978 |
| H8B | 4e | 0.39645 | 0.54618 | 0.25449 | 0.10978 |
| H8C | 4e | 0.33075 | 0.60465 | 0.28328 | 0.10978 |
| C9 | 4e | 0.1737(4) | 0.5331(2) | 0.5922(3) | 0.060(1) |
| H9A | 4e | 0.11557 | 0.54791 | 0.63091 | 0.07177 |
| H9B | 4e | 0.12187 | 0.53222 | 0.53833 | 0.07177 |
| C10 | 4e | 0.2132(4) | 0.4711(2) | 0.6158(3) | 0.071(2) |
| H10A | 4e | 0.27099 | 0.47203 | 0.66767 | 0.08499 |
| H10B | 4e | 0.26452 | 0.45480 | 0.57455 | 0.08499 |
| C11 | 4e | 0.0954(4) | 0.4299(3) | 0.6247(3) | 0.101(2) |
| H11A | 4e | 0.02917 | 0.43421 | 0.57695 | 0.12133 |
| H11B | 4e | 0.12629 | 0.38899 | 0.62671 | 0.12133 |
| C12 | 4e | 0.03565 | 0.44243 | 0.69606 | 0.131(2) |
| H12A | 4e | 0.10390 | 0.44669 | 0.74196 | 0.19673 |
| H12B | 4e | -0.02320 | 0.41041 | 0.70659 | 0.19673 |
| H12C | 4e | -0.01463 | 0.47873 | 0.68844 | 0.19673 |
| C13 | 4e | 0.3796(4) | 0.5742(2) | 0.6668(2) | 0.058(1) |
| H13A | 4e | 0.42059 | 0.53505 | 0.67187 | 0.06941 |
| H13B | 4e | 0.45030 | 0.60289 | 0.66231 | 0.06941 |
| C14 | 4e | 0.3183(4) | 0.5868(2) | 0.7430(2) | 0.070(1) |
| H14A | 4e | 0.24503 | 0.55945 | 0.74744 | 0.08405 |
| H14B | 4e | 0.28272 | 0.62701 | 0.74081 | 0.08405 |

Table 4.11: Atomic co-ordinates and equivalent thermal displacement parameters for $[N(C_4H_9)_4]_2[B_6H_6]$

| Atom | Wyck. | x /a | y /b | z /c | $U_{eq}$ |
|---|---|---|---|---|---|
| C15 | 4e | 0.4219(4) | 0.5803(3) | 0.8168(3) | 0.076(1) |
| H15A | 4e | 0.45737 | 0.54012 | 0.81826 | 0.09122 |
| H15B | 4e | 0.49529 | 0.60750 | 0.81148 | 0.09122 |
| C16 | 4e | 0.3671(5) | 0.5925(3) | 0.8939(3) | 0.103(2) |
| H16A | 4e | 0.33483 | 0.63273 | 0.89356 | 0.15402 |
| H16B | 4e | 0.43590 | 0.58721 | 0.93929 | 0.15402 |
| H16C | 4e | 0.29464 | 0.56558 | 0.89955 | 0.15402 |
| C17 | 4e | -0.1595(4) | 0.6255(3) | 0.8795(3) | 0.075(2) |
| H17A | 4e | -0.15926 | 0.63145 | 0.82081 | 0.09036 |
| H17B | 4e | -0.23883 | 0.60263 | 0.88710 | 0.09036 |
| C18 | 4e | -0.0403(5) | 0.5897(3) | 0.9102(4) | 0.092(2) |
| H18A | 4e | -0.03599 | 0.58516 | 0.96940 | 0.11150 |
| H18B | 4e | 0.04001 | 0.61017 | 0.89829 | 0.11150 |
| C19 | 4e | -0.0464(7) | 0.5288(4) | 0.8701(4) | 0.121(3) |
| H19A | 4e | 0.03964 | 0.50921 | 0.88239 | 0.14406 |
| H19B | 4e | -0.06387 | 0.53336 | 0.81080 | 0.14406 |
| C20 | 4e | -0.1551(9) | 0.4899(4) | 0.8999(5) | 0.179(4) |
| H20A | 4e | -0.14082 | 0.48694 | 0.95889 | 0.26868 |
| H20B | 4e | -0.15177 | 0.45083 | 0.87635 | 0.26868 |
| H20C | 4e | -0.24128 | 0.50730 | 0.88341 | 0.26868 |
| C21 | 4e | -0.1746(4) | 0.6801(2) | 1.0082(2) | 0.063(1) |
| H21A | 4e | -0.18991 | 0.71956 | 1.02915 | 0.07609 |
| H21B | 4e | -0.08751 | 0.66689 | 1.03362 | 0.07609 |
| C22 | 4e | -0.2781(5) | 0.6393(3) | 1.0340(3) | 0.073(2) |
| H22A | 4e | -0.26417 | 0.59968 | 1.01296 | 0.08772 |
| H22B | 4e | -0.36590 | 0.65277 | 1.01027 | 0.08772 |
| C23 | 4e | -0.2737(5) | 0.6366(3) | 1.1249(3) | 0.083(2) |
| H23A | 4e | -0.18469 | 0.62463 | 1.14849 | 0.10018 |
| H23B | 4e | -0.29024 | 0.67613 | 1.14550 | 0.10018 |
| C24 | 4e | -0.3730(5) | 0.5947(3) | 1.1526(3) | 0.095(2) |
| H24A | 4e | -0.46156 | 0.60723 | 1.13120 | 0.14237 |
| H24B | 4e | -0.36485 | 0.59439 | 1.21166 | 0.14237 |
| H24C | 4e | -0.35669 | 0.55549 | 1.13285 | 0.14237 |
| C25 | 4e | -0.2994(4) | 0.7093(3) | 0.8761(3) | 0.069(2) |
| H25A | 4e | -0.29254 | 0.71188 | 0.81757 | 0.08234 |
| H25B | 4e | -0.37125 | 0.68170 | 0.88336 | 0.08234 |
| C26 | 4e | -0.3357(4) | 0.7684(3) | 0.9056(3) | 0.078(2) |
| H26A | 4e | -0.25978 | 0.79509 | 0.90646 | 0.09361 |
| H26B | 4e | -0.35916 | 0.76515 | 0.96122 | 0.09361 |
| C27 | 4e | -0.4450(7) | 0.7928(3) | 0.8512(5) | 0.171(4) |
| H27A | 4e | -0.48625 | 0.82357 | 0.88376 | 0.20556 |
| H27B | 4e | -0.40958 | 0.81358 | 0.80844 | 0.20556 |
| C28 | 4e | -0.544(1) | 0.7695(5) | 0.8168(8) | 0.269(8) |
| H28A | 4e | -0.52594 | 0.72771 | 0.81196 | 0.40414 |
| H28B | 4e | -0.56324 | 0.78647 | 0.76283 | 0.40414 |
| H28C | 4e | -0.61873 | 0.77504 | 0.84703 | 0.40414 |
| C29 | 4e | -0.0549(4) | 0.7237(2) | 0.9059(3) | 0.069(2) |

Table 4.11: Atomic co-ordinates and equivalent thermal displacement parameters for $[N(C_4H_9)_4]_2[B_6H_6]$

| Atom | Wyck. | x /a | y /b | z /c | $U_{eq}$ |
|------|-------|------|------|------|----------|
| H29A | 4e | -0.05940 | 0.75911 | 0.93939 | 0.08349 |
| H29B | 4e | 0.02746 | 0.70303 | 0.92528 | 0.08349 |
| C30 | 4e | -0.0498(5) | 0.7421(3) | 0.8192(3) | 0.078(2) |
| H30A | 4e | -0.06935 | 0.70808 | 0.78330 | 0.09350 |
| H30B | 4e | -0.11775 | 0.77210 | 0.80422 | 0.09350 |
| C31 | 4e | 0.0824(5) | 0.7663(3) | 0.8072(3) | 0.102(2) |
| H31A | 4e | 0.15008 | 0.73593 | 0.82083 | 0.12233 |
| H31B | 4e | 0.10295 | 0.79966 | 0.84414 | 0.12233 |
| C32 | 4e | 0.0864(5) | 0.7863(3) | 0.7203(3) | 0.103(2) |
| H32A | 4e | 0.06180 | 0.75373 | 0.68352 | 0.15454 |
| H32B | 4e | 0.17524 | 0.79932 | 0.71344 | 0.15454 |
| H32C | 4e | 0.02462 | 0.81853 | 0.70819 | 0.15454 |
| B1 | 4e | -0.0985(5) | 0.6274(3) | 0.6688(3) | 0.061(2) |
| H1 | 4e | -0.008(4) | 0.626(1) | 0.723(2) | 0.050(1) |
| B2 | 4e | -0.1295(5) | 0.6517(3) | 0.5718(3) | 0.060(2) |
| H2 | 4e | -0.067(4) | 0.673(2) | 0.524(2) | 0.051(1) |
| B3 | 4e | -0.1663(5) | 0.5817(3) | 0.5945(3) | 0.057(2) |
| H3 | 4e | -0.147(3) | 0.539(2) | 0.569(2) | 0.051(1) |
| B4 | 4e | -0.2899(5) | 0.6293(3) | 0.5691(3) | 0.060(2) |
| H4 | 4e | -0.374(3) | 0.634(2) | 0.523(2) | 0.061(1) |
| B5 | 4e | -0.2258(5) | 0.6763(3) | 0.6431(3) | 0.064(2) |
| H5 | 4e | -0.253(4) | 0.721(2) | 0.669(2) | 0.052(1) |
| B6 | 4e | -0.2606(5) | 0.6060(3) | 0.6664(3) | 0.064(2) |
| H6 | 4e | -0.321(4) | 0.583(2) | 0.713(3) | 0.078(1) |

Table 4.11: Atomic co-ordinates and equivalent thermal displacement parameters for $[N(C_4H_9)_4]_2[B_6H_6]$

| Atom | U11 | U22 | U33 | U23 | U13 | U12 |
|------|-----|-----|-----|-----|-----|-----|
| N1 | 0.016(2) | 0.103(3) | 0.041(2) | -0.001(2) | 0.001(2) | -0.005(2) |
| N2 | 0.041(2) | 0.094(3) | 0.051(3) | -0.010(2) | 0.009(2) | 0.005(2) |
| C1 | 0.026(2) | 0.103(4) | 0.047(3) | -0.004(3) | 0.003(2) | -0.001(3) |
| C2 | 0.038(3) | 0.113(5) | 0.055(3) | -0.004(3) | -0.001(2) | -0.002(3) |
| C3 | 0.067(4) | 0.121(6) | 0.055(3) | 0.006(3) | 0.012(3) | -0.003(4) |
| C4 | 0.124(5) | 0.119(5) | 0.082(4) | 0.004(4) | 0.018(4) | -0.027(5) |
| C5 | 0.020(2) | 0.098(4) | 0.047(3) | -0.001(3) | 0.003(2) | -0.004(2) |
| C6 | 0.025(2) | 0.099(4) | 0.041(3) | 0.001(3) | 0.001(2) | -0.004(2) |
| C7 | 0.028(2) | 0.098(4) | 0.047(3) | 0.001(3) | 0.005(2) | -0.004(2) |
| C8 | 0.054(3) | 0.114(5) | 0.053(3) | 0.001(3) | 0.010(2) | -0.002(3) |
| C9 | 0.020(2) | 0.118(5) | 0.040(3) | 0.002(3) | -0.001(2) | -0.014(3) |
| C10 | 0.036(3) | 0.124(5) | 0.049(3) | 0.021(3) | -0.009(2) | -0.012(3) |
| C11 | 0.034(3) | 0.215(7) | 0.057(4) | -0.054(4) | 0.014(2) | -0.032(4) |
| C12 | 0.066(4) | 0.206(8) | 0.118(6) | 0.003(5) | -0.005(4) | -0.022(5) |
| C13 | 0.020(2) | 0.109(4) | 0.042(3) | 0.002(3) | -0.005(2) | -0.003(2) |
| C14 | 0.027(2) | 0.132(5) | 0.048(3) | -0.005(2) | -0.003(2) | 0.001(3) |
| C15 | 0.043(3) | 0.141(5) | 0.044(3) | -0.013(3) | 0.005(2) | -0.012(3) |
| C16 | 0.063(4) | 0.184(7) | 0.059(4) | -0.018(4) | -0.002(3) | 0.005(4) |
| C17 | 0.039(3) | 0.125(5) | 0.061(3) | -0.007(3) | 0.002(2) | 0.005(3) |
| C18 | 0.046(3) | 0.134(6) | 0.095(4) | -0.013(4) | -0.003(3) | 0.008(3) |
| C19 | 0.100(5) | 0.142(7) | 0.119(6) | -0.008(6) | 0.020(4) | -0.023(5) |
| C20 | 0.207(9) | 0.198(9) | 0.114(6) | -0.018(6) | -0.053(7) | 0.040(8) |
| C21 | 0.035(3) | 0.112(4) | 0.042(7) | 0.001(3) | -0.001(2) | 0.011(3) |
| C22 | 0.050(3) | 0.114(5) | 0.054(3) | 0.003(3) | 0.002(2) | 0.003(3) |
| C23 | 0.070(4) | 0.122(5) | 0.057(3) | 0.010(3) | -0.001(3) | 0.070(4) |
| C24 | 0.071(4) | 0.134(5) | 0.081(4) | 0.020(4) | 0.015(3) | -0.005(4) |
| C25 | 0.030(3) | 0.125(5) | 0.048(3) | -0.004(3) | -0.010(2) | -0.008(3) |
| C26 | 0.041(3) | 0.116(5) | 0.073(4) | -0.005(3) | -0.012(3) | 0.009(3) |
| C27 | 0.122(6) | 0.179(8) | 0.184(8) | -0.081(6) | -0.101(6) | 0.075(6) |
| C28 | 0.178(9) | 0.23(1) | 0.35(2) | -0.14(1) | -0.19(1) | 0.110(8) |
| C29 | 0.034(3) | 0.118(5) | 0.056(3) | -0.008(3) | -0.001(2) | -0.001(3) |
| C30 | 0.056(3) | 0.124(5) | 0.054(3) | -0.012(3) | 0.009(3) | -0.009(3) |
| C31 | 0.047(3) | 0.195(7) | 0.064(4) | -0.008(4) | 0.006(3) | -0.025(4) |
| C32 | 0.069(4) | 0.179(7) | 0.065(4) | -0.010(4) | 0.022(3) | -0.027(4) |
| B1 | 0.022(3) | 0.105(5) | 0.057(4) | -0.001(3) | 0.006(2) | -0.004(3) |
| B2 | 0.024(3) | 0.096(5) | 0.057(4) | 0.002(3) | -0.003(2) | -0.003(3) |
| B3 | 0.032(3) | 0.085(5) | 0.055(4) | -0.004(3) | 0.006(2) | -0.010(3) |
| B4 | 0.020(3) | 0.098(5) | 0.062(4) | 0.001(3) | -0.002(2) | -0.006(3) |
| B5 | 0.029(3) | 0.101(6) | 0.061(4) | -0.009(4) | 0.002(3) | 0.004(3) |
| B6 | 0.021(3) | 0.117(6) | 0.052(4) | -0.003(4) | 0.001(2) | -0.006(3) |

Table 4.12: Anisotropic thermal displacement parameters for $[N(C_4H_9)_4]_2[B_6H_6]$

The hexahydro-*closo*-hexaborate cage is built up by six boron and six hydrogen atoms respectively, forming the well-known shape of $[B_6H_6]^{2-}$ similar to an octahedron. This $[B_6H_6]^{2-}$ cluster is surrounded by two $[N(C_4H_9)_4]$ cations. The B-B, C-C and C-N distances are shown in table 4.13. The C(29)-C(30) distance is relatively

short compared to other C-C distances. The anisotropic thermal displacement parameters obtained were not reasonable. B-B-B bond angles vary between $89.1(4)°$ to $90.8(4)°$ in the boron square plane and within $59.1(3)°$ and $61.0(3)°$ in the boron triangle of the octahedron cage. All the apical boron atoms are centered within $2°$ and located about $1.222$ Å above a r.m.s. plane through their corresponding boron square plane. The primitive unit cell of $[N(C_4H_9)_4]_2[B_6H_6]$ is shown in figure 4.10.

| Bond | Length /Å | Bond | Length /Å |
|------|-----------|------|-----------|
| B(1)-B(2) | 1.706(8) | B(4)-B(5) | 1.712(8) |
| B(1)-B(6) | 1.732(7) | B(5)-B(6) | 1.707(9) |
| B(2)-B(3) | 1.703(9) | B(5)-B(1) | 1.737(8) |
| B(2)-B(5) | 1.731(8) | B(6)-B(3) | 1.722(8) |
| B(3)-B(4) | 1.690(8) | B(6)-B(4) | 1.702(8) |
| N(1)-C(1) | 1.509(5) | N(2)-C(17) | 1.501(6) |
| N(1)-C(9) | 1.515(5) | N(2)-C(21) | 1.513(5) |
| N(1)-C(13) | 1.515(5) | N(2)-C(25) | 1.529(5) |
| N(1)-C(5) | 1.522(2) | N(2)-C(29) | 1.531(6) |
| C(1)-C(2) | 1.519(6) | C(17)-C(18) | 1.513(6) |
| C(2)-C(3) | 1.509(7) | C(18)-C(19) | 1.547(8) |
| C(3)-C(4) | 1.518(7) | C(19)-C(20) | 1.557(5) |
| C(5)-C(6) | 1.509(6) | C(21)-C(22) | 1.516(6) |
| C(6)-C(7) | 1.519(5) | C(22)-C(23) | 1.516 (6) |
| C(7)-C(8) | 1.507(8) | C(23)-C(24) | 1.512(7) |
| C(9)-C(10) | 1.517 (6) | C(25)-C(26) | 1.505(6) |
| C(10)-C(11) | 1.555 (6) | C(26)-C(27) | 1.503(7) |
| C(11)-C(12) | 1.432(7) | C(27)-C(28) | 1.186 (9) |
| C(13)-C(14) | 1.513 (6) | C(29)-C(30) | 1.186 (9) |
| C(14)-C(15) | 1.537 (5) | C(30)-C(31) | 1.501(6) |
| C(15)-C(16) | 1.492 (6) | C(31)-C(32) | 1.527(7) |

Table 4.13: Selected bond lengths for $[N(C_4H_9)_4]_2[B_6H_6]$

### 4.2.3.4 Powder diffraction and IR analysis

The structure model of $[N(C_4H_9)_4]_2[B_6H_6]$ based on the refinement described here is not completely satisfactory. To investigate the reasons for this, a crystalline powder of $[N(C_4H_9)_4]_2[B_6H_6]$ was synthesized according to the literature procedure [126] and additional techniques such as X-ray powder diffraction and IR were used for characterization. The powder pattern of $[N(C_4H_9)_4]_2[B_6H_6]$ is not recorded in the PDF database. CSD and ICSD database contains no structural data for this compound. IR data of the $[N(C_4H_9)_4]_2[B_6H_6]$ was found to be identical to the compound described in literature [127]. The IR data recorded in this study will be
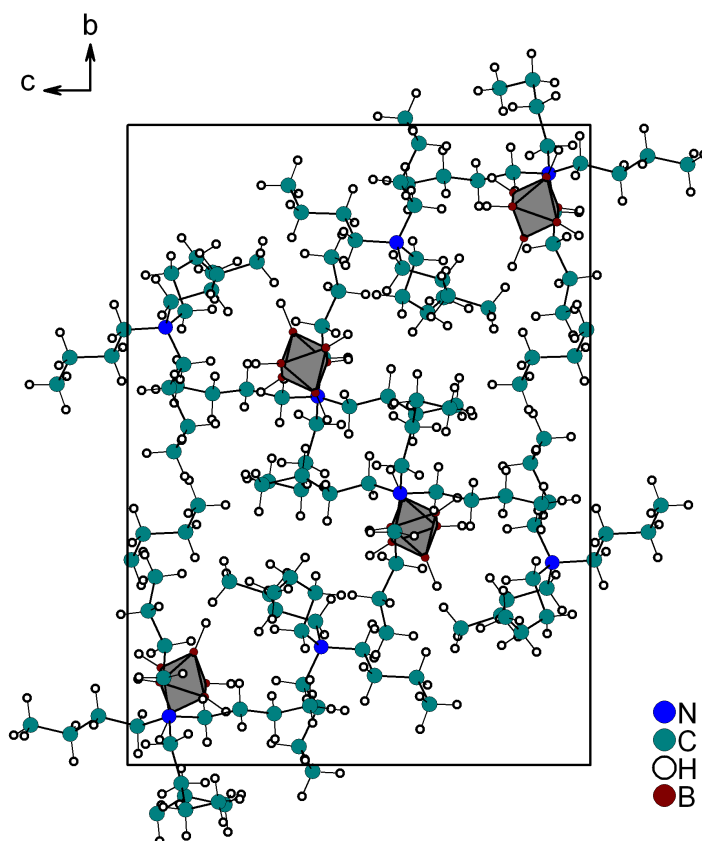
Figure 4.10: The crystal structure of $[N(C_4H_9)_4]_2[B_6H_6]$. The boron atoms of *closo*-hexahydroborates are shown as polyhedrons
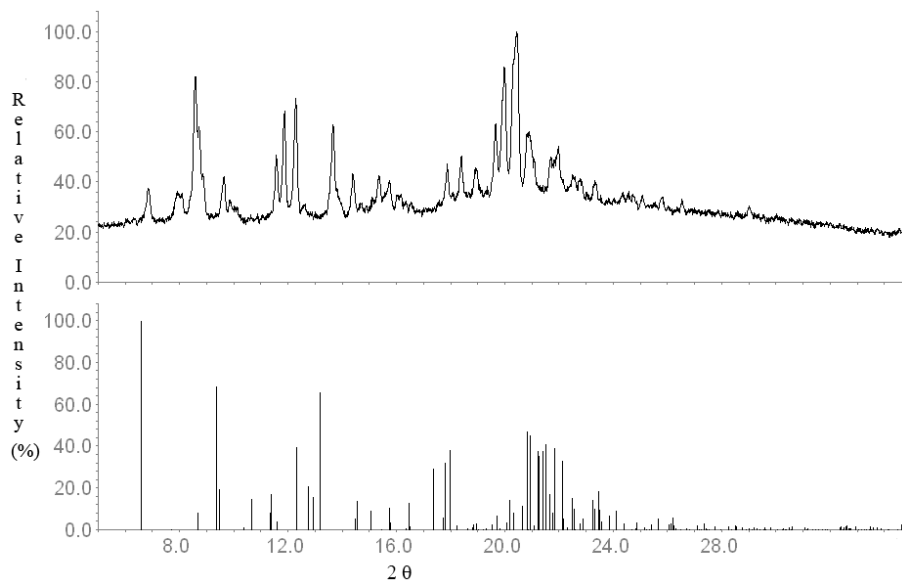
Figure 4.11: Comparison of X-ray powder diffractogram of $[N(C_4H_9)_4]_2[B_6H_6]$ (T = 298 K) (top) and simulated diffractogram of $[N(C_4H_9)_4]_2[B_6H_6]$ (T = 123 K) (bottom)

discussed later.

The diffractogram of the $[N(C_4H_9)_4]_2[B_6H_6]$ at room temperature is shown in figure 4.11 (top). It is compared with the simulated pattern based on the structural model obtained from the single crystal data as described in 4.2.3.2 (figure 4.11, bottom). The reflection positions for the structural model are found to be shifted to higher $2\theta$ values compared with the room temperature measurement. This is due to the shrinkage of lattice parameters at 123 K.

Therefore, a low temperature X-ray powder diffraction measurement was carried out at 123 K for $[N(C_4H_9)_4]_2[B_6H_6]$. A comparison between room temperature and low temperature measurements is shown in figure 4.12. Although the quality of data is not that good, the match between experimental and calculated peaks is much better now.

X-ray powder diffraction of the bulk product (starting material) after evaporating the ammonia and drying in vacuum $6 \times 10^{-3}$ mbar led to a diffractogram as shown in figure 4.13 (top). This matches with the X-ray pattern of $[N(C_4H_9)_4][B_6H_6H^{fac}]$ as described by Hofmann et al. [122] and shown in figure 4.13 (bottom). In the bulk product, the reflections of $[N(C_4H_9)_4]_2[B_6H_6]$ were not observed.

From the above observations it can be inferred that $[N(C_4H_9)_4]_2[B_6H_6]$ was obtained as single crystals during the storage of $[N(C_4H_9)_4][B_6H_6H^{fac}]$ in liquid ammo-
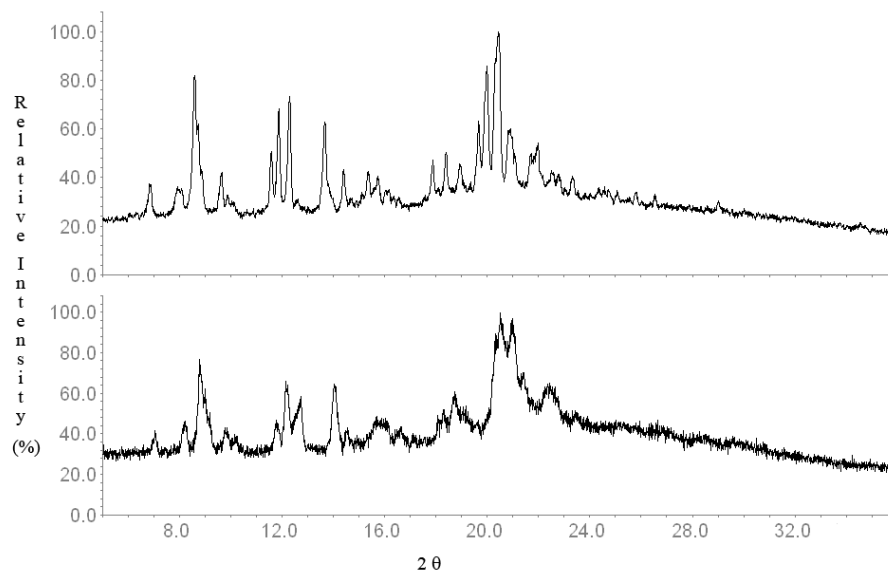
Figure 4.12: Comparison of X-ray powder diffractogram of $[N(C_4H_9)_4]_2[B_6H_6]$ at room temperature (top) and low temperature 123 K (bottom)
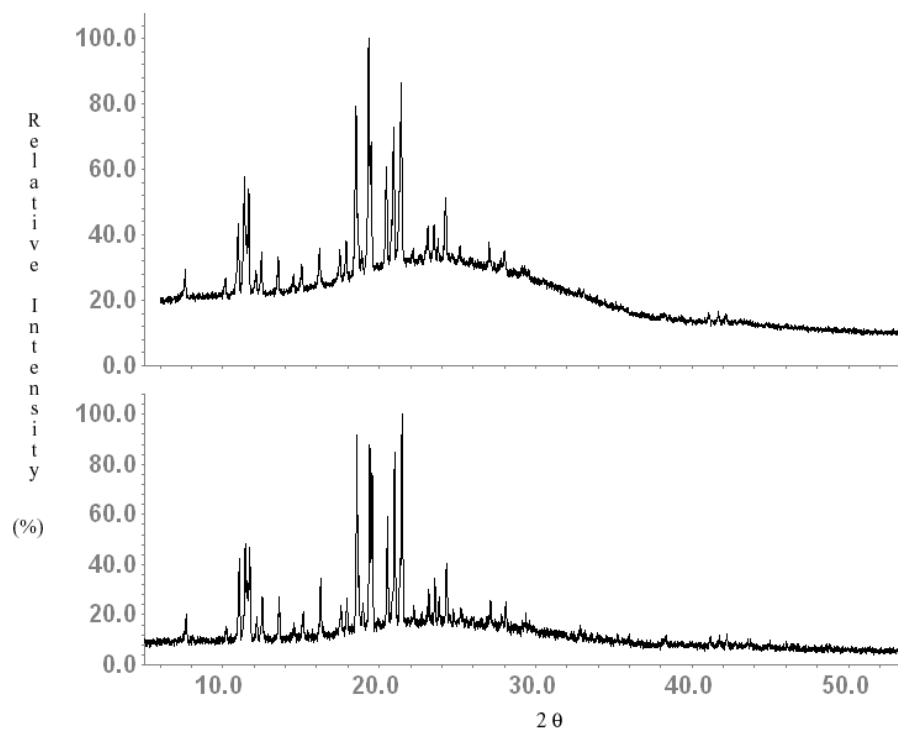


Figure 4.13: Comparison of X-ray powder diffractogram of the sample obtained from liquid ammonia (top) and $[nBu_4N][B_6H_6H^{fac}]$ [122] (bottom)

nia. But the amount of single crystals was very little compared to the powder that was identified as $[N(C_4H_9)_4][B_6H_6H^{fac}]$.

The IR measurements were carried out for $[N(C_4H_9)_4]_2[B_6H_6]$ (**a**) , $[N(C_4H_9)_4]$ $[B_6H_6H^{fac}]$ (**b**) and the product obtained after reacting with liquid ammonia (**c**). The IR spectra are shown in figure 4.14. The infrared spectra show that the characteristic vibrations for cations at 2960 $\nu_{C-N}$, 2880 $\nu_{C-H}$, 1470, 1380 $\delta_{C-H}$ are same for all the compounds.

The characteristic vibrations of boron-cage are shown in table 4.14. The $\nu_{B-H}$ for reported compounds containing $[B_6H_6]^{2-}$ varies from 2414 to 2470 cm$^{-1}$ depending on the cation. The value of $\nu_{B-H}$ at 2420 cm$^{-1}$ for synthesized $[N(C_4H_9)_4]_2[B_6H_6]$ agrees well with the value reported in Ref. [127]. The $\nu_{B-H}$ vibration for compounds containing $[B_6H_6H^{fac}]^{1-}$ appears at 2530 cm$^{-1}$ and is the same for the reported and the synthesized one. In the product, a broad band consisting of a main peak at 2530 cm$^{-1}$ and a shoulder at 2420 cm$^{-1}$ corresponds to the $\nu_{B-H}$ of $[N(C_4H_9)_4][B_6H_6H^{fac}]$ and $[N(C_4H_9)_4]_2[B_6H_6]$. The $\nu_{B-B}$ observed for synthesized $[N(C_4H_9)_4]_2[B_6H_6]$ and $[N(C_4H_9)_4][B_6H_6H^{fac}]$ agree well with [126]. In the product, it is difficult to differentiate the $\nu_{B-B}$ of $[B_6H_6]^{2-}$ and $[B_6H_6H^{fac}]^{1-}$ as the peaks overlap. It is already mentioned in the literature [127] that the assignment of $\nu_{B-B}$ for $[N(C_4H_9)_4]$ containing compounds are ambiguous due to the presence of this cation. There were some extra peaks observed below 1100 cm$^{-1}$ for all the synthesized compounds. Based on the values of $\nu_{B-H}$, the product can be assigned as a mixture of $[N(C_4H_9)_4]_2[B_6H_6]$ and $[N(C_4H_9)_4][B_6H_6H^{fac}]$.

|  | Comp. Containing $[B_6H_6]^{2-}$ | | | | Comp. containing $[B_6H_7]^{1-}$ | | | Product (c) |
|---|---|---|---|---|---|---|---|---|
| Ref. | TBA [127] | Cs [126] | HPy−2NH [115] | TBA [this work] | TBA [127] | Cs [126] | TBA [this work] | [this work] |
| $\nu_{B-H}$ | 2414 | 2432 | 2470<br>2445 | 2420 | 2530<br>2509 | 2532<br>2545 | 2530 | 2530<br>2414 |
| $\nu_{B-B}$ |  | 1050<br>731 |  | 1030<br>739 | 1078<br>1048<br>1015<br>947<br>844<br>765<br>696<br>652 | 1061<br>1030<br>1020<br>827<br>737 |  | 1066<br>1030<br>1026<br>922<br>827<br>797<br>739 |

Table 4.14: Comparison of IR-bands of literature and now synthesized products before and after treating with liquid ammonia. TBA = $[N(C_4H_9)_4]$ cation
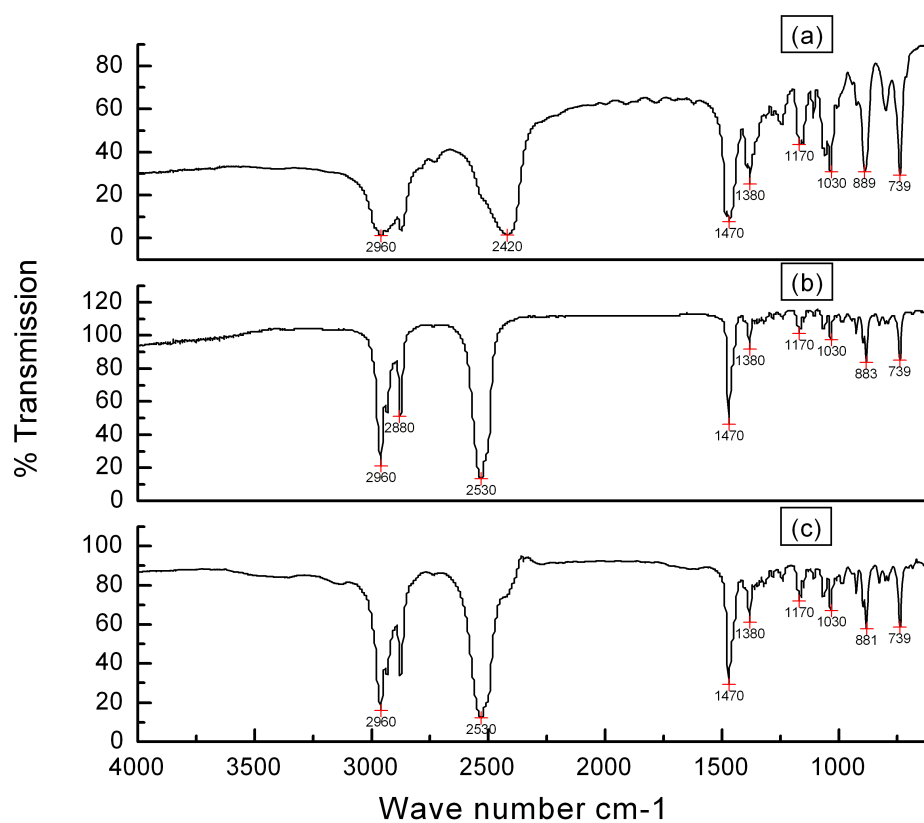
Figure 4.14: Comparison of IR spectra among $[N(C_4H_9)_4]_2[B_6H_6]$ **(a)**, $[N(C_4H_9)_4][B_6H_6H^{fac}]$ **(b)**, and the product after reacting with liquid ammonia **(c)**

From the powder XRD and IR measurements, it can be concluded that the product **(c)** contains both $[N(C_4H_9)_4]_2[B_6H_6]$ and $[N(C_4H_9)_4][B_6H_6H^{fac}]$.

## 4.3 Alkali metal compounds containing the $[B_{10}H_{10}]^{2-}$ anion

Early NMR studies as well as the application of the MO theory led to the assumption, that the arrangement of ten boron atoms is that of a *closo*-cluster in the form of a bicapped square antiprism as shown in figure 4.15. In this anion, two groups of symmetry equivalent boron atoms (i.e two apical and eight equitorial) are found. Therefore, in the $^{11}$B NMR spectrum of $Li_2[B_{10}H_{10}]$ (left side of figure 4.15), one low field doublet is observed to which both the apical boron atoms can be assigned and a high field doublet with an intensity four times higher is observed to which eight equitorial B atoms can be assigned.



(a)          (b)
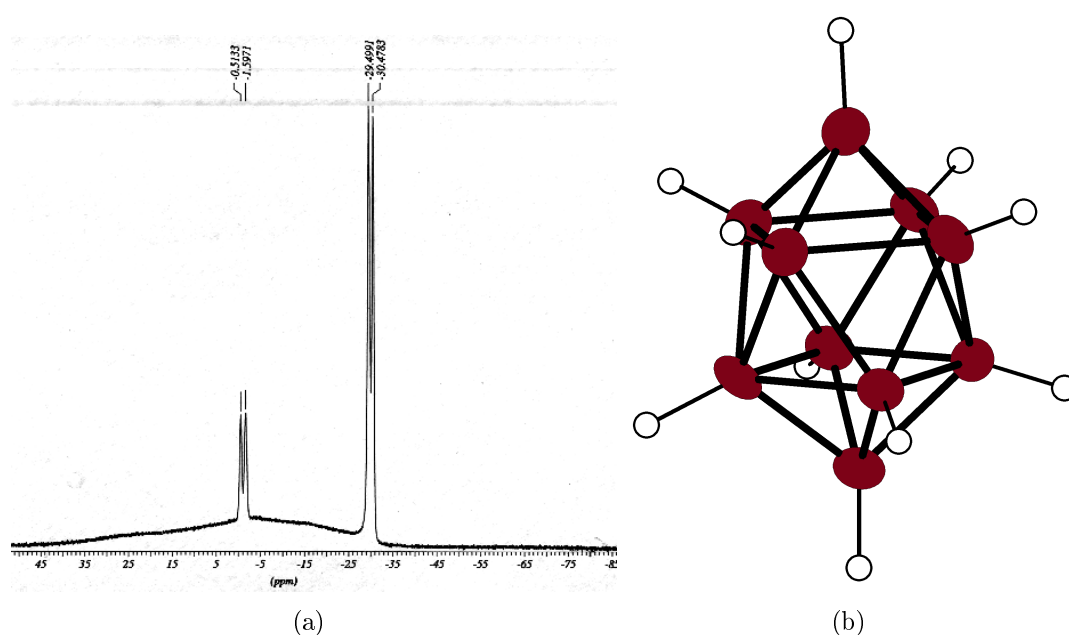
Figure 4.15: $^{11}$B NMR spectrum of the $[B_{10}H_{10}]^{2-}$ ion (left) and the corresponding *closo*-cluster

The infrared spectrum of $Li_2[B_{10}H_{10}]$ shows the characteristic vibrations of the $[B_{10}H_{10}]^{2-}$ ion at 2470 ($\nu_{B-H}$) and 1034 ($\delta_{B-B}$) which are comparable to the literature values [128].

## 4.3.1 Synthesis and characterization of $M_2[B_{10}H_{10}] \cdot 5\,NH_3$ (M = Rb, Cs)

### 4.3.1.1 Synthesis

$Rb_2[B_{10}H_{10}] \cdot 5\,NH_3$ and $Cs_2[B_{10}H_{10}] \cdot 5\,NH_3$ were obtained from distilled alkali metals (M = Rb, Cs) and $Li_2[B_{10}H_{10}]$. $Li_2[B_{10}H_{10}]$ was dried at 413 K for 18 h in $3 \times 10^{-3}$ mbar. $Rb_2[B_{10}H_{10}] \cdot 5\,NH_3$ was synthesized from 1.093 g (12.79 mmol) of rubidium and 0.167 g (1.26 mmol) of $Li_2[B_{10}H_{10}]$. $Cs_2[B_{10}H_{10}] \cdot 5\,NH_3$ was synthesized from 0.293 g (2.2 mmol) of cesium and 0.058 g (0.4 mmol) $Li_2[B_{10}H_{10}]$. The weighed amounts were placed in a Schlenk tube and the evacuated vessel was cooled by a dry ice/isopropanol slush. Approximately 15 mL of liquid ammonia was condensed into the tube through a vacuum line, yielding a blue solution of alkali metal. It was then stored at 235 K for 10 days resulting in colorless crystals in the form of needles for $Rb_2[B_{10}H_{10}] \cdot 5\,NH_3$ and approximately for one month resulting in colourless crystals in the form of plates for $Cs_2[B_{10}H_{10}] \cdot 5\,NH_3$. Alternatively the $Cs_2[B_{10}H_{10}] \cdot 5\,NH_3$ can be also synthesized from 0.191 g (0.50 mmol) of $Cs_2[B_{10}H_{10}]$ and 0.006 g (1.0 mmol) of lithium. Crystals with the dimensions of 0.22 mm $\times$ 0.14 mm $\times$ 0.1 mm ( $Rb_2[B_{10}H_{10}] \cdot 5\,NH_3$) and 0.36 mm $\times$ 0.22 mm $\times$ 0.24 mm ($Cs_2[B_{10}H_{10}] \cdot 5\,NH_3$) were measured on the diffractometer.

### 4.3.1.2 X-ray investigation

Details of the data collection and refinement parameters are given in table 4.15. Systematic extinctions suggested space group $P2_1/c$ for the ammoniated rubidium compound and $Pnma$ for the cesium compound. This gives rise to chemically reasonable and computationally stable results of the refinements. The structure was solved by direct methods, followed by subsequent difference Fourier syntheses, and refined by a full-matrix least-squares procedure. The thermal parameters of all the non-hydrogen atoms were refined anisotropically. The hydrogen atoms were located from the difference maps. To verify the selection of the space groups, searches for additional symmetry were performed. No additional symmetry was found for the cesium compound whereas, for the rubidium compound higher symmetry was found which suggested the space group $Pnma$. Therefore both the crystal structures are described in $Pnma$.

| Empirical formula | $H_{25}B_{10}N_5Rb_2$ | $H_{25}B_{10}N_5Cs_2$ |
|---|---|---|
| Formula weight /g/mol | 374.29 | 469.15 |
| Crystal system | Orthorhombic | Orthorhombic |
| Space group | *Pnma* (No. 61) | *Pnma* (No. 61) |
| $a$ /Å | 13.9510(7) | 14.0856(4) |
| $b$ /Å | 8.6750(11) | 8.8918(3) |
| $c$ /Å | 13.9660(11) | 14.2622(4) |
| $V$ /Å$^3$ | 1690.2(3) | 1786.29(9) |
| $Z$ | 4 | 4 |
| $\rho_c$ /g/cm$^3$ | 1.525 | 1.745 |
| Wave length /Å | 0.71073 | 0.71073 |
| Detector distance /mm | 60 | 60 |
| $\omega$- Increment | 0.3° | 0.3° |
| Temperature /K | 123 | 123 |
| $F(000)$ | 736 | 880 |
| $\mu(\text{MoK}_\alpha)$ /mm$^{-1}$ | 5.77 | 4.062 |
| $\theta$-Range | 2.06° to 27.54° | 2.03° to 28.01° |
| Number of collected reflections | 37094 | 40021 |
| Number of unique reflections | 2072 | 2289 |
| Reflections with I >4$\sigma$ (I) | 1368 | 2078 |
| $R_{int}$ | 0.1405 | 0.0506 |
| $h$ | -18 to 18 | -18 to 18 |
| $k$ | -11 to 11 | -11 to 11 |
| $l$ | -18 to 18 | -18 to 18 |
| Refinement method | Full-matrix least-squares on F$^2$ | |
| Final $R$ indices [I>4$\sigma$(I)] | 0.0265 | 0.0187 |
| $R$ indices (all data) | $R_1 = 0.0489$ | $R_1 = 0.0209$ |
| | $wR_2 = 0.0472$ | $wR_2 = 0.0486$ |
| Goodness-of-fit(S) | 0.75 | 1.058 |
| Number of parameters | 145 | 145 |
| $w=1/[\sigma^2(\text{Fo}^2)+(0.0285P)^2+0.0000P]$ | | |
| P=(Fo$^2$+2Fc$^2$)/3 | | |
| $\Delta\rho_{max}$ /eÅ$^{-3}$ | 0.61 | 0.92 |
| $\Delta\rho_{min}$ /eÅ$^{-3}$ | -0.31 | -0.55 |

Table 4.15: Crystal data and structure refinement for $M_2[B_{10}H_{10}] \cdot 5\,NH_3$ (M = Rb, Cs)

### 4.3.1.3 Description of the crystal structures

$Rb_2[B_{10}H_{10}] \cdot 5\,NH_3$ and $Cs_2[B_{10}H_{10}] \cdot 5\,NH_3$ crystallize in the orthorhombic space-group *Pnma* (No. 61) with four formula units per unit cell. The asymmetric unit contains one metal atom which is situated at the general position 8$d$. All the atomic co-ordinates, isotropic and anisotropic thermal parameters are shown in table 4.16, 4.17, 4.18 and 4.19 . The asymmetric unit is shown in the figure 4.16.
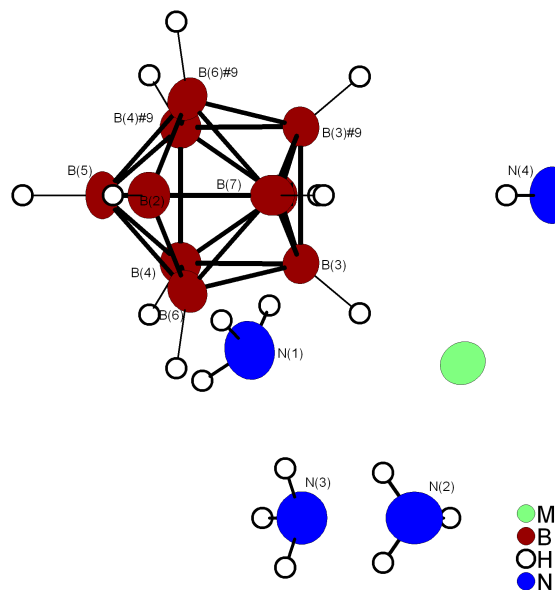
Figure 4.16: Asymmetric unit of $M_2[B_{10}H_{10}] \cdot 5\,NH_3$. Ellipsoids of the thermal displacement parameters are drawn for Rb containing compound at 70 % probability

The decahydro-*closo*-decaborate cage is built up by seven boron and hydrogen atoms and their symmetry equivalents forming the well-known $[B_{10}H_{10}]^{2-}$ cluster which is similar to a bicapped square antiprism. All B-B bond lengths in the apical boron atoms are 1.69 Å and the B-B-bond lengths in the square antiprism lie between 1.81 Å and 1.84 Å. B-B-B-angles lie between $89.8(1)$ and $90.2(1)°$ in the boron atom squares and between $57.2(1)$ and $60.7(2)°$ in the boron atom triangles of the cluster. Both apical boron atoms reside 1.09 Å above a r.m.s. plane through their corresponding boron atom squares, with the two planes being parallel within standard deviation. The boron-hydrogen bond lengths vary between 1.03 Å and 1.11 Å for $Rb_2[B_{10}H_{10}] \cdot 5\,NH_3$ and between 1.05 Å and 1.15 Å for $Cs_2[B_{10}H_{10}] \cdot 5\,NH_3$. The $[B_{10}H_{10}]^{2-}$ cage is coordinated by six metal cations (Rb or Cs). The metal cation (Rb or Cs) shows a coordination number of eleven, since one *closo*-hydroboate cage is coordinating $\eta_3$- like, two symmetry equivalent hydroborate ions are coordinating $\eta_2$- like and four symmetry independent ammonia molecules are bonded to it, which is shown in figure 4.17. The Rb-H-distances vary between 2.92 and 3.23 Å and Cs-H-distances varying between 3.10 and 3.31 Å respectively. The two ammonia molecules are acting as bridging ligands between M and its symmetry equivalent. For example, N(2) and N(3) are acting as bridging ligands between Rb(1) and its

symmetry equivalent Rb(1)#8, N(4) bridges between Rb(1) and Rb(1)#9. Additionally N(2) forms two hydrogen bonds using H(2A) and H(2A)#8 to N(1) and N(1)#8, respectively as shown in figure 4.18). Hydrogen bond lenghts (in Å) and angles (in °) for $Rb_2[B_{10}H_{10}] \cdot 5\,NH_3$ are N(2)-H(2B) 0.76(5), N(1)$\cdots$ H(2B) 2.610, N(2)-H(2B)$\cdots$ N(1) 142.3. Thus, a $[M_2(NH_3)_5]$-chain is formed running along the b-axis where each metal ion is additionally surrounded by three $[B_{10}H_{10}]^{2-}$ cages. The primitive unit cell is shown in figure 4.19.

| Atom | Wyck. | x /a | y /b | z /c | $U_{eq}$ |
|---|---|---|---|---|---|
| Rb1 | 8d | 0.07674(2) | -0.01039(3) | 0.66140(2) | 0.02300(8) |
| N1 | 8d | -0.0290(2) | 0.0094(4) | 0.8667(2) | 0.0326(6) |
| H1A | 8d | -0.076(2) | 0.079(4) | 0.848(2) | 0.06(1) |
| H1B | 8d | -0.064(2) | -0.038(4) | 0.912(2) | 0.07(1) |
| H1C | 8d | 0.012(2) | 0.055(4) | 0.894(2) | 0.07(1) |
| N2 | 4c | -0.0822(3) | -0.2500 | 0.7080(4) | 0.0318(9) |
| H2A | 4c | -0.122(6) | -0.2500 | 0.674(6) | 0.15(4) |
| H2B | 8d | -0.096(3) | -0.180(6) | 0.738(3) | 0.15(2) |
| N3 | 4c | 0.1527(4) | -0.2500 | 0.8162(3) | 0.0326(9) |
| H3A | 8d | 0.184(2) | -0.173(3) | 0.832(2) | 0.07(1) |
| H3B | 4c | 0.111(4) | -0.2500 | 0.854(4) | 0.10(2) |
| N4 | 4c | 0.2202(3) | 0.2500 | 0.5755(3) | 0.0302(9) |
| H4A | 8d | 0.240(2) | 0.170(4) | 0.547(2) | 0.07(1) |
| H4B | 4c | 0.254(3) | 0.2500 | 0.619(3) | 0.05(2) |
| B1 | 4c | 0.1801(3) | 0.2500 | 0.8383(3) | 0.0190(9) |
| H1 | 4c | 0.111(2) | 0.2500 | 0.800(2) | 0.021(9) |
| B2 | 4c | 0.4138(3) | 0.2500 | 0.9634(3) | 0.0207(9) |
| H2 | 4c | 0.484(2) | 0.2500 | 0.998(2) | 0.019(9) |
| B3 | 8d | 0.2800(2) | 0.1439(3) | 0.8173(2) | 0.0181(6) |
| H3 | 8d | 0.279(2) | 0.067(2) | 0.760(1) | 0.020(6) |
| B4 | 8d | 0.7045(2) | 0.2500 | 0.5017(2) | 0.0164(5) |
| H4 | 8d | 0.716(2) | 0.2500 | 0.575(2) | 0.020(7) |
| B5 | 4c | 0.3012(3) | 0.2500 | 1.0082(3) | 0.0189(9) |
| H5 | 4c | 0.292(3) | 0.2500 | 1.085(3) | 0.045(1) |
| B6 | 8d | 0.3451(2) | 0.1009(3) | 0.9265(2) | 0.0187(6) |
| H6 | 8d | 0.371(1) | -0.019(2) | 0.937(1) | 0.013(6) |
| B7 | 4c | -0.6115(3) | 0.2500 | 0.8447(3) | 0.0182(9) |
| H7 | 4c | -0.549(2) | 0.2500 | 0.795(2) | 0.02(1) |

Table 4.16: Atomic co-ordinates and equivalent thermal displacement parameters for $Rb_2[B_{10}H_{10}] \cdot 5\,NH_3$

| Atom | U11 | U22 | U33 | U23 | U13 | U12 |
|------|-----|-----|-----|-----|-----|-----|
| RB1 | 0.0213(1) | 0.0227(1) | 0.0250(1) | -0.0023(1) | 0.0009(1) | 0.0017(1) |
| B1 | 0.019(2) | 0.021(2) | 0.017(2) | 0.00000 | -0.001(2) | 0.00000 |
| B2 | 0.013(2) | 0.026(2) | 0.022(2) | 0.00000 | -0.001(2) | 0.00000 |
| B3 | 0.018(2) | 0.020(1) | 0.017(2) | -0.001(1) | -0.001(1) | -0.003(1) |
| B4 | 0.014(1) | 0.022(2) | 0.021(1) | 0.0001(1) | 0.002(1) | -0.005(1) |
| B5 | 0.015(2) | 0.028(2) | 0.014(2) | 0.00000 | 0.001(2) | 0.00000 |
| B6 | 0.015(2) | 0.022(2) | 0.019(2) | 0.003(1) | -0.001(1) | 0.001(1) |
| B7 | 0.011(2) | 0.020(2) | 0.024(2) | 0.00000 | 0.004(2) | 0.00000 |
| N1 | 0.025(1) | 0.042(2) | 0.031(1) | 0.003(2) | -0.001(1) | -0.003(1) |
| N2 | 0.022(2) | 0.033(2) | 0.040(2) | 0.00000 | -0.002(2) | 0.00000 |
| N3 | 0.032 | 0.034(2) | 0.032(2) | 0.00000 | -0.004(2) | 0.00000 |
| N4 | 0.025(2) | 0.040(2) | 0.025(2) | 0.00000 | 0.001(2) | 0.00000 |

Table 4.17: Anisotropic thermal displacement parameters for $Rb_2[B_{10}H_{10}] \cdot 5\,NH_3$

| Atom | Wyck. | x /a | y /b | z /c | $U_{eq}$ |
|------|-------|------|------|------|----------|
| CS1 | 8d | 0.57641(1) | 0.00898(1) | 0.65791(1) | 0.01855(6) |
| N1 | 8d | 0.4649(2) | -0.0071(2) | 0.8674(2) | 0.0323(4) |
| H1A | 8d | 0.428(2) | -0.069(5) | 0.843(2) | 0.065(1) |
| H1B | 8d | 0.512(2) | -0.057(4) | 0.893(2) | 0.060(9) |
| H1C | 8d | 0.437(2) | 0.034(4) | 0.908(3) | 0.073(1) |
| N2 | 4c | 0.6468(2) | 0.2500 | 0.8226(2) | 0.0336(6) |
| H2A | 4c | 0.591(3) | 0.2500 | 0.850(3) | 0.078(2) |
| H2B | 8d | 0.668(2) | 0.174(4) | 0.843(2) | 0.084(1) |
| N3 | 4c | 0.7280(2) | -0.2500 | 0.5691(2) | 0.0298(6) |
| H3A | 8d | 0.742(2) | -0.173(3) | 0.536(2) | 0.042(7) |
| H3B | 4c | 0.768(3) | -0.2500 | 0.609(3) | 0.064(1) |
| N4 | 4c | 0.4079(2) | 0.2500 | 0.7100(2) | 0.0310(6) |
| H4A | 8d | 0.376(3) | 0.165(4) | 0.71(3) | 0.12(1) |
| H4B | 4c | 0.409(4) | 0.2500 | 0.767(4) | 0.11(2) |
| B1 | 4c | 0.5927(2) | 0.2500 | 0.4573(2) | 0.0158(5) |
| H1 | 4c | 0.526(2) | 0.2500 | 0.490(2) | 0.032(8) |
| B2 | 4c | 0.6191(2) | -0.7500 | 0.3412(2) | 0.0157(5) |
| H2 | 4c | 0.562(2) | -0.7500 | 0.288(2) | 0.020(8) |
| B3 | 8d | 0.6616(3) | 0.1044(2) | 0.4217(1) | 0.0155(4) |
| H3 | 8d | 0.638(2) | -0.011(2) | 0.434(2) | 0.034(7) |
| B4 | 4c | 0.7045(2) | 0.2500 | 0.5017(2) | 0.0164(5) |
| H4 | 4c | 0.716(2) | 0.2500 | 0.575(2) | 0.020(7) |
| B5 | 8d | 0.7874(1) | 0.1469(2) | 1.4291(1) | 0.0166(4) |
| H5 | 8d | 0.836(1) | 0.059(2) | 1.464(1) | 0.022(5) |
| B6 | 8d | 0.7268(1) | -0.6467(2) | 1.3151(1) | 0.0151(4) |
| H6 | 8d | 0.725(1) | -0.566(2) | 1.258(1) | 0.020(5) |
| B7 | 4c | 0.8259(2) | 0.2500 | 1.3363(2) | 0.0159(5) |
| H7 | 4c | 0.892(2) | 0.2500 | 1.301(2) | 0.013(6) |

Table 4.18: Atomic co-ordinates and equivalent thermal displacement parameters for $Cs_2[B_{10}H_{10}] \cdot 5\,NH_3$

(a) Co-ordination sphere of $[B_{10}H_{10}]^{2-}$      (b) Co-ordination sphere of the cation
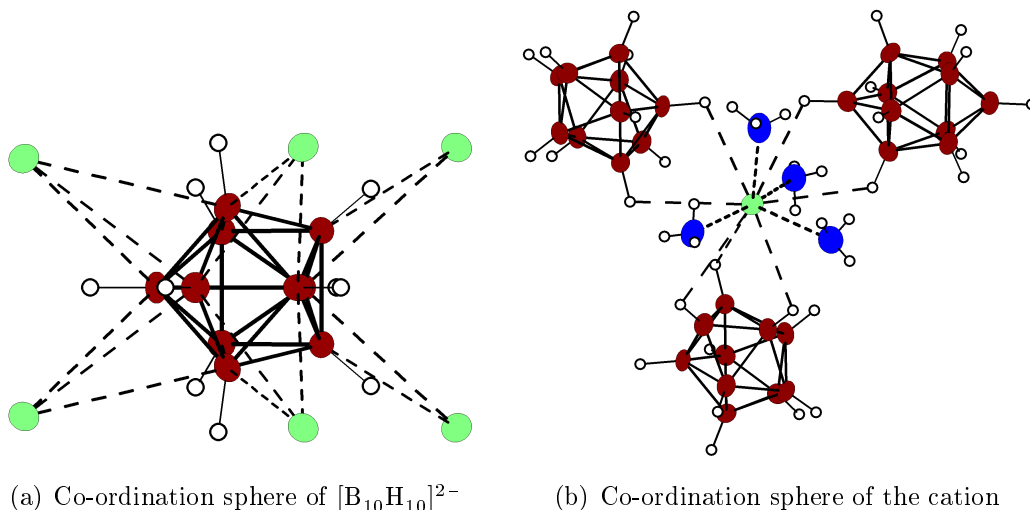
Figure 4.17: Co-ordination sphere of both anion and cation. Ellipsoids of thermal displacement parameter are drawn for Rb containing compound at 70 % probability
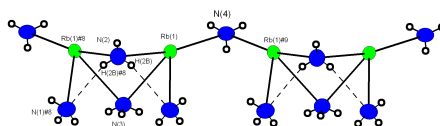


Figure 4.18: [Projection of a fragment of the $[Rb_2(NH_3)_5]$-chain. Ellipsoids of thermal displacement parameters are drawn at 70 % probability level. Symmetry transformations to generate equivalent atoms: $\#8 = x, -0.5-y, z$

| Atom | U11 | U22 | U33 | U23 | U13 | U12 |
|------|-----|-----|-----|-----|-----|-----|
| CS1 | 0.01927(9) | 0.01887(8) | 0.01752(9) | 0.00284(4) | -0.00047(4) | -0.00147(4) |
| N1 | 0.0296(2) | 0.0423(2) | 0.0249(9) | -0.0026(8) | 0.0030(9) | 0.0035(9) |
| N2 | 0.0367(2) | 0.0319(2) | 0.0322(2) | 0.00000 | -0.007(1) | 0.00000 |
| N3 | 0.034(1) | 0.031(1) | 0.025(1) | 0.00000 | 0.003(1) | 0.00000 |
| N4 | 0.026(1) | 0.027(1) | 0.041(1) | 0.00000 | 0.001(1) | 0.00000 |
| B1 | 0.015(1) | 0.019(1) | 0.013(1) | 0.00000 | 0.0016(9) | 0.00000 |
| B2 | 0.015(1) | 0.018(1) | 0.014(1) | 0.00000 | -0.00013 | 0.00000 |
| B3 | 0.0171(9) | 0.0169(9) | 0.0124(9) | 0.0018(7) | -0.0007(7) | -0.0012(7) |
| B4 | 0.017(1) | 0.019(1) | 0.013(1) | 0.00000 | -0.0008(9) | 0.00000 |
| B5 | 0.0150(9) | 0.0199(9) | 0.0150(9) | 0.0006(7) | -0.0015(7) | 0.0020(7) |
| B6 | 0.0174(8) | 0.0160(8) | 0.0120(8) | 0.0006(7) | 0.0004(7) | -0.0006(7) |
| B7 | 0.014(1) | 0.019(1) | 0.015(1) | 0.00000 | -0.0002(9) | 0.00000 |

Table 4.19: Anisotropic thermal displacement parameters for $Cs_2[B_{10}H_{10}] \cdot 5\,NH_3$
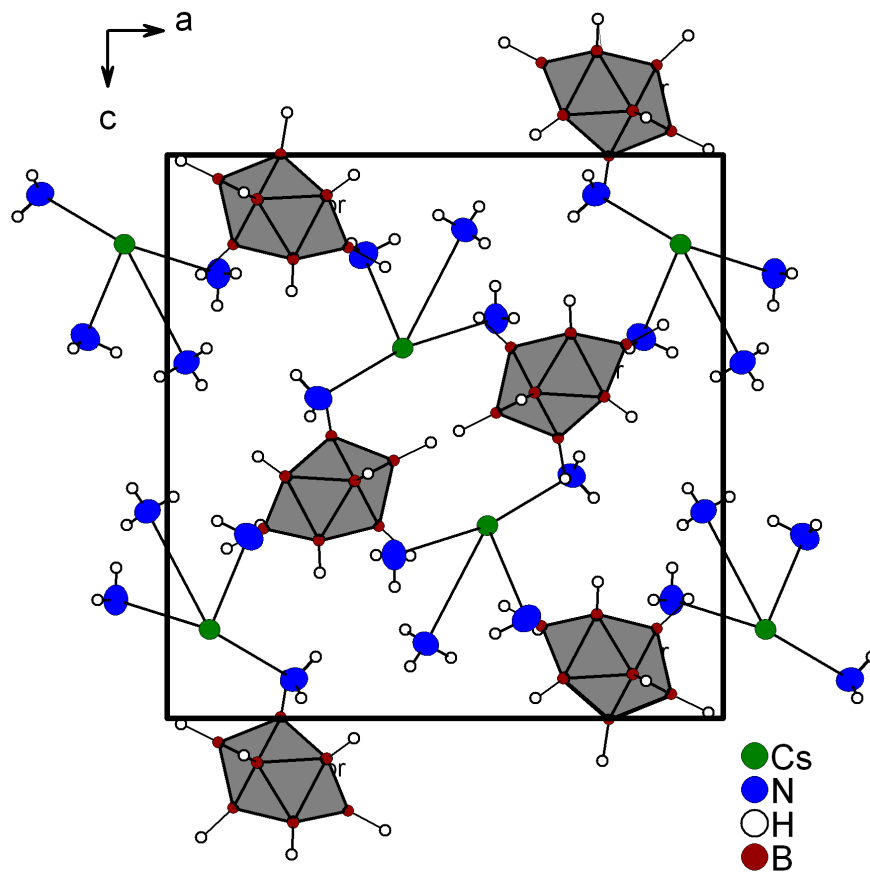
Figure 4.19: The crystal structure of $Cs_2[B_{10}H_{10}] \cdot 5\,NH_3$ projected on the *ac*-plane. The boron atoms of *closo*-hexahydroborates are shown as polyhedrons. Ellipsoids of thermal displacement parameter are drawn at 70 % probability

## 4.4 Alkali metal compounds containing the $[B_{12}H_{12}]^{2-}$ anion

Among many thousands of known boron hydrogen compounds, one of the most central places belongs to the dodecahydro-*closo*-dodecaborate anion $[B_{12}H_{12}]^{2-}$. The structure of this anion is described as a regular icosahedron and looks as an incarnation of the highest simplicity and the highest symmetry. An icosahedron is a rigid body with point symmetry $I_h$ (fig. 4.20). Therefore, it has the following point symmetries: 24 $C_5$, 20 $C_3$, 15 $C_2$, i, 12 $S_{10}$, 12 $S_{10}^3$, 20 $S_6$ and 15 $\sigma$. Due to the 5 fold rotation axes, it is impossible to derive a closed packed crystalline structure with ideal icosahedra. Compounds like $LiB_{13}$ contain a boron atom framework consisting of icosahedra. A molecular compound with an unsubstituted $[B_{12}H_{12}]^{2-}$ unit and a lithium atom would be perfect to compare to $LiB_{13}$ for analysing the ideality of icosahedra in molecular chemistry and solid state chemistry of boron rich materials.

Using ammonia as solvent, we were able to synthesize and structurally characterize ammoniates of lithium containing the $[B_{12}H_{12}]^{2-}$ ion for the first time. An ammoniate of a mixed cationic compound containing lithium and sodium was also synthesized. The crystal structure of these compounds will be described here.
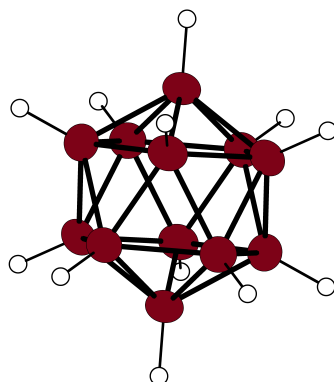


Figure 4.20: $[B_{12}H_{12}]^{2-}$ unit

## 4.4.1 Synthesis and characterization of Bis-(tetraamminelithium)-dodecahydro-*closo*-dodeca--borate-ammonia (1/2) $[Li(NH_3)_4]_2[B_{12}H_{12}] \cdot 2\,NH_3$

### 4.4.1.1 Synthesis

$[Li(NH_3)_4]_2[B_{12}H_{12}].2NH_3$ was synthesized by reacting lithium and $[N(C_4H_9)_4]_2[B_{12}H_{12}]$. All the reactions were carried out excluding moisture in an atmosphere of purified and dry argon. $[N(C_4H_9)_4]_2[B_{12}H_{12}]$ was dried at room temperature for 18 h in $3\times10^{-3}$ mbar. The infrared spectrum of $[N(C_4H_9)_4]_2[B_{12}H_{12}]$ shows the characteristic vibrations of the $[B_{12}H_{12}]^{2-}$ ion which are comparable to the literature values [129–131]. The IR spectrum is shown in figure 4.21 and the assignment of peaks to particular groups are shown in the table 4.20.

| Wavenumber /cm$^{-1}$ | Assignment of characteristic group |
|---|---|
| 2961 | C-N stretching vibration ($\nu_{C-N}$) |
| 2873 | C-H stretching vibration ($\nu_{C-N}$) |
| 2471 | B-H stretching vibration ($\nu_{B-H}$) |
| 1471, 1381 | C-H bending vibration ($\delta_{C-H}$) |
| 709, 740, 1054, 1108 | B-B cage vibration ($\delta_{B-B}$) |

Table 4.20: IR-bands of $[N(C_4H_9)_4]_2[B_{12}H_{12}]$
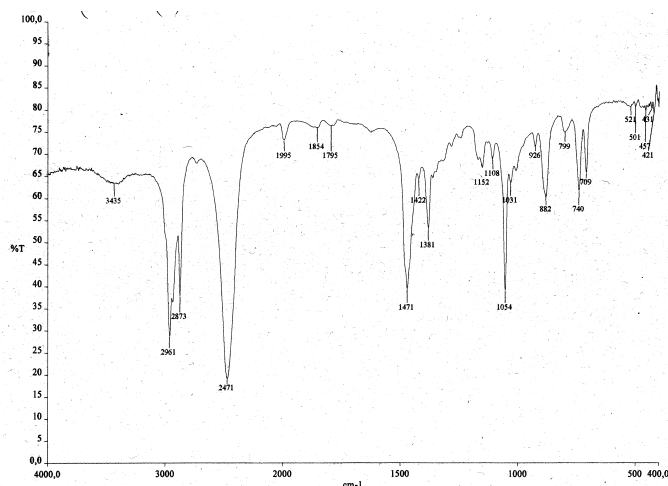


Figure 4.21: Infrared spectrum of $[N(C_4H_9)_4]_2[B_{12}H_{12}]$

0.017 g (2.45 mmol) of lithium and 0.313 g (0.50 mmol) of $[N(C_4H_9)_4]_2[B_{12}H_{12}]$ were placed in a Schlenk tube and the evacuated vessel was cooled by a dry ice/ isopropanol slush. Approximately 15 mL of liquid ammonia was condensed into the

117

tube through a vacuum line, yielding a blue solution of the alkali metal. It was then stored at 235 K for one month resulting in colorless crystals in the form of cubes. A crystal with dimensions of 0.23 mm × 0.19 mm × 0.14 mm was measured on the diffractometer.

### 4.4.1.2 X-ray investigation

Crystallographic details of the data collection and the refinement parameters are given in table 4.21. No evidence of symmetry higher than monoclinic was observed in the diffraction data. Systematic extinctions suggested the possible space group $P2_1/c$, which yielded chemically reasonable and computationally stable results of refinement. The structure was solved by direct methods, completed by subsequent difference Fourier syntheses and refined by the full-matrix least-squares procedure. All the non-hydrogen atoms were refined with anisotropic thermal displacement parameters. The hydrogen atoms were located from the difference maps. To verify the selection of the space group $P2_1/c$, searches for additional symmetry were performed, which did not indicate further symmetries.

| Empirical formula | $H_{42}B_{12}Li_2 N_{10}$ |
|---|---|
| Formula weight /g/mol | 326.04 |
| Crystal system | Monoclinic |
| Space group | $P2_1/c$ (No. 14) |
| $a$ /Å | 9.183(2) |
| $b$ /Å | 8.1330(10) |
| $c$ /Å | 16.357(3) |
| $\beta$ /° | 110.540(10) |
| $V$ /Å$^3$ | 1144.0(4) |
| $Z$ | 2 |
| $\rho_c$ /g/cm$^3$ | 0.947 |
| Wave length /Å | 0.71073 |
| Detector distance /mm | 60 |
| $\omega$- Increment | 0.3° |
| Temperature /K | 123 |
| $F(000)$ | 356 |
| $\mu(\text{MoK}_\alpha)$ /mm$^{-1}$ | 0.054 |
| $\theta$-Range | 2.37° to 28.04° |
| Collected reflections | 13396 |
| Unique reflections | 2696 |
| Reflections with I $>4\sigma$ (I) | 1258 |
| $R_{int}$ | 0.0691 |
| $h$ | -12 to 11 |
| $k$ | -10 to 10 |
| $l$ | -21 to 21 |
| Refinement method | Full-matrix least-squares on F$^2$ |
| Final $R$ indices [I$>4\sigma$(I)] | $R_1 = 0.0422$ |
| $R$ indices (all data) | $R_1 = 0.0907$, $wR_2 = 0.0746$ |
| Goodness-of-fit (S) | 0.714 |
| Number of parameters | 193 |
| $w=1/[\sigma^2(\text{Fo}^2)+(0.0285\text{P})^2+0.0000\text{P}]$ | |
| P=(Fo$^2$+2Fc$^2$)/3 | |
| $\Delta\rho_{max}$ /eÅ$^{-3}$ | 0.199 |
| $\Delta\rho_{min}$ /eÅ$^{-3}$ | -0.209 |

Table 4.21: Crystal data and structure refinement for $[\text{Li(NH}_3)_4]_2[\text{B}_{12}\text{H}_{12}] \cdot 2\,\text{NH}_3$

### 4.4.1.3 Description of crystal structure

$[\text{Li(NH}_3)_4]_2[\text{B}_{12}\text{H}_{12}] \cdot 2\,\text{NH}_3$ crystallizes in a monoclinic crystal system with two formula units per unit cell. The asymmetric unit contains one lithium atom, one dodecahydro-*closo*-dodecaborate unit and five ammonia molecules. All the atoms are situated at the general positions 4$e$. All the atomic co-ordinates, isotropic and anisotropic thermal parameters are shown in table 4.22 and 4.23. The asymmetric unit is shown in figure 4.22.

119
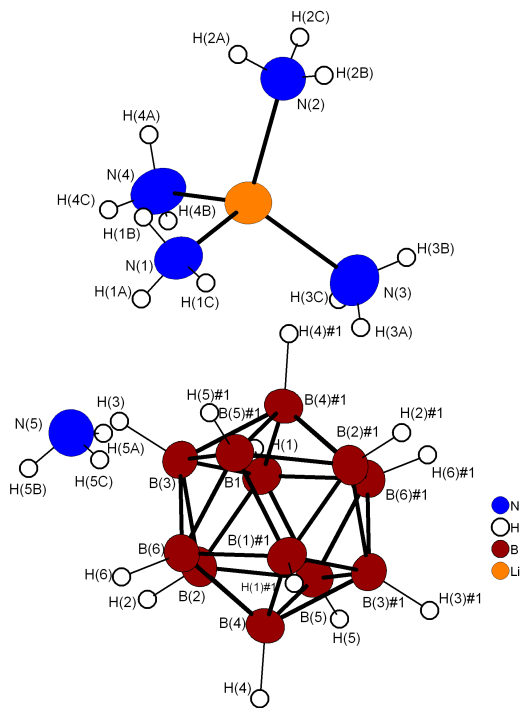
Figure 4.22: Asymmetric unit of $[Li(NH_3)_4]_2[B_{12}H_{12}] \cdot 2NH_3$. Ellipsoids of the thermal displacement parameters are drawn at 70 % probability

The dodecahydro-*closo*-dodecaborate cage is built up by six boron and six hydrogen atoms and their symmetry equivalents respectively, forming the well-known shape of $[B_{12}H_{12}]^{2-}$ which is similar to an icosahedron. The bond lengths of B-B and B-H are shown in the table 4.24. The B-B-bond lengths are found at approximately 1.77 Å and B-H at approximately 1.11 Å. B-B-B bond angles are approximately 107° in the boron pentagon and close to 60° in the boron triangles of the cage. All the apical boron atoms are centered within 0.3° and located about 0.936(2) Å above a root mean square (r.m.s). plane through their corresponding boron pentagons, with the greatest r.m.s. deviation being only 0.0016. The $[B_{12}H_{12}]^{2-}$ cage is surrounded by six symmetry equivalent tetraammine lithium complexes with a Li-B distance in the range from 4.23 to 4.88 Å and with a geometry similar to an octahedron. The lithium cation is coordinated by four molecules of ammonia yielding almost a tetrahedron and is shown in figure 4.23. The Li-N bond lengths extend from 2.04 to 2.09 Å in the range of the sum of the covalent radii (2.09 Å) [124], indicating the presence of covalent Li-N bonding. One ammonia molecule in the asymmetric unit is forming N-H···N hydrogen bond to the ammonia molecules of the coordination sphere of lithium cation. These hydrogen bonds result in the formation of a
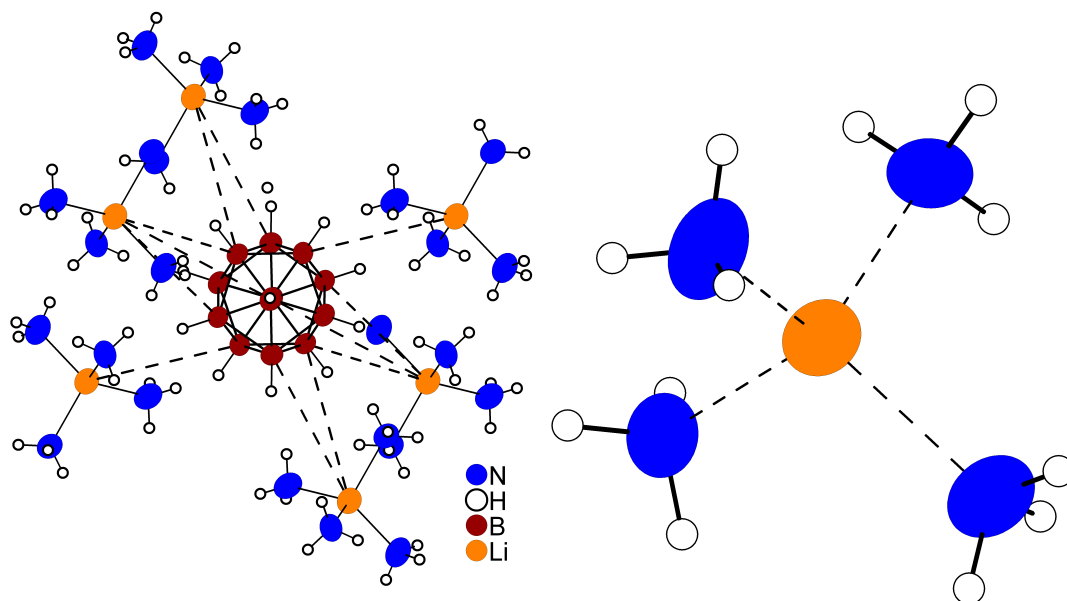
(a) Co-ordination sphere of the $[B_{12}H_{12}]^{2-}$ unit

(b) Co-ordination sphere of lithium

Figure 4.23: Co-ordination sphere of both anion and cation. Ellipsoids of the thermal displacement parameters are drawn at 70 % probability

$[Li(NH_3)_4 \cdot NH_3]$ -zig-zag chain running along the b-axis (fig. 4.24). The hydrogen bonded zig-zag strands are separated by dodecahydro-*closo*-dodecaborate cages. Selected bond lengths (in Å) and angles (in °) found in hydrogen bonds are N(1)-H(1A) 0.90(2), N(5)$\cdots$ H(1A) 2.54, N(1)-H(1A)$\cdots$ N(5) 165.9, N(4)#1-H(4A)#1 0.88(2), N(5)$\cdots$ H(4A)#1 2.32, N(4)#1-H(4A)#1 $\cdots$ N(5) 170.5. The primitive unit cell of $[Li(NH_3)_4]_2[B_{12}H_{12}].2NH_3$ is shown in figure 4.26, where $[B_{12}H_{12}]$ clusters are located at the corners as well as at the edges. The center of the unit cell is occupied by tetraammine lithium ions and ammonia molecules. The packing scheme is displayed in figure 4.25. It can be derived from a slightly distorted hexagonal arrangement of the anions with cations (lithium ions) in the tetrahedral interstices. Each of the boronate anions is surrounded by twelve others, the mean distance between their centers of gravity is 9.51 Å for this compound. The mean distance between the lithium ions and the centers of gravity of the boronate anions is 6.20 Å.

(a) Fragment of zig-zag chain.

(b) Projection of chains in *bc*-plane.
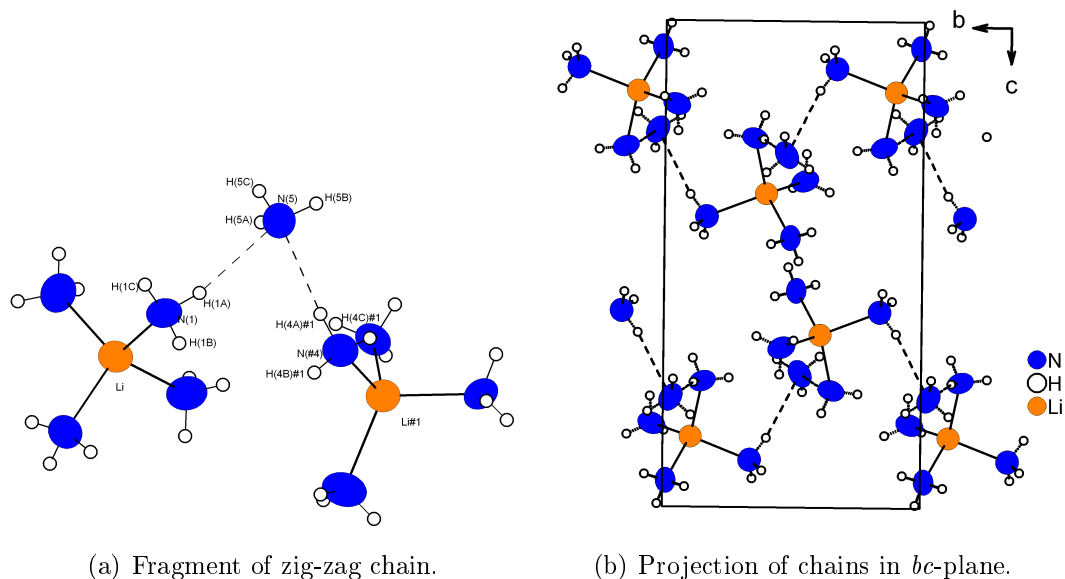
Figure 4.24: $[\mathrm{Li(NH_3)_4 \cdot NH_3}]$ zig-zag chains due to hydrogen bonds. Symmetry transformations to generate equivalent atoms: $\#\, 1 = -x+1, y-0.5, -z+0.5$. Ellipsoids of thermal displacement parameters are drawn at $70\,\%$ probability
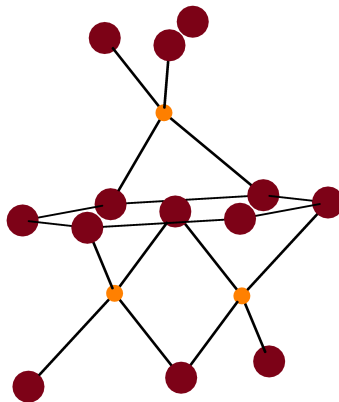


Figure 4.25: Packing scheme for $[\mathrm{Li(NH_3)_4}]_2[\mathrm{B_{12}H_{12}}] \cdot 2\,\mathrm{NH_3}$ . For the $\mathrm{B_{12}}$-polyhedra the centers of gravity are represented as large spheres (red), the lithium atoms are represented as small spheres (orange)
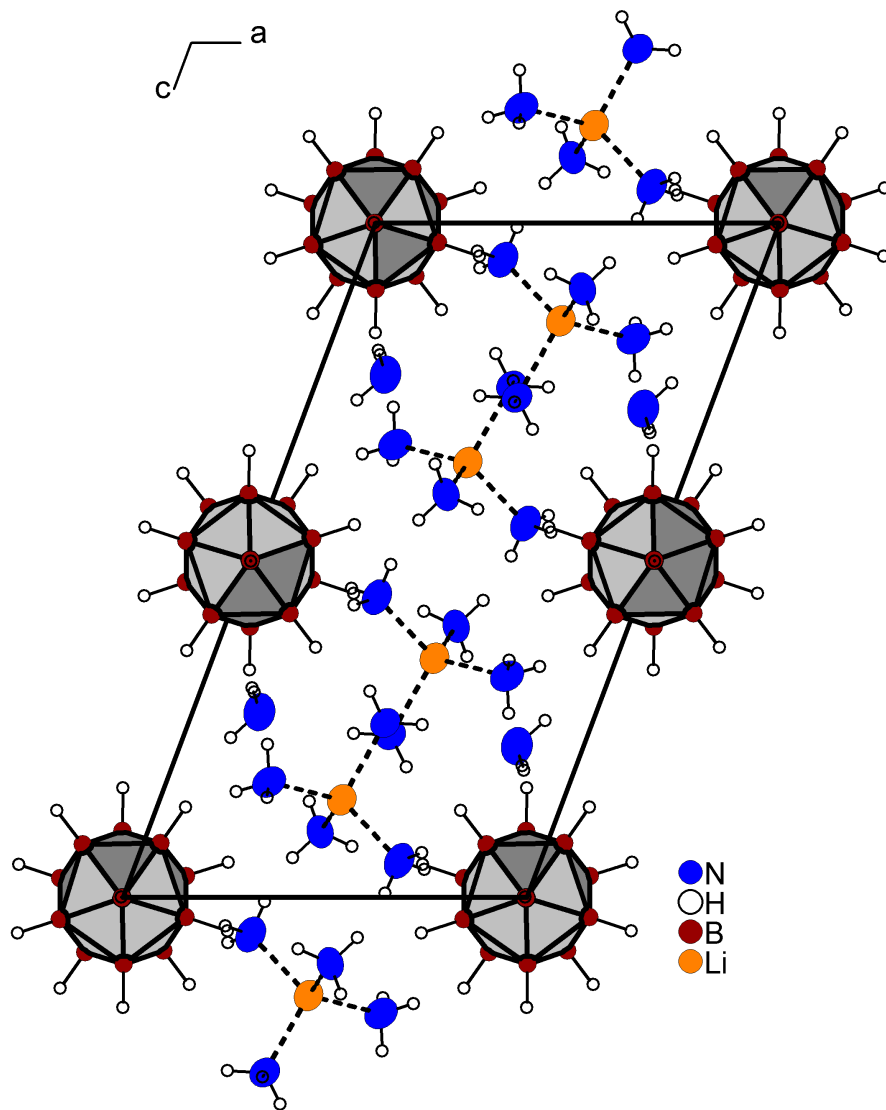
Figure 4.26: The crystal structure of [Li(NH$_3$)$_4$]$_2$[B$_{12}$H$_{12}$].2NH$_3$. The boron atoms of *closo*-dodecahydroborates are shown as polyhedrons. Ellipsoids of the thermal displacement parameters are drawn at 70 % probability

| Atom | Wyck. | x /a | y /a | z /c | $U_{eq}$ |
|------|-------|------|------|------|------|
| N1 | 4e | 0.5735(2) | 0.3368(2) | 0.0976(1) | 0.0334(4) |
| H1A | 4e | 0.628(2) | 0.401(2) | 0.143(1) | 0.076(7) |
| H1B | 4e | 0.481(2) | 0.385(2) | 0.076(1) | 0.060(6) |
| H1C | 4e | 0.617(2) | 0.347(2) | 0.059(1) | 0.055(6) |
| N2 | 4e | 0.3498(2) | 0.0127(2) | 0.0545(1) | 0.0348(4) |
| H2A | 4e | 0.279(2) | 0.087(2) | 0.041(1) | 0.070(7) |
| H2B | 4e | 0.355(2) | -0.020(3) | 0.006(2) | 0.118(1) |
| H2C | 4e | 0.301(2) | -0.070(2) | 0.066(1) | 0.094(9) |
| N3 | 4e | 0.7459(2) | -0.0432(2) | 0.1716(1) | 0.0416(4) |
| H3A | 4e | 0.818(2) | 0.005(2) | 0.1572(1) | 0.089(9) |
| H3B | 4e | 0.737(2) | -0.139(3) | 0.1485(1) | 0.093(9) |
| H3C | 4e | 0.784(2) | -0.050(2) | 0.227(1) | 0.072(7) |
| N4 | 4e | 0.5124(2) | 0.1521(2) | 0.2590(1) | 0.0368(4) |
| H4A | 4e | 0.419(2) | 0.118(2) | 0.2565(9) | 0.050(6) |
| H4B | 4e | 0.580(2) | 0.116(2) | 0.306(1) | 0.067(7) |
| H4C | 4e | 0.512(2) | 0.255(2) | 0.266(1) | 0.060(7) |
| N5 | 4e | 0.8348(2) | 0.5296(2) | 0.2752(1) | 0.0413(4) |
| H5A | 4e | 0.866(2) | 0.441(2) | 0.305(1) | 0.071(8) |
| H5B | 4e | 0.875(2) | 0.608(2) | 0.311(1) | 0.063(7) |
| H5C | 4e | 0.882(2) | 0.539(2) | 0.237(1) | 0.079(8) |
| B1 | 4e | 0.9575(2) | 0.4054(2) | 0.0809(1) | 0.0226(4) |
| H1 | 4e | 0.929(2) | 0.3405(1) | 0.1342(7) | 0.017(3) |
| B2 | 4e | 1.0632(2) | 0.5928(2) | 0.0986(1) | 0.0233(4) |
| H2 | 4e | 1.102(1) | 0.6567(1) | 0.1627(7) | 0.017(3) |
| B3 | 4e | 0.8637(2) | 0.5910(2) | 0.0321(1) | 0.0218(4) |
| H3 | 4e | 0.773(1) | 0.6472(1) | 0.0526(7) | 0.018(3) |
| B4 | 4e | 0.8268(2) | 0.4061(2) | -0.0287(1) | 0.0223(4) |
| H4 | 4e | 0.711(1) | 0.347(1) | -0.0491(6) | 0.012(3) |
| B5 | 4e | 1.0022(2) | 0.2915(2) | -0.0002(1) | 0.0225(4) |
| H5 | 4e | 1.005(1) | 0.155(1) | 0.0011(7) | 0.016(3) |
| B6 | 4e | 1.1489(2) | 0.4085(2) | 0.0787(1) | 0.0218(4) |
| H6 | 4e | 1.245(1) | 0.351(1) | 0.1290(7) | 0.019(3) |
| Li | 4e | 0.5495(3) | 0.1073(3) | 0.1450(2) | 0.0324(6) |

Table 4.22: Atomic co-ordinates and equivalent thermal displacement parameters for $[Li(NH_3)_4]_2[B_{12}H_{12}] \cdot 2\,NH_3$

| Atom | U11 | U22 | U33 | U23 | U13 | U12 |
|------|-----|-----|-----|-----|-----|-----|
| N1 | 0.0289(9) | 0.0367(9) | 0.038(1) | 0.0009(8) | 0.0163(8) | -0.0025(8) |
| N2 | 0.0280(8) | 0.028(1) | 0.044(1) | -0.0007(8) | 0.0072(7) | 0.0019(8) |
| N3 | 0.034(1) | 0.052(1) | 0.034(1) | -0.0074(9) | 0.0053(8) | 0.0071(8) |
| N4 | 0.0291(9) | 0.048(1) | 0.0302(9) | 0.0069(8) | 0.0064(8) | 0.0032(8) |
| N5 | 0.0347(9) | 0.039(1) | 0.050(1) | -0.012(1) | 0.0146(9) | -0.0011(8) |
| B1 | 0.0206(9) | 0.024(1) | 0.024(1) | 0.0027(8) | 0.0082(8) | 0.0018(8) |
| B2 | 0.0243(9) | 0.022(1) | 0.022(1) | -0.0030(8) | 0.0063(8) | 0.0012(8) |
| B3 | 0.0199(9) | 0.022(1) | 0.023(1) | -0.0011(8) | 0.0067(8) | 0.0025(8) |
| B4 | 0.0197(9) | 0.0198(9) | 0.0254(9) | -0.0003(8) | 0.0053(8) | -0.0016(8) |
| B5 | 0.0217(9) | 0.016(1) | 0.028(1) | 0.0002(8) | 0.0064(8) | 0.0014(7) |
| B6 | 0.0200(9) | 0.021(1) | 0.022(1) | 0.0026(8) | 0.0045(8) | 0.0024(8) |
| Li | 0.028(1) | 0.034(2) | 0.033(2) | -0.0002(1) | 0.009(1) | -0.001(1) |

Table 4.23: Anisotropic thermal displacement parameters for
$[\mathrm{Li(NH_3)_4}]_2[\mathrm{B_{12}H_{12}}] \cdot 2\,\mathrm{NH_3}$

| Bond | Length /Å | Bond | Length /Å |
|------|-----------|------|-----------|
| B(1)-B(6) | 1.771(2) | B(4)-B(5) | 1.776(2) |
| B(1)-B(4) | 1.772(2) | B(5)-B(3)#1 | 1.775(2) |
| B(1)-B(2) | 1.776(2) | B(5)-B(2)#1 | 1.777(2) |
| B(1)-B(5) | 1.780(2) | B(5)-B(6) | 1.780(2) |
| B(1)-B(3) | 1.782(2) | B(6)-B(4)#1 | 1.767(2) |
| B(2)-B(3) | 1.772(2) | B(6)-B(3)#1 | 1.775(2) |
| B(2)-B(6) | 1.775(2) | B(1)-H(1) | 1.13(1) |
| B(2)-B(4)#1 | 1.771(2) | B(2)-H(2) | 1.11(1) |
| B(2)-B(5)#1 | 1.777(2) | B(3)-H(3) | 1.10(1) |
| B(3)-B(4) | 1.769(2) | B(4)-H(4) | 1.11(1) |
| B(3)-B(6)#1 | 1.775(2) | B(5)-H(5) | 1.11(1) |
| B(3)-B(5)#1 | 1.775(2) | B(6)-H(6) | 1.08(1) |
| B(4)-B(6)#1 | 1.767(2) | | |

Table 4.24: Bond lengths of the $[\mathrm{B_{12}H_{12}}]^{2-}$ cluster

## 4.5 Symmetry analysis of polyhedra in alkali metal borides and *closo*-hydroborates

The crystal structures of boron-rich solids are described by frameworks of interconnected boron atom polyhedra. The electronic situation of boron atom frameworks in boron-rich solids is not easy to understand. As described by Albert [55], to understand the bonding situation in boron-rich solids, it is necessary to understand the electron count of boron atom polyhedra in well-defined compounds. The electronic situation of the boron atom clusters found in the *closo*-hydroborates has already been well studied and reported by Longuet-Higgins and de V. Roberts [95] and K. Wade [132]. Then the geometric situation between boron atom polyhedra in molecules and in solids has to be compared. It is often desirable to know how ideal these polyhedra are in boron-rich solids.

In this study, the type of polyhedra studied in boron-rich alkali metal solids are ochahedra in $Li_2B_9$ and $Na_3B_{20}$, bicapped square antiprisms in $Li_3B_{14}$, and icosahedra in $LiB_{13}$. These polyhedra are comparable to $[B_6H_6]^{2-}$, $[B_{10}H_{10}]^{2-}$ and $[B_{12}H_{12}]^{2-}$ anions found in *closo*-hydroborates. The overall regularity of these polyhedra was confirmed from single crystal or powder X-ray structure determination.

As discussed in 2.2.1.7, (by using the computer program SYMMOL) the symmetry of these polyhedron can be checked and the r.m.s. values can be computed. These values characterize the degree of distortion of the polyhedra. These values are always higher than zero when crystallographic symmetry is not present. For example, in $K_2[B_6H_6]$ [97] the value is zero due to crystallographic symmetry.

There r.m.s. values and symmetries for studied alkali metal borides are given in table 4.25.

| Compound name | Symmetry | R.M.S. values |
|---|---|---|
| $Li_2B_9$ | $D_{2h}$ | 0.0940 |
| $Li_2B_9$ | $D_{4h}$ | 0.1104 |
| $Na_3B_{20}$ | $O_h$ | 0.0155 |
| $Li_3B_{14}$ | $D_{4d}$ | 0.0543 |
| $LiB_{13}$ | $I_h$ | 0.0524 |

Table 4.25: Symmetry and degree of polyhedral distortion (r.m.s. values) for different boron cages of the alkali metal borides

The r.m.s. values for $[B_6H_6]^{2-}$, $[B_{10}H_{10}]^{2-}$ and $[B_{12}H_{12}]^{2-}$ ions in the studied ammoniated compounds are given the table 4.26.

| Compound name | Symmetry | R.M.S. values |
|---|---|---|
| $[\mathrm{Li(NH_3)_4}]_2[\mathrm{B_6H_6}] \cdot 2\,\mathrm{NH_3}$ | $O_h$ | 0.0026 |
| $[\mathrm{Na(NH_3)_4}]_2[\mathrm{B_6H_6}] \cdot 2\,\mathrm{NH_3}$ | $O_h$ | 0.0155 |
| $\mathrm{Rb_2}[\mathrm{B_{10}H_{10}}] \cdot 5\,\mathrm{NH_3}$ | $D_{4d}$ | 0.0003 |
| $\mathrm{Cs_2}[\mathrm{B_{10}H_{10}}] \cdot 5\,\mathrm{NH_3}$ | $D_{4d}$ | 0.0013 |
| $[\mathrm{Li(NH_3)_4}]_2[\mathrm{B_{12}H_{12}}] \cdot 2\,\mathrm{NH_3}$ | $I_h$ | 0.0067 |

Table 4.26: Degree of polyhedral distortion (r.m.s values) for different boron cages in ammoniated alkali metal *closo*-hydroborate

As discussed, in 3.2.4.1 the arrangement of the B-atoms in $\mathrm{Li_2B_9}$ has lost the $O_h$ symmetry and can be decsribed as $D_{2h}$ or $D_{4h}$ symmetry. Comparing the r.m.s. values in the tables 4.25 and 4.26, it can be concluded that polyhedra are more distorted in compounds with extended frameworks than in ammoniated *closo*-hydroborates, except for $[\mathrm{Na(NH_3)_4}]_2[\mathrm{B_6H_6}] \cdot 2\,\mathrm{NH_3}$. The r.m.s. values of the polyhedra in $[\mathrm{Na(NH_3)_4}]_2[\mathrm{B_6H_6}] \cdot 2\,\mathrm{NH_3}$ and $\mathrm{Na_3B_{20}}$ are comparable. In the ammoniated *closo*-hydroborates, ammonia molecules plays the role as space filling molecules which separate cations from anions. Therefore, the interaction between cation and anion is weak.

# 4.6 Concluding remarks

Liquid ammonia was used as a solvent and reactant which gives access to single crystals of alkali metal *closo*-hydroborates as ammoniates. All these ammoniated alkali metal *closo*- hydroborates were synthesised via ion-exchange reactions. Lithium and sodium containing compounds were obtained via exchange of tetrabutylammonium cations of a corresponding *closo*-hydroborates. Rb and Cs containing compounds were obtained with exchange of the Li ion of the corresponding *closo*-hydroborates. All of the cations in the presented structures, *i.e.* $[\mathrm{Li(NH_3)_4}]^+$, $[\mathrm{Na(NH_3)_4}]^+$, $\mathrm{Rb}^+$ and $\mathrm{Cs}^+$ can be regarded as relatively soft acids according to Pearson principle [133]. The lithiumtetraammine cation is typical for lithium containing ammoniates. A non ammoniated *closo*-hydroborate compound $[\mathrm{N(C_4H_9)_4}]_2[\mathrm{B_6H_6}]$ was crystallized in form of single crystal using liquid ammonia.

Based on symmol calculations only minute distortions from $O_h$ for the $[\mathrm{B_6H_6}]^{2-}$ (Li and Na), $D_{4d}$ for the $[\mathrm{B_{10}H_{10}}]^{2-}$ and $I_h$ for the $[\mathrm{B_{12}H_{12}}]^{2-}$ anions were found. It is shown in this study that these compounds are very adequate to study coordination spheres and coordination numbers of the alkali metal ions.

# 5 Conclusions

This work is focussed on the syntheses and characterization of alkali metal borides and *closo*-hydroborates. Alkali metal borides were synthesized from the elements and various precursors. Alkali metal *closo*-hydroborates were crystallized as ammoniates using liquid ammonia. This route of using liquid ammonia is a new method for the synthesis and crystallization of hydroborates.

X-ray single crystal and powder diffraction methods were used for structural characterization. In addition, IR, NMR and EEL spectroscopy techniques were applied. Impedance spectroscopy was used to study conductivity in solids.

A lithium-boron compound ($Li_2B_9$) was synthesized without presence of any impurities like oxygen and nitrogen. The obtained product was found to be inhomogeneous and separated mechanically by the colour difference of the sample (*i.e.* gray and brown). The gray part was found to be more crystalline than the brown one. According to Schmitt *et al.* [16] and Wörle *et al.* [15], the crystal structure of this compound was described in the space group $P6/mmm$. The structure consists of a three dimensionally interconnected framework of boron atom octahedra. The existence of boron-atom octahedra was verified from the analysis of the near-edge structure of the $B_K$ ionization edges in EELS. Synchrotron and laboratory X-ray powder diffraction patterns indicated a reduction of symmetry compared with earlier investigations. Hence, the crystal structure was described in *Ibmm*. Due to the presence of only light elements and strongly overlapping reflections, the structure solution from powder data was not completely unambiguous. It might be further clarified in future by growing single crystals and using a higher dimensional space group. Also, additional characterization techniques like solid state NMR and neutron diffraction might be applied in future. Impedance spectroscopy measurements show electronic conductivity at room temperature and ionic conductivity at higher temperatures for $Li_2B_9$. Due to its extremely low density and the ionic conductivity, $Li_2B_9$ might be used as an electrode in modern solid state electrolyte battery technology.

The use of precursors for synthesizing alkali metal borides is also a relatively new technique. *closo*-Hydroborates were used as precursor materials for synthesizing $Li_2B_9$, $Na_3B_{20}$ and sodium azide for $Na_2B_{29}$.

Liquid ammonia turned out to be a very promising solvent or reactant for crystallizing new alkali metal *closo*-hydroborates as ammoniates. In this work, for the first time the crystal structures of lithium *closo*-hydroborates were solved. They were obtained in form of single crystals as ammoniates such as $[Li(NH_3)_4]_2[B_6H_6] \cdot 2\,NH_3$ and $[Li(NH_3)_4]_2[B_{12}H_{12}] \cdot 2\,NH_3$. Other *closo*-hydroborates discussed in this work are $[Na(NH_3)_4]_2[B_6H_6] \cdot 2\,NH_3$ and $M_2[B_{10}H_{10}] \cdot 5\,NH_3$ (M = Rb and Cs). A non-ammoniated *closo*-hydroborate $[N(C_4H_9)_4]_2[B_6H_6]$ was synthesized from $[N(C_4H_9)_4][B_6H_6H^{fac}]$ in liquid ammonia and obtained in form of a single crystal. The crystal structures of $[Li(NH_3)_4]_2[B_6H_6] \cdot 2\,NH_3$, $M_2[B_{10}H_{10}] \cdot 5\,NH_3$ (M = Rb and Cs) and $[Li(NH_3)_4]_2[B_{12}H_{12}] \cdot 2\,NH_3$ were solved and described. The structure models derived for $[N(C_4H_9)_4]_2[B_6H_6]$ and $[Na(NH_3)_4]_2[B_6H_6] \cdot 2\,NH_3$ will have to be optimized in future. Due to their symmetry and electron-deficiency, *closo*-hydroborates $[B_nH_n]^{2-}$ containing light elements are highly interesting for the deeper investigation of multi-centres bonds. After removal of ammonia, these *closo*-hydroborates might be used as a potential precursor molecules for the synthesis of ultra-pure borides.

Based on symmol calculations, only minute distortions from $O_h$ for the $[B_6H_6]^{2-}$ $D_{4d}$ for the $[B_{10}H_{10}]^{2-}$ and $I_h$ for the $[B_{12}H_{12}]^{2-}$ were found for ammoniated *closo*-hydroborates. Comparing the r.m.s. values of polyhedras in between studied *closo*-hydroborates and borides, it is concluded that the polyhedra in borides are more distorted.

# 6 Safety data sheet

| Chemical | R-Phrase | S-Phrase | Hazard symbols |
|---|---|---|---|
| Acetone | 11-36-66-67 | 9-16-26 | [F] [Xi] |
| Ammonia | 34-50 | 26-36/37/39-45-61 | [C] [N] |
| Boron | 11-22 | 16 | [F] [Xn] |
| Cesium | 14/15-34 | 8-20-26-30-36/37/39-45 | [F] [C] |
| $[(C_5H_5)_3NH]_2[B_{10}H_{10}]$ | | not fully examined compound | |
| Decaborane | 5-11-26-24/25 | 16-45-37/38/39 | [T] [F] |
| Ethanol | 11 | 7-16 | [F] |
| Hydrofluoric acid | 34, 23/24/25 | 7/9-20-26 36/37/39-45-60 | [C][T] |
| Hydrocloric acid | 34-37 | 26-36/37/39-45 | [C] |
| Lithium | 14/15-34 | (1/2)-8-43-45 | [F] [C] |
| Lithium hydroxide monohydrate | 34 | 26-37/39 | [C] |
| $Li_2[B_{10}H_{10}]$ | | not fully examined compound | |
| Mercury | 23-33 | 45-7 | [T] |
| Nitric acid | 8-35 | 23-26-36-45 | [F] [C] |
| $[N(C_4H_9)_4]_2[B_6H_6]$ | | not fully examined compound | |
| $[N(C_4H_9)_4][B_6H_7]$ | | not fully examined compound | |
| $[N(C_4H_9)_4]_2[B_{12}H_{12}]$ | | not fully examined compound | |
| Potasium bromide | 22-36/37/38 | 22-26-36 | [Xn] |
| Rubidium | 14/15-17-34 | - | [F] [C] |
| Triethylamine | 11-20/21/22-35 | 3-16-26-29-36/37/39-45 | [F] [C] |
| Sodium | 14/15-34 | 5.3-8-43.7-45 | [F] [C] |
| Sodium azide | 28-32-50/53 | 1/2-28-45-60-61 | [T+] |
| Sodium borohydride | 15-24/25-26-34 | 22-26-36/37/39-43.13-45 | [F] [T+] |
| $Na_2[B_{10}H_{10}]$ | | not fully examined compound | |
| Sodium Hydroxide | 35 | 26-37/39-45 | [C] |
| Sulphuric acid | 35 | 2-26-30 | [C] |
| Xylene | 10-20/21-38 | 24/25 | [Xn] |

Table 6.1: Risk (R-), safety precaution (S-) phrases and hazard symbols for the used chemicals

**Risk (R-) phrases :**

**R 1** : Explosive when dry

**R 2** : Risk of explosion by shock, friction, fire or other sources of ignition

**R 3** : Extreme risk of explosion by shock, friction, fire or other sources of ignition

**R 4** : Forms very sensitive explosive metallic compounds

**R 5** : Heating may cause an explosion

**R 6** : Explosive with or without contact with air

**R 7** : May cause fire

**R 8** : Contact with combustible material may cause fire

**R 9** : Explosive when mixed with combustible material

**R 10** : Flammable

**R 11** : Highly flammable

**R 12** : Extremely flammable

**R 13** : Extremely flammable liquefied gas

**R 14** : Reacts violently with water

**R 15** : Contact with water liberates extremely flammable gases

**R 16** : Explosive when mixed with oxidising substances

**R 17** : Spontaneously flammable in air

**R 18** : In use, may form flammable/explosive vapour-air mixture

**R 19** : May form explosive peroxides

**R 20** : Harmful by inhalation

**R 21** : Harmful in contact with skin

**R 22** : Harmful if swallowed

**R 23** : Toxic by inhalation

**R 24** : Toxic in contact with skin

**R 25** : Toxic if swallowed

**R 26** : Very toxic by inhalation

**R 27** : Very toxic in contact with skin

**R 28** : Very toxic if swallowed

**R 29** : Contact with water liberates toxic gas

**R 30** : Can become highly flammable in use

**R 31** : Contact with acids liberates toxic gas

**R 32** : Contact with acids liberates very toxic gas

**R 33** : Danger of cumulative effects

**R 34** : Causes burns

**R 35** : Causes severe burns

**R 36** : Irritating to eyes

**R 37** : Irritating to respiratory system

**R 38** : Irritating to skin

**R 39** : Danger of very serious irreversible effects

**R 40** : Limited evidence of a carcinogenic effect

**R 41** : Risk of serious damage to eyes

**R 42** : May cause sensitisation by inhalation

**R 43** : May cause sensitisation by skin contact

**R 44** : Risk of explosion if heated under confinement

**R 45** : May cause cancer

**R 46** : May cause heritable genetic damage

**R 47** : May cause birth defects

**R 48** : Danger of serious damage to health by prolonged exposure

**R 49** : May cause cancer by inhalation

**R 50** : Very toxic to aquatic organisms

**R 51** : Toxic to aquatic organisms

**R 52** : Harmful to aquatic organisms

**R 53** : May cause long-term adverse effects in the aquatic environment

**R 54** : Toxic to flora

**R 55**: Toxic to fauna

**R 56** : Toxic to soil organisms

**R 57** : Toxic to bees

**R 58** : May cause long-term adverse effects in the environment

**R 59** : Dangerous for the ozone layer

**R 60** : May impair fertility

**R 61** : May cause harm to the unborn child

**R 62** : Possible risk of impaired fertility

**R 63** : Possible risk of harm to the unborn child

**R 64** : May cause harm to breast-fed babies

**R 65** : Harmful: may cause lung damage if swallowed

**R 66** : Repeated exposure may cause skin dryness or cracking

**R 67** : Vapours may cause drowsiness and dizziness

**R 68** : Possible risk of irreversible effects

**Combination of risk (R-) phrases :**

**R14/15** : Reacts violently with water, liberating extremely flammable gases

**R15/29** : Contact with water liberates toxic, extremely flammable gases

**R20/21** : Harmful by inhalation and in contact with skin

**R20/22** : Harmful by inhalation and if swallowed

**R20/21/22** : Harmful by inhalation, in contact with skin and if swallowed

**R21/22** : Harmful in contact with skin and if swallowed

**R23/24**: Toxic by inhalation and in contact with skin

**R23/25** : Toxic by inhalation and if swallowed

**R23/24/25** : Toxic by inhalation, in contact with skin and if swallowed

**R24/25** : Toxic in contact with skin and if swallowed

**R26/27** : Very toxic by inhalation and in contact with skin

**R26/28** : Very toxic by inhalation and if swallowed

**R26/27/28** : Very toxic by inhalation, in contact with skin and if swallowed

**R27/28** : Very toxic in contact with skin and if swallowed

**R36/37** : Irritating to eyes and respiratory system

**R36/38** : Irritating to eyes and skin

**R36/37/38** : Irritating to eyes, respiratory system and skin

**R37/38** : Irritating to respiratory system and skin

**R39/23** : Toxic: danger of very serious irreversible effects through inhalation

**R39/24** : Toxic: danger of very serious irreversible effects in contact with skin

**R39/25** : Toxic: danger of very serious irreversible effects if swallowed

**R39/23/24** : Toxic: danger of very serious irreversible effects through inhalation and in contact with skin

**R39/23/25** : Toxic: danger of very serious irreversible effects through inhalation and if swallowed

**R39/24/25** : Toxic: danger of very serious irreversible effects in contact with skin and if swallowed

**R39/23/24/25** : Toxic: danger of very serious irreversible effects through inhalation, in contact with skin and if swallowed

**R39/26** : Very Toxic: danger of very serious irreversible effects through inhalation

**R39/27** : Very Toxic: danger of very serious irreversible effects in contact with skin

**R39/28** : Very Toxic: danger of very serious irreversible effects if swallowed

**R39/26/27** : Very Toxic: danger of very serious irreversible effects through inhalation and in contact with skin

**R39/26/28** : Very Toxic: danger of very serious irreversible effects through inhalation and if swallowed

**R39/27/28** : Very Toxic: danger of very serious irreversible effects in contact with skin and if swallowed

**R39/26/27/28** : Very Toxic: danger of very serious irreversible effects through inhalation, in contact with skin and if swallowed

**R42/43** : May cause sensitisation by inhalation and skin contact

**R48/20** : Harmful: danger of serious damage to health by prolonged exposure through inhalation

**R48/21** : Harmful: danger of serious damage to health by prolonged exposure in contact with skin

**R48/22** : Harmful: danger of serious damage to health by prolonged exposure if swallowed

**R48/20/21**: Harmful: danger of serious damage to health by prolonged exposure through inhalation and in contact with skin

**R48/20/22** : Harmful: danger of serious damage to health by prolonged exposure through inhalation and if swallowed

**R48/21/22** : Harmful: danger of serious damage to health by prolonged exposure in contact with skin and if swallowed

**R48/20/21/22** : Harmful: danger of serious damage to health by prolonged exposure through inhalation, in contact with skin and if swallowed

**R48/23** : Toxic: danger of serious damage to health by prolonged exposure through inhalation

**R48/24** : Toxic: danger of serious damage to health by prolonged exposure in contact with skin

**R48/25** : Toxic: danger of serious damage to health by prolonged exposure if swallowed

**R48/23/24** : Toxic: danger of serious damage to health by prolonged exposure through inhalation and in contact with skin

**R48/23/25** : Toxic: danger of serious damage to health by prolonged exposure through inhalation and if swallowed

**R48/24/25** : Toxic: danger of serious damage to health by prolonged exposure in contact with skin and if swallowed

**R48/23/24/25** : Toxic: danger of serious damage to health by prolonged exposure through inhalation, in contact with skin and if swallowed

**R50/53** : Very toxic to aquatic organisms, may cause long-term adverse effects in the aquatic environment

**R51/53** : Toxic to aquatic organisms, may cause long-term adverse effects in the aquatic environment

**R52/53** : Harmful to aquatic organisms, may cause long-term adverse effects in the aquatic environment

**R68/20** : Harmful: possible risk of irreversible effects through inhalation

**R68/21** : Harmful: possible risk of irreversible effects in contact with skin

**R68/22** : Harmful: possible risk of irreversible effects if swallowed

**R68/20/21** : Harmful: possible risk of irreversible effects through inhalation and in contact with skin

**R68/20/22** : Harmful: possible risk of irreversible effects through inhalation and if swallowed

**R68/21/22** : Harmful: possible risk of irreversible effects in contact with skin and if swallowed

**R68/20/21/22** : Harmful: possible risk of irreversible effects through inhalation, in contact with skin and if swallowed

**Safety precaution (S-) phrases :**

**S1** : Keep locked up

**S2** : Keep out of the reach of children

**S3** : Keep in a cool place

**S4** : Keep away from living quarters

**S5** : Keep contents under $\cdots$ (appropriate liquid to be specified by the manufacturer)

**S6** : Keep under $\cdots$ (inert gas to be specified by the manufacturer)

**S7** : Keep container tightly closed

**S8** : Keep container dry

**S9** : Keep container in a well-ventilated place

**S12** : Do not keep the container sealed

**S13** : Keep away from food, drink and animal feedingstuffs

**S14** : Keep away from $\cdots$ (incompatible materials to be indicated by the manufacturer)

**S15** : Keep away from heat

**S16** : Keep away from sources of ignition - No smoking

**S17** : Keep away from combustible material

**S18** : Handle and open container with care

**S20** : When using do not eat or drink

**S21** : When using do not smoke

**S22** : Do not breathe dust

**S23** : Do not breathe gas/fumes/vapour/spray (appropriate wording to be specified by the manufacturer)

**S24** : Avoid contact with skin

**S25** : Avoid contact with eyes

**S 26** : In case of contact with eyes, rinse immediately with pleanty of water and seek medical advice

**S27** : Take off immediately all contaminated clothing

**S28** : After contact with skin, wash immediately with plenty of ⋯ (to be specified by the manufacturer)

**S29** : Do not empty into drains

**S30** : Never add water to this product

**S33** : Take precautionary measures against static discharges

**S35** : This material and its container must be disposed of in a safe way

**S36** : Wear suitable protective clothing

**S37** : Wear suitable gloves

**S38** : In case of insufficient ventilation wear suitable respiratory equipment

**S39** : Wear eye/face protection

**S40** : To clean the floor and all objects contaminated by this material use ⋯ (to be specified by the manufacturer)

**S41** : In case of fire and/or explosion do not breathe fumes

**S42** : During fumigation/spraying wear suitable respiratory equipment (appropriate wording to be specified by the manufacturer)

**S43** : In case of fire use ⋯ (indicate in the space the precise type of fire-fighting equipment. If water increases the risk add - Never use water)

**S 45**: In case of accident or if you feel unwell, seek medical advice immedietely (show the label where possible)

**S46** : If swallowed, seek medical advice immediately and show this container or label

**S47** : Keep at temperature not exceeding ⋯ °C (to be specified by the manufacturer)

**S48** : Keep wet with · · · (appropriate material to be specified by the manufacturer)

**S49** : Keep only in the original container

**S50**: Do not mix with · · · (to be specified by the manufacturer)

**S51** : Use only in well-ventilated areas

**S52** : Not recommended for interior use on large surface areas

**S53** : Avoid exposure - obtain special instructions before use

**S56** : Dispose of this material and its container at hazardous or special waste collection point

**S57** : Use appropriate containment to avoid environmental contamination

**S59** : Refer to manufacturer/supplier for information on recovery/recycling

**S60** : This material and its container must be disposed of as hazardous waste

**S61** : Avoid release to the environment. Refer to special instructions/safety data sheet

**S62** : If swallowed, do not induce vomiting: seek medical advice immediately and show this container or label

**S63** : In case of accident by inhalation: remove casualty to fresh air and keep at rest

**S64** : If swallowed, rinse mouth with water (only if the person is conscious)

**Combination of safety precaution (S-) phrases :**

**S1/2** : Keep locked up and out of the reach of children

**S3/7** : Keep container tightly closed in a cool place

**S3/7/9** : Keep container tightly closed in a cool, well-ventilated place

**S3/9/14** : Keep in a cool, well-ventilated place away from · · · (incompatible materials to be indicated by the manufacturer)

**S3/9/14/49** : Keep only in the original container in a cool, well-ventilated place away from · · · (incompatible materials to be indicated by the manufacturer)

**S3/9/49** : Keep only in the original container in a cool, well-ventilated place

**S3/14** : Keep in a cool place away from · · · (incompatible materials to be indicated by the manufacturer)

**S7/8** : Keep container tightly closed and dry

**S7/9** : Keep container tightly closed and in a well-ventilated place

**S7/47** : Keep container tightly closed and at temperature not exceeding · · · °C (to be specified by the manufacturer)

**S20/21** : When using do not eat, drink or smoke **S24/25**: Avoid contact with skin

and eyes

**S27/28** : After contact with skin, take off immediately all contaminated clothing, and wash immediately with plenty of · · · (to be specified by the manufacturer)

**S29/35** : Do not empty into drains; dispose of this material and its container in a safe way

**S29/56** : Do not empty into drains, dispose of this material and its container at hazardous or special waste collection point

**S36/37** : Wear suitable protective clothing and gloves

**S36/37/39** : Wear suitable protective clothing, gloves and eye/face protection

**S36/39** : Wear suitable protective clothing and eye/face protection

**S 37/39** : Wear suitable gloves and eye/face protection

**S47/49** : Keep only in the original container at temperature not exceeding · · · °C (to be specified by the manufacturer)

# Bibliography

[1] N. N. Greenwood and A. Earnshaw, *Chemistry of the elements*, Pergamon Press, England, **1984**.

[2] T. B. Massalski, H. Okamoto, and P. R. L. Subramanian, *Binary alloy phase diagrams*, ASM international, Metals Park. Ohio, **1990**.

[3] M. Kobayashi, I. Higashi, H. Matsuda, and K. Kimura, *J. Alloys Compd.*, 221, 120, **1995**.

[4] G. Mair, R. Nesper, and H. G. von Schnering, *J. Solid State Chem.*, 75, 30, **1988**.

[5] H. G. von Schnering, G. Mair, M. Wörle, and R. Nesper, *Z. Anorg. Allg. Chem.*, 625, 1207, **1999**.

[6] M. Wörle and R. Nesper, *Angew. Chem.*, 112(13), 2439, **2000**.

[7] D. R. Secrist, *J. Am. Ceram. Soc.*, 50, 520, **1967**.

[8] I. I. Serebryakova, V. I. Lyashenko, and V. D. Levandovskii, *Powder Metallurgy Met. Ceram.*, 33, 49, **1994**.

[9] A. Lipp, *Fr. Pat.*, Dec. 9, 1,461,878, **1966**.

[10] V. P. Sorokin, P. I. Gavrilov, and E. V. Levakov, *Russ. J. Inorg. Chem.*, 22, 329, **1977**.

[11] S. Dallek, D. W. Ernst, and B. F. Larrick, *J. Electrochem. Soc.*, 126, 866, **1979**.

[12] F. E. Wang, M. A. Mitchell, R. A. Sutula, J. R. Holden, and L. H. Bennet, *J. Less-Comm. Met.*, 57, 161, **1978**.

[13] S. D. James and L. E. DeVries, *J. Electrochem. Soc.*, 123, 321, **1976**.

[14] A. Meden, J. Mavri, M. Bele, and S. Pejovnik, *J. Phys. Chem.*, 99, 4252, **1995**.

[15] M. Wörle, Ph.D. thesis, ETH Zürich, **1995**.

[16] K. Schmitt, Ph.D. thesis, Justus-Liebig-Universität Giessen, **1997**.

[17] P. Hagenmuller and R. Naslain, *Compt. Rend.*, 257, 1924, **1963**.

[18] R. Naslain and J. S. Kasper, *J. Solid State Chem.*, 1, 150, **1970**.

[19] R. Naslain, A. Guette, and P. Hagenmuller, *J. Less-Comm. Met.*, 47, 1, **1976**.

[20] B. Albert, K. Hofmann, C. Fild, H. Eckert, M. Schleifer, and R. Gruehn, *Chem. Eur. J*, 6(14), 2531, **2000**.

[21] B. Albert, *Angew. Chem. Int. Ed.*, 37(8), 1117, **1998**.

[22] B. Albert and K. Hofmann, *Z. Anorg. Allg. Chem.*, 625, 709, **1999**.

[23] W. Schlenk and H. Thal, *Ber. Dtsch. Chem. Ges.*, 46, 2840, **1913**.

[24] R. Pöttgen, T. Gulden, and A. Simon, *GIT laborfachzeitschrift*, 43, 133, **1999**.

[25] A. R. West, *Basic Solid State Chemistry*, John Wiley and Sons, New York, **1988**.

[26] *Stoe Stadi P*, STOE and Cie GmbH, Darmstadt, **2002**.

[27] H. M. Rietveld, *J. Appl. Cryst.*, 2, 65, **1969**.

[28] J. E. Post, *Reviews in Mineralogy: Modern Powder Diffraction, Washington D. C. USA*, 20, S278, **1989**.

[29] A. C. Larson and R. B. V. Dreele, *General Structure Analysis System*, Los Alamos National Laboratory, Los Alamos, NM 87545, **2000**.

[30] B. H. Toby, *J. Appl. Cryst.*, 34, 210, **2001**.

[31] J. Durbin and G. Watson, *Biometrika*, 38, 159, **1951**.

[32] *Bruker SMART*, Bruker AXS: Madison, Wisconsin, USA, **2000**.

[33] *Bruker SAINT, Integration software for single crystal data*, Bruker AXS: Madison, Wisconsin, USA, **2000**.

[34] *Bruker SADABS*, Bruker AXS: Madison, Wisconsin, USA, **2000**.

[35] G. M. Sheldrick, *SHELXS-97*, Göttingen, Germany, **1997**.

[36] G. M. Sheldrick, *SHELXL-97*, Göttingen, Germany, **1997**.

[37] T. Pilati and A. Forni, *J. Appl. Crystallogr.*, 31, 503, **1998**.

[38] H. Zabrodsky, S. Peleg, and D. Avnir, *J. Am. Chem. Soc*, 115, 8278, **1993**.

[39] H. L. Tuller and P. K. Moon, *Mat. Sci. Eng. B*, 1, 171, **1988**.

[40] J. T. S. Irvine, D. C. Sinclair, and A. R. West, *Adv. Mater.*, 2(3), 132, **1990**.

[41] H. Rickert, *Electrochemistry of Solids*, Springer-Verlag, New York, **1982**.

[42] J. R. Macdonald, *Impedance Spectroscopy: Emphasizing Solid Materials and Systems*, John Wiley and Sons, Inc., New York, **1987**.

[43] A. R. West, D. C. Sinclair, and N. Hirose, *J. Electrocer.*, 1, 65, **1997**.

[44] G. Hsieh, S. J. Ford, T. O. Mason, and L. R. Pederson, *Solid State Ionics*, 100, 297, **1997**.

[45] J. R. Dygas, G. Fafilek, and M. W. Breiter, *Solid State Ionics*, 119, 115, **1999**.

[46] R. F. Egerton, *Electron Energy-Loss Spectroscopy in the Electron Microscope*, Plenum press, New York, **1996**.

[47] J. C. H. Spence, *Rep. Prog. Phys.*, 69, 725, **2006**.

[48] R. Brydson, *EMSA Bulletin*, 21(2), 57, **1991**.

[49] K. Hofmann and B. Albert, personal communication.

[50] F. Settle, *Handbook of instrumental techniques for analytical chemistry*, Prentice-Hall, Inc., New Jersey, **1997**.

[51] C. N. R. Rao and J. R. Ferraro, *Spectroscopy in Inorganic Chemistry*, Academic press, Inc., New York, **1970**.

[52] V. I. Matkovich, editor, *Boron and Refractory Borides*, Springer-Verlag, New York, **1977**.

[53] R. Naslain and J. Etourneau, *Compt. Rend.*, 263(6), 484, **1966**.

[54] R. Naslain, J. Etourneau, and P. Hagenmuller, *Bull. Soc. Chim. Fr.*, 7, 2529, **1967**.

[55] B. Albert, *Eur. J. Inorg. Chem.*, 2000(8), 1679, **2000**.

[56] L. W. Rupp and D. J. Hodges, *J. Phys. Chem. Solids*, 35, 617, **1974**.

[57] F. E. Wang, *Trans. Amer. Inst. Metal. Pet. Eng.*, 10A, 343, **1979**.

[58] G. E. Mcmanis, A. N. Fletcher, and M. H. Miles, *J. Electrochem. Soc.*, 134, 286, **1984**.

[59] P. Sanchez, C. Belin, G. Crepy, and A. D. Guibert, *J. Mat. Sci.*, 27, 240, **1992**.

[60] A. Meden, B. Pihlar, and S. Pejovnik, *J. Appl. Electrochem.*, 24, 78, **1994**.

[61] S. Gunji and H. Kamimura, *Proc. 11th Int. Symp. Boron, Borides and Rel. Comp., JJAP Series*, 10, 35, **1994**.

[62] Z. Liu, X. Qu, B. Huang, and Z. Li, *J. Alloys Compd.*, 311, 256, **2000**.

[63] H. Rosner and W. E. Picket, *Phys. Rev. B*, 67, 054104, **2003**.

[64] L. Zhijian, Q. Xuanhui, L. Zhiyou, and H. Baiyun, *Science in China (Series E)*, 46(4), 391, **2003**.

[65] M. Winter, J. O. Besenhard, M. E. Spahr, and P. Novak, *Adv. Mater.*, 10(10), 725, **1998**.

[66] R. J. Brodd, *J. Electrochem. Soc. Interface*, 8(3), 20, **1999**.

[67] M. M. Thackeray, J. O. Thomas, and M. S. Whittingham, *MRS Bulletin*, 39, **2000**.

[68] J. M. Tarascon and M. Armand, *Nature*, 414, 359, **2001**.

[69] H. Yamane, S. Kikkawa, H. Horiuchi, and M. Koizumi, *J. Solid State Chem.*, 65, 6, **1986**.

[70] H. Yamane, S. Kikkawa, and M. Koizumi, *J. Solid State Chem.*, 71, 1, **1987**.

[71] R. S. Pease, *Acta Crystallogr.*, 5, 356, **1952**.

[72] K. Hofmann, R. Gruehn, and B. Albert, *Z. Anorg. Allg. Chem.*, 628, 2691, **2002**.

[73] M. V. Stackelberg and F. Neumann, *Z. Phys. Chem.*, B19, 314, **1932**.

[74] T. Ito, T. Kasukawa, I. Higashi, and Y. Satow, *Proc. 11th Int. Symp. Boron, Borides and Rel. Comp., JJAP Series*, 10, 11, **1994**.

[75] H. R. Ott, M. Chernikov, E. Felder, L. Degiorgi, E. G. Moshopulou, and Z. Fisk, *Z. Phys.*, B102, 337, **1997**.

[76] K. Schmitt, C. Stückel, H. Ripplinger, and B. Albert, *Solid State Sci.*, 3, 321, **2001**.

[77] *WinXPOW Ver(1.10)*, STOE and Cie GmbH, Darmstadt, **2002**.

[78] H. Bärnighausen, *MATCH, Commun. Math. Chem.*, 9, 139, **1980**.

[79] H. Bärnighausen, U. Müller, R. Pöttgen, and H. Wondratschek, *Seminar über Anwendungen der kristallographischen Gruppentheorie in der Kristallchemie*, Hofgeismar, Germany, **2005**.

[80] T. Hahn, editor, *International tables for crystallography, Volume A*, D. Reidel Publishing Company, Holland, **1983**.

[81] H. Wondratschek and U. Müller, editors, *International tables for crystallography, Volume A1*, Kluwer academic publishers, The Netherlands, **2004**.

[82] W. Kraus and G. Nolze, *PowderCell for Windows*, Federal Institute of Materials Research and Testing, Rudower Chaussee 5, Berlin Germany, **2000**.

[83] G. W. Rice and R. L. Woodin, *J. Am. Ceram. Soc.*, 71, 181, **1988**.

[84] A. L. Wayda, L. F. Schneemeyer, and R. L. Opila, *Appl. Phys. Lett.*, 53(5), 361, **1988**.

[85] H. Itoh, Y. Tsuzuki, T. Yogo, and S. Naka, *Mat. Res. Bull.*, 22, 1259, **1987**.

[86] N. T. Kuznetsov, K. A. Solntsev, and V. Y. Shevchenko, *Proc. 9th Int. Symp. Boron, Borides and Rel. Comp.*, 281, **1987**.

[87] M. Sofin, E. M. Peters, and M. Jansen, *J. Solid State Chem.*, 117, 2550, **2004**.

[88] D. Trinschek and M. Jansen, *Z. Anorg. Allg. Chem.*, 622, 245, **1996**.

[89] D. Trinschek and M. Jansen, *Z. Naturforsch.*, 51b, 711, **1996**.

[90] M. Sofin, Ph.D. thesis, MPI für Festkörperforschung Stuttgart, **2003**.

[91] N. Arumugam, A. Hönnerscheid, and M. Jansen, *Z. Anorg. Allg. Chem.*, 629, 939, **2003**.

[92] J. W. Johnson and J. F. Brody, *J. Electrochem. Soc.*, 129, 2213, **1982**.

[93] K. Hofmann, Ph.D. thesis, Justus-Liebig-Universität Giessen, **2000**.

[94] M. F. Hawthorne, R. L. Pilling, and W. H. Knoth, *Inorg. Synth.*, 9, 16, **1967**.

[95] H. C. Longuet-Higgins and M. de V. Roberts, *Proc. Roy. Soc. London*, A230, 110, **1955**.

[96] M. F. Hawthorne and A. R. Pitochelli, *J. Am. Chem. Soc*, 82, 3228, **1960**.

[97] I. Y. Kuznetsov, D. M. Vinitskii, K. A. Solntsev, N. T. Kuznetsov, and L. A. Butman, *Russ. J. Inorg. Chem.*, 32, 1803, **1987**.

[98] J. A. Wunderlich and W. N. Lipscomb, *J. Am. Chem. Soc.*, 82, 4427, **1960**.

[99] S. I. Uspenskaya, K. A. Solntsev, and N. T. Kuznetsov, *Zh. Strukt. Khim.*, 16, 482, **1975**.

[100] I. Tiritiris, T. Schleid, K. Müller, and W. Preetz, *Z. Anorg. Allg. Chem.*, 626, 323, **2000**.

[101] K. A. Solntsev, N. T. Kuznetsov, L. N. Kolba, V. M. Agre, and V. I. Ponomarev, *Russ. J. Inorg. Chem.*, 22(2), 171, **1977**.

[102] I. Tiritiris and T. Schleid, *Z. Anorg. Allg. Chem.*, 627, 1836, **2001**.

[103] V. I. Ponomarev, T. Y. Lyubeznova, K. A. Solntsev, and N. T. Kuznetsov, *Koord. Khim.*, 17, 21, **1991**.

[104] K. A. Solntsev, N. T. Kuznetsov, V. K. Trunov, O. G. Karpinskii, G. S. Klimchuk, S. I. Uspenskaya, and Y. V. Oboznenko, *Russ. J. Inorg. Chem.*, 22(12), 1744, **1977**.

[105] G. Shoham, D. Schomburg, and W. L. Lipscomb, *Cryst. Struct. Comm.*, 9, 429, **1980**.

[106] S. B. Katser, E. A. Malinina, V. N. Mustyatsa, K. A. Solntsev, and N. T. Kuznetsov, *Koord. Khim.*, 18, 387, **1992**.

[107] W. N. Lipscomb, A. R. Pitocelli, and M. F. Hawthorne, *J. Am. Chem. Soc.*, 81, 5833, **1959**.

[108] Y. Zhang, Z. Cai, Z. Chen, K. Pan, J. Lu, G. Zhang, and H. Zhu, *Jiegou Huaxne*, 1, 45, **1982**.

[109] D. J. Fuller, D. L. Kepert, B. W. Skelton, and A. H. White, *Aust. J. Chem.*, 40, 2097, **1987**.

[110] C. T. Chantler and E. N. Maslen, *Acta Crystallogr.*, B45, 290, **1989**.

[111] A. V. Virovets, N. Vakulenko, V. V. Volkov, and N. V. Podberezskaya, *Zh. Strukt. Khim.*, 35, 72, **1994**.

[112] K. Hofmann and B. Albert, *Z. Naturforsch.*, 55b, 499, **2000**.

[113] S. Chitsaz, H. Folkerts, J. Grebe, T. Grob, K. Harms, W. Hiller, M. Krieger, W. Massa, J. Merle, M. Mohlen, B. Neumuller, and K. Dehnicke, *Z. Anorg. Allg. Chem.*, 626, 775, **2000**.

[114] K. Hofmann and B. Albert, *Z. Krist.*, 220, 142, **2005**.

[115] A. M. Orlova, V. N. Mustyatsa, L. V. Goeva, S. B. Kaster, K. A. Solntsev, and N. T. Kuznetsov, *Russ. J. Inorg. Chem.*, 41, 1956, **1996**.

[116] K. Hofmann and B. Albert, *Z. Kristallogr. Suppl.*, 18, 88, **2001**.

[117] J. T. Gill and S. L. Lippard, *Inorg. Chem.*, 14, 751, **1975**.

[118] F. Kraus and B. Albert, *Z. Anorg. Allg. Chem.*, 631, 152, **2005**.

[119] W. Preetz and G. Peters, *Eur. J. Inorg. Chem*, 6(14), 1831, **1999**.

[120] R. M. Kabbani, *Polyhedron*, 15(12), 1951, **1996**.

[121] I. Y. Kuznetsov, D. N. Vinitskii, K. A. Solntsev, N. T. Kunetsov, and L. A. Butman, *Dokl. Akad. Nauk. SSSR*, 283(4), 873, **1985**.

[122] K. Hofmann and B. Albert, personal communication.

[123] A. L. Speck, *PLATON-A Multipurpose Crystallographic Tool*, Utrecht, The Netherlands, **2003**.

[124] J. E. Huheey, E. A. Keiter, and R. L. Keiter, *Inoragnic chemistry: priciples of structure and reactivity, 4. ed.*, HarperCollins College Publishers, India, **1993**.

[125] N. Korber and M. Reil, *Chem. Commun.*, 1, 84, **2002**.

[126] W. Preetz, A. Heinrich, and J. Thesing, *Z. Naturforsch.*, 43(b), 1319, **1988**.

[127] T. Schaper and W. Preetz, *Inorg. Chem.*, 37, 363, **1998**.

[128] E. L. Muetterties, J. H. Balthis, Y. T. Chai, W. H. Knoth, and H. C. Miller, *Inorg. Chem.*, 3, 444, **1964**.

[129] W. E. Keller and H. L. Johnston, *J. Chem. Phys.*, 20, 1749, **1952**.

[130] E. L. Muetterties, R. E. Merrifield, H. C. Miller, W. H. Knoth, and J. R. Downing, *J. Am. Chem. Soc*, 84, 2506, **1962**.

[131] K. O. Christe, W. W. Wilson, R. D. Wilson, R. Bau, and J. Feng, *J. Am. Chem. Soc*, 112, 7619, **1990**.

[132] K. Wade, *Inorg. Chem. Radiochem.*, 18, 1, **1976**.

[133] R. G. Pearson, *J. Am. Chem. Soc*, 85, 3533, **1963**.